NASA Contractor Report 158905
ASI-TR-76-39

(NASA-CR-158905) DISPLAY/CONTROL REQUIREMENTS FOR AUTOMATED VTOL AIRCRAFT Final Report (Aerospace Systems, Inc., Burlington, Mass.) 161 p HC A04/MF A01 CSCL 01D G3/06

N79-20112

Unclas
17248

DISPLAY/CONTROL REQUIREMENTS FOR AUTOMATED VTOL AIRCRAFT

FINAL TECHNICAL REPORT

W. C. Hoffman, D. L. Kleinman, and L. R. Young

Aerospace Systems, Inc.
Burlington, MA 01803

Contract No. NAS 1-13653
October 1976

National Aeronautics and Space Administration

Langley Research Center
Hampton, Virginia 23665

ASI-TR-76-39
NASA CR-158905

DISPLAY/CONTROL REQUIREMENTS FOR AUTOMATED VTOL AIRCRAFT

FINAL TECHNICAL REPORT

by

William C. Hoffman
David L. Kleinman
Laurence R. Young

AEROSPACE SYSTEMS, INC.
Burlington, Massachusetts 01803

Prepared under

Contract No. NAS 1-13653

for

Langley Research Center
National Aeronautics and Space Administration
Hampton, Virginia 23665

October 1976

FOREWORD

This report was prepared by Aerospace Systems, Inc. (ASI), Burlington, Massachusetts, for the National Aeronautics and Space Administration (NASA) under Contract No. NAS1-13653. The report documents the results of research performed during the period October 1975 to October 1976. The study was sponsored by the Flight Instrumentation Division, Navigation and Guidance Research Branch, the NASA Langley Research Center (LaRC), Hampton, Virginia. Dr. J. F. Creedon served as Technical Monitor on the contract.

The effort was directed by Mr. William C. Hoffman as the Project Engineer with Mr. John Zvara as the Technical Director and President of ASI. Dr. Renwick E. Curry, formerly of the MIT Department of Aeronautics and Astronautics, Dr. David L. Kleinman of the University of Connecticut Department of Electrical Engineering and Computer Science, and Dr. Laurence R. Young, Director of the MIT Man-Vehicle Laboratory, contributed to the study as technical consultants and principal investigators. Miss Kristine M. Doyle participated in the mathematical analysis and the computer program development and applications. Contributions to the overall program by Dr. Walter M. Hollister, consultant to ASI and Associate Professor in the Department of Aeronautics and Astronautics at MIT, are gratefully acknowledged.

TABLE OF CONTENTS

TABLE OF CONTENTS (Continued)

LIST OF FIGURES

LIST OF FIGURES (Concluded)

LIST OF TABLES

NOMENCLATURE

a	indifference thresholds for observations y
A	system homogeneous response matrix
$\hat{A}$	closed loop filter matrix
b	aerodynamic reference length
β	system control distribution matrix
c_1, c_2	constants
C	state distribution matrix for observations
D	control distribution matrix for observations
$e(t)$	estimation error
E	system noise distribution matrix
$E(1/2)$	percentage estimation error
f	workload
f_c	workload for control
f_{c_i}	attention allocated to y_i for control purposes
f_m	workload for monitoring
f_{mA}	fractional monitoring attention for longitudinal axes
f_{mB}	fractional monitoring attention for lateral axes
f_{m_i}	fraction of monitoring attention allocated to y_i
f_T	total workload
FD_i	flight director signal
g	acceleration of gravity
g_f	unconstrained gradient vector
g_f^p	projection of g_f on constraint surface
G	Kalman filter gain matrix

h	vertical position
h_i	flight director gains for FD_i
I_{xx}, I_{yy}, I_{zz}	vehicle moments of inertia
J_{xz}	vehicle product of inertia
J	cost functional
J_m	monitoring performance cost
J_{mA}	fractional monitoring cost for longitudinal axes
J_{mB}	fractional monitoring cost for lateral axes
k	error fraction for monitoring
$\hat{\ell}_i'$	i^{th} row of $\hat{L}$
L	pilot's feedback control gain matrix
$\hat{L}$	equivalent to L with gains on unmeasurable noise shaping states set to zero
L_{cs}	control system feedback gains
L_e	"equivalent" gain
L_p, L_r, L_y, L_δ	aerodynamic rolling moment derivatives
L_u, L_v, L_w	scale distances for gust model
m	vehicle mass
M_i	weighting term on FD_i in control cost J_c
M_q, M_u, M_w, M_δ	aerodynamic pitching moment derivatives
N_A	number of longitudinal axis instruments to be monitored
N_B	number of lateral axis instruments to be monitored
N_i	describing function gain for observation threshold
N_i	weighting term on FD_i in control cost J_c
NI	number of displacements of state variables
NU	number of pilot-generated corrective control inputs

NX	number of states for which $x_{i,max} < \infty$
NY	number of displayed outputs
p	aerodynamic roll rate
p(t)	best estimate of delayed state x and control u
p_{uj}	control input limits
P	performance cost functional
P_c	control performance
P_m	monitoring performance
P_0	steady state yaw rate
q	aerodynamic pitch rate
$\dot{q}_{max}$	pitch acceleration limit
$q_{\dot{u}_i}$	control rate weightings
q_{y_i}	cost functional weightings
Q_0	steady state pitch rate
Q_u	performance weighting matrix on controls
$Q_{\dot{u}}$	performance weighting matrix on control rates
Q_x	performance weighting matrix on states
Q_y	performance weighting matrix on observations
r	aerodynamic yaw rate
R_0	steady-state yaw rate
s	Laplace operator
t	time
t_{D_i}	mean time to detect an additive failure on instrument i
T_N	pilot's neuromuscular time constant
u	control inputs
u_c	commanded control

U_0	steady-state longitudinal body axis velocity component
$V_u(t)$	motor noise
$V_y(t)$	observation noise
V	airspeed
V_{u_i}	covariance of $v_u(t)$
V_x	forward velocity
V_y	lateral velocity
V_y	observation noise covariance
V_z	vertical velocity
w	gust disturbance inputs
$w(t)$	Gaussian white-noise process for modeling external disturbances (e.g., wind)
W	covariance of w
W_0	steady-state vertical velocity
x	forward position
x	state variable vector
X	input covariance matrix
X_q, X_u, X_w, X_δ	longitudinal aerodynamic force derivatives
y	lateral position
y	observation vector
y_{FD}	flight director displays
y_p	total signal perceived by human
Y	output covariance matrix
Y_p, Y_r, Y_v, Y_δ	lateral aerodynamic force derivatives
z	vertical position
Z_u, Z_w, Z_q, Z_δ	vertical aerodynamic force derivatives

α	fraction of f_{c_i} used implicitly for monitoring
β	fraction of signal rms
γ_i	constant related to probability and magnitude of failure
Γ	transformation matrix
δ	control inputs
δ_a	lateral control inputs
δ_c	vertical control inputs
δ_e	forward control inputs
δ_{FB}	control system feedback inputs
δ_r	directional control inputs
ζ	damping ratio
η_i	Gaussian white driving noise with zero mean and unity variance
θ	forward attitude
θ_0	trim pitch attitude
ρ_{u_i}	motor noise/signal ratio
ρ_{y_i}	observation noise/signal ratio with shared attention
$\rho^o_{y_i}$	observation noise/signal ratio for full attention
σ	standard deviation unit
σ_{e_i}	standard deviation in the pilot's estimation error
$\sigma^2_{r_i}$	unfailed residual covariance for failure detection
σ_{x_i}	standard deviation of state x_i
σ_{y_i}	standard deviation of y_i
Σ	estimation error covariance matrix
τ	human's perceptual time-delay
τ	time constants
ϕ	roll attitude

ϕ_0	steady-state roll attitude
χ	augmented state
ψ	directional (yaw) attitude
ω	natural frequency

SUBSCRIPTS

avail	available
A	longitudinal axes
B	lateral axes
c	control
des	desired value
FD_1	flight director signal 1
FD_2	flight director signal 2
g	gust disturbance variable
lat	lateral axes
long	longitudinal axes
m	monitoring
max	maximum value
0	system matrices for automated vehicle
0L	system matrices for manual vehicle
req	required value to meet performance specifications
s	status variable
x_i	refers to state x_i
y_i	refers to observation y_i

SUPERSCRIPTS

$(\dot{\ })$	rate
$(\hat{\ })$	best estimate
$(\ )^{-1}$	inverse of matrix
$(\ )'$	transpose of matrix

SECTION 1

INTRODUCTION

1.1 BACKGROUND

Vertical takeoff and landing (VTOL) aircraft have considerable potential for use in a viable short-haul air transportation system. The VTOL aircraft used in this context would provide convenient, safe and reliable access to long-haul air transportation by providing air service from major and smaller cities to regional airports. They would also contribute to the achievement of a more balanced total transportation system by providing direct links between smaller cities and major cities and between nearby major cities.

In order for such a VTOL short-haul system to be economically feasible, the aircraft must provide schedule reliability in all-weather conditions, acceptable levels of ride quality, and direct access to the city centers for passenger convenience. Before a viable VTOL system can become a reality, technology developments are needed in a number of areas. During the past several years many advanced VTOL aircraft design programs have been conducted to develop economical vehicles with improved ride qualities and controllability which would be suitable for a commercial VTOL transportation system. However, to effectively utilize these vehicles and to exploit their unique characteristics for minimizing noise and both air and ground space requirements, corresponding advances must be made in handling qualities, operating procedures, and all-weather avionics.

The NASA Langley Research Center (LaRC) has undertaken a research program to develop the navigation, guidance, control, display and flight management technology base needed to establish systems design concepts and operating procedures for VTOL

short-haul transportation systems in the 1980s time period and beyond. The VALT (VTOL Automatic Landing Technology) Program encompasses: investigation of operating systems and piloting techniques associated with VTOL operations under all-weather conditions from downtown vertiports; analysis of terminal air traffic and airspace requirements; and development of avionics including navigation, guidance, controls, and displays for automated takeoff, cruise, and landing operations.

In support of the VALT Program, Aerospace Systems, Inc. (ASI) has conducted a number of research studies for LaRC which provide a technology base for the present study. In the initial effort (Reference 1), ASI analyzed the navigation and guidance requirements for commercial VTOL operations in the takeoff, cruise, terminal area, and landing phases of flight in weather conditions up to and including Category III. A digital computer simulation was developed to provide a means for evaluating the performance of candidate VTOL avionics systems, and was used to conduct a sensitivity study of several VTOL guidance and control concepts (Reference 2).

One conclusion in Reference 1 was that curved decelerating approaches will be required for safe, efficient, and independent VTOL operations. To facilitate these maneuvers, a spiral descent technique was formulated as a possible standard VTOL approach procedure (Reference 3). The spiral descent uses minimal airspace, accommodates arrivals from any direction, and can service multipad landings; it also provides the benefits of a vertical descent, but avoids the vortex ring state, maintains a stable airspeed, and uses less fuel.

The control of a VTOL along the spiral descent trajectory or other flight path constitutes a challenging task for the pilot. To reduce the workload for the guidance and control tasks to a tolerable level for multiple daily landings, the aircraft controls will be partially or completely automated. As the level of automation increases,

the pilot's role shifts from primarily that of a controller towards that of a system monitor and manager. Reference 4 documents the first phase of a study to examine which tasks should be allocated to the pilot of an automated VTOL aircraft utilized as part of a short-haul air transportation system, and to determine what displayed information will be required in performing these tasks.

1.2 REVIEW OF PRELIMINARY CONTROL/DISPLAY ANALYSIS

The preliminary study (Reference 4) was intended to provide insight into the problems associated with pilot tasks in an automated VTOL aircraft in general. Several guidelines were established to provide a frame of reference and to ensure that the results could be readily used and evaluated in the context of the VALT program. These guidelines included the following:

- Flight Profile - The emphasis of the study was on the approach and landing phase of flight; however, sufficient general consideration to the takeoff and enroute phases of flight was included to ensure that the study results would be compatible with the overall task of operating the vehicle as a commercial transport.
- Vehicle Dynamics - The study utilized the CH-46C and CH-47 helicopters used in the LaRC flight research programs.
- Crew - Crew tasks were configured to permit operation by one pilot. Routine calls, communication channel selection, or other tasks which might be handled by a second crew member in an operational context were not included in the scope of work.
- Pilot Involvement - The levels of automation considered were varied over a range extending from a fully automatic system with the pilot in a passive mode with respect to control activity to a system with full manual control.
- Technology Date - In defining a level of system automation, allocating tasks to automatic systems, and in conceiving displays for the control/display concept, decisions were based on the relevant technology projected as being available in the mid 1980s.
- Pilot/Hardware Experiments - Hardware tests, flight tests, and pilot/hardware interaction experiments were specifically excluded from the scope of the work.

The primary accomplishment of the investigation in Reference 4 was the development of a systematic methodology for evaluating pilot display/control trade-offs and information requirements. This design approach accounts for various levels of control automation and display sophistication. It is based on the optimal control model for the human operator, but includes several significant extensions in the state-of-the-art of pilot modeling. An explicit attention allocation procedure was established which determines the optimal division of the pilot's total attention between monitoring and control tasks, and among the various displays available to him for each task.

The design methodology separated the model into three levels of detail. At the "information level," all of the state variables were assumed to be perfectly displayed to the pilot. Thus, the pilot would have perfect knowledge of each state variable, and the allocation of his attention among these indicates their relevant importance in the ideal situation. At the "display element level" the effects of pilot indifference thresholds were introduced, and the pilot's ability to detect both position and rate from a given display element was included. At this level the relative importance of each display element can be determined, and a more realistic estimate of the overall system performance can be obtained. Finally, at the "display format level" realistic performance estimates due to display thresholds, maximum deflections, instrument noise, scan frequency, etc. can be determined for an actual display format which has been designed from the display element results.

The design methodology included a model for simultaneous monitoring and control, which was based on the premise that the pilot first attempts to control the aircraft to a given level of performance, and then uses any additional capability for monitoring status information and/or automatic system performance. The model used a quadratic function of the state errors as a metric for control performance. The control workload metric was the pilot's total control attention to all the displayed elements that

would be required to achieve a desired level of system performance. The model optimized the control performance metric by allocating this total control attention among the available displayed elements. Then his available attention for monitoring was determined as the difference between his total capacity and that required for control to the given performance level. The model next determined the optimum allocation of monitoring attention among the available status displays and evaluated the overall monitoring performance metric, which was a quadratic index similar to the control performance metric.

A computer program (Program PIREP) was developed to implement the extended optimal control/monitoring model for the pilot. It can be used to determine the optimal allocation of pilot's attention for either monitoring or control, as well as the associated system performance. The principal inputs of PIREP are the system dynamics (automation level, external disturbances, etc.), the display model (display elements, threshold, etc.), and the total attention (control/monitoring). The primary outputs of PIREP are the optimum attention allocation (control/monitoring), the system performance metrics (J_c, J_m, cost gradients), and the rms predictions (state, display, control).

The extended optimal control model for the pilot was validated by attempting to reproduce flight results obtained by NASA/LaRC with the CH-46 tandem rotor helicopter. Descriptions of the CH-46 model-following control system, evaluation display panel, and the flight director algorithms were obtained from NASA. The optimal control model was exercised at the display format level for hover flight condition, and the results were compared with limited flight data. Both the analytical and experimental results show that the pilot could not adequately hover without the flight director, but that he had very little difficulty in hover with the flight director.

A flight director design technique using quadratic synthesis was developed as a straightforward means of generating flight director algorithms. These algorithms were designed to relate to the pilot task objectives, i.e., minimize his workload and/or improve his control performance, and to satisfy the pilot's desired goal of behaving approximately as a gain and time delay. The flight director signals were obtained as linear functions of the system states as a byproduct from the optimal control model. When applied to the CH-46 helicopter, the flight director design technique produced nearly identical time constants to those of the flight director algorithms developed by NASA/LaRC in flight tests.

A similar approach using quadratic synthesis was applied to determine flight control systems at several automation levels for the helicopter. By appropriately specifying the control and state weights in a quadratic performance index, various levels of automatic feedback control systems could be systematically designed. These ranged from a totally manual basic vehicle with no feedback to the fully automatic system with complete position feedback.

The display/control design methodology was applied to predict the longitudinal performance of the LaRC CH-47 helicopter, which will be used as the VALT research aircraft. Two flight conditions were investigated: hover at sea level, and a straight approach condition at 60 knots and 1,000 ft/min descent. Seven levels of control automation and five display system levels were considered. Cost weighting functions and indifference thresholds for the CH-47 were selected based on the desired performance requirements for an advanced VTOL commercial helicopter.

In general, the preliminary results indicated that the flight director improved system performance. Although this was an obvious and expected result, the model provided quantitative indications of the performance improvement with the flight director. The results also showed that the vertical flight director provided marginal performance

improvement; most of the performance gain was produced by the forward flight director. The CH-47 results also showed that control automation generally improved performance. Again, this was an obvious conclusion, but the model provided quantitative measures of the performance improvement for various automation systems. Moreover, Reference 4 concluded that in order to achieve the desired system performance, some level of automation will be required for most advanced VTOL missions, since at hover and approach the CH-47 helicopter could not be flown to an acceptable performance level without control automation. The results also indicated that the hover condition is considerably more difficult than the approach. However, increasing system automation tended to reduce the difference in difficulty between the two flight conditions. Also, the more automatic systems were found to be less sensitive to pilot workload variations; as automation was increased, the slope of the performance curve versus workload was lower. This means that other temporary demands on the pilot's attention would cause less deterioriation in system performance as automation increased.

The relative importance of the individual display elements was clearly demonstrated for all display sophistication and control automation levels. The model provided a quantitative measure of the relative importance of each display element by means of the optimum attention allocation. For example, as the display sophistication increased the pilot paid less attention to the situation displays and more to the flight director signals. Similarly, as system automation increased for a given display configuration, the pilot adjusted his attention accordingly.

The monitoring model confirmed the a priori conjecture that more monitoring generally improves system performance, since more monitoring time implies less control workload. However, the preliminary results showed that monitoring performance itself does not necessarily improve either with increased system automation or with display

sophistication. Several questions were raised regarding the interpretation of the monitoring model and combining the monitoring results with the control results.

Although the actual design of a display format is more of an art than a science, several design principles were delineated that could be used to simplify the translation of display element analytical results to the instrument format. Using these principles, a straw-man display concept was developed in an attempt to satisfy the results of the optimal control/monitor model for the CH-47 with two control/display configurations.

1.3 RESEARCH OBJECTIVES AND REPORT ORGANIZATION

This report documents the second phase of ASI's research to determine the display/control requirements for commercial VTOL aircraft. Specifically, the design and analysis methodologies developed in Reference have been refined and have been demonstrated in a more thorough manner. The major portion of the second phase effort was expended on performing a combined longitudinal and lateral control/design tradeoff analysis for the CH-47 VALT Research Aircraft. Secondary objectives involved a reassessment of the monitoring model developed in the first phase, and the definition of further analytical and experimental research areas preparatory to the VALT flight test program.

Section 2 provides a complete discussion of the display/control system design methodology that was developed and applied to the CH-47. Our philosophy is that the pilot's first priority is to control the aircraft to some acceptable performance level, then he uses any remaining capacity to fulfill his monitoring role. The design process involves four metrics for system evaluation:

1. Control task performance
2. Control task workload

3. Monitoring task performance
4. Monitoring task workload

The well-known optimal control model of the human operator has been extended to provide predictions of these system measures during a simultaneous control and monitoring situation.

The application of the design methodology requires the specification of competing control/display system configurations by the analyst. These can be either obtained independently from some other source, or defined through some systematic procedure as a corollary to the main analysis. Subsections 3.1 and 3.2 of the report describe the procedures utilized in this study to develop levels of control automation and display sophistication for the candidate systems. These procedures are adaptations of those presented in Reference 4. The control system design process uses quadratic synthesis to generate successive closed-loop systems which are based on the bandwidth characteristics of a predetermined model. The flight director design approach attempts to provide the pilot with the information that he needs for control of the aircraft. The flight director signals are generated to allow the pilot to respond to them strictly as a gain. The remainder of Section 3 presents the numerical application of the control/display design procedures to the CH-47 helicopter. Six flight conditions were evaluated:

- Hover
- 3° Straight Approach
- 9° Straight Approach
- 15° Straight Approach
- Spiral Approach
- Cruise

Eight control systems were designed, ranging from fully manual to automatic; and four flight director combinations were examined.

Section 4 returns to the main issue of evaluating the candidate display/control configurations. The control system and flight directors designed in Section 3 for the CH-47 helicopter are evaluated via the methodology described in Section 2. The resulting control performance and workload metrics are determined for all the candidate systems at the most difficult flight condition-hover. These hover results reveal that many of the display/control configurations cannot achieve the desired control performance, and several others are only marginal in terms of the available workload for monitoring. The remaining configurations are analyzed further in terms of their monitoring performance and other characteristics. These results are evaluated and three systems are identified as potential candidates for experimental analysis.

In Section 5, the recommended display/control configurations are used to generate display formats according to established design guidelines. The process of translating the analytical model results into display formats is described and subjective decisions are explained.

The final section of the report presents a summary of the important conclusions obtained during the study, and several recommendations for additional research. Topics deserving further analysis are delineated, and suggested experimental investigations (ground based and inflight) are outlined.

A list of references cited in the text is followed by an appendix which contains detailed numerical results for one of the leading candidate control/display systems.

SECTION 2

VTOL DISPLAY/CONTROL SYSTEM EVALUATION

Efficient evaluation of candidate pilot-vehicle control/display systems is best accomplished via a balanced program of modeling and experimentation. The modeling effort provides maximum advantage in the preliminary stages, where a wide variety of potential systems can be explored and rank-ordered with a relatively small amount of effort and cost. The experimental programs, which would normally include both ground-based and in-flight tests, study the more promising systems in realistic settings. These detailed man-in-the-loop simulations should tend to confirm the model-based predictions, and resolve the minor details between competing control/display systems.

2.1 A MODEL-BASED APPROACH FOR SYSTEM EVALUATION

The VTOL display/control design and evaluation procedure developed and utilized in this study is shown in Figure 1. There are four major phases in this process:

1. Formulation and information requirements
2. Control/monitoring performance
3. Pilot/automatic task allocation
4. Display format design

Each of these phases consists of one or more steps, as outlined in Table 1, and discussed below.

2.1.1 FORMULATION AND INFORMATION REQUIREMENTS

Performance requirements, and the design (or selection) of candidate control display systems are the objectives of the information requirements category. The steps are as follows.

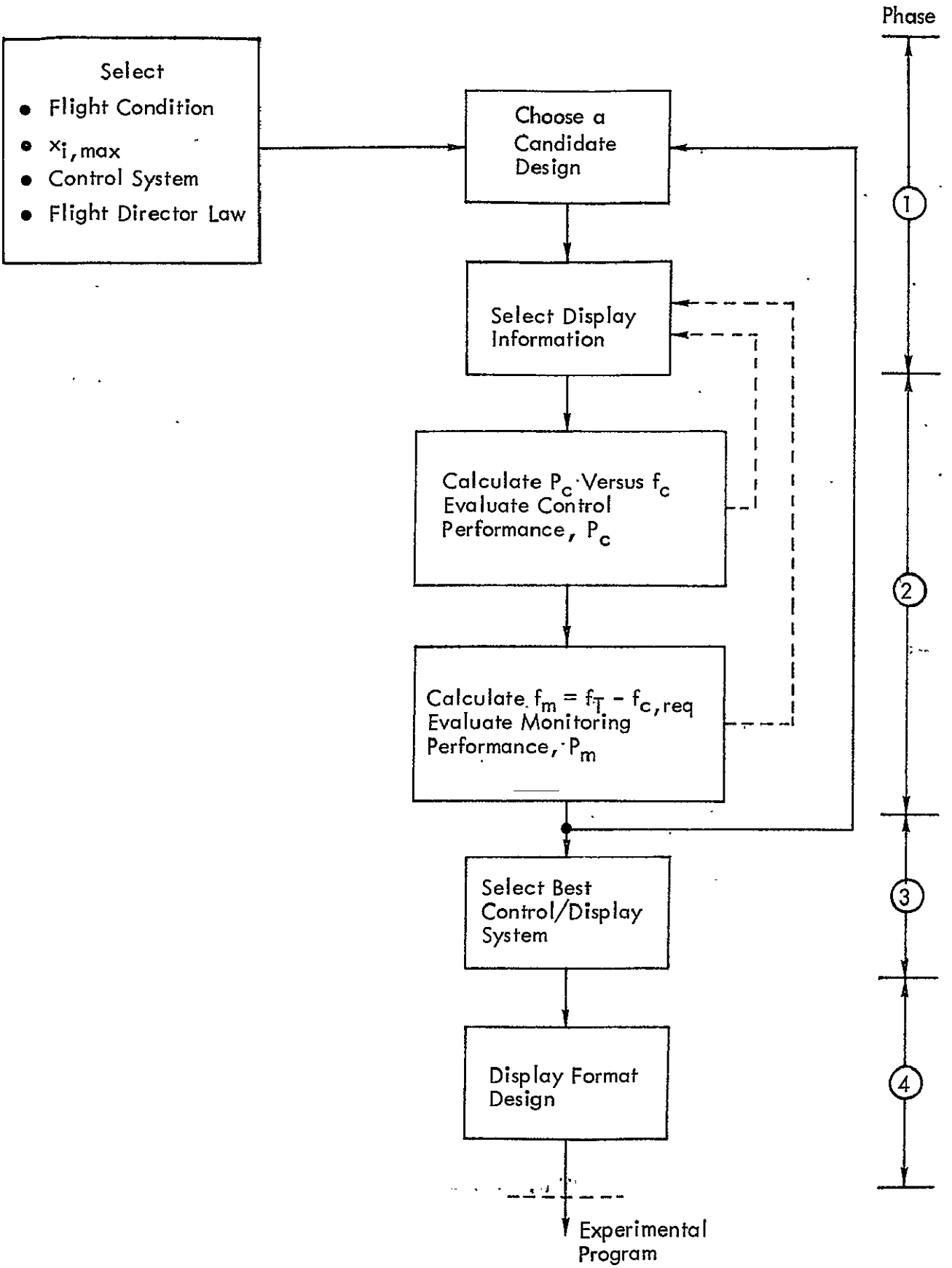

Figure 1. VTOL System Evaluation Process.

Table 1. VTOL System Evaluation Process.

Phase	Step
1. Formulation and Information Requirements	1. Determine Maximum Value of x_i 2. Select Candidate Control Systems 3. Select Flight Director Signals 4. Select Display Information
2. Control and Monitoring	5. Predict Control Performance 6. Predict Monitoring Performance
3. Pilot versus Automatic Task Allocation	7. Select Control/Display System
4. Display Format Design	8. Suggest Display Format

Step 1. Determine Maximum Value of x_i

The maximum deviations of the system states are selected according to flight condition requirements, pilot acceptance criteria, and passenger acceptance criteria. These maximum values of x_i will be used in subsequent phases of the design process, including flight director design, pilot modeling and performance evaluation. Under a Gaussian assumption, the $x_{i,max}$ can be interpreted conveniently as either 1σ, 2σ or 3σ values for the underlying time history $x_i(t)$. However, it is necessary to be consistent in this interpretation throughout the design process. We choose the 1σ interpretation for the numerical analysis of the CH-47. Thus, the design objective is for $|x_i(t)| \leq x_{i,max}$ with 0.68 probability, or about two-thirds of the time. This will occur when the standard deviation $\sigma_{x_i} \leq x_{i,max}$, so that selection of $x_{i,max}$ is equivalent to specifying desirable rms statistics for vehicle states. In the design process we select values $x_{i,max}$ for all vehicle states. If some states are not of concern from a performance viewpoint, we set those $x_{i,max} = \infty$.

Step 2. Select Candidate Control Systems

In this step, the candidate control systems that utilize different levels of augmentation are designed and/or selected. These levels of automation may span a wide range of possibilities from the unaugmented vehicle to complete position feedback (i.e., fully automatic control). Once a level of augmentation is selected, it is necessary to determine a feedback controller that realizes the system structure. Often, such a controller already exists from preceding or concommitent study efforts, or from ongoing flight control programs. If this is not the case, a candidate control system must be designed. The conceptual control system design procedure used for this study involves a blend of model-following and quadratic synthesis techniques. Subsection 3.1 describes the procedure.

Thus, through either selection or design, the outcome of this step of the procedure is a set of dynamics

$$\dot{x}(t) = A_0 x(t) + B_0 u(t) + E_0 w(t) \qquad (1)$$

that interact with the pilot via control inputs u(t), and with the environment via gust disturbances w(t).

Step 3. Select Flight Director Signals

This step considers the process of display automation through selection of flight director signals, or steering commands, that would be displayed to the pilot in addition to other information. For a candidate automation level and control system, as selected in Step 2, the flight director signals can be designed to improve pilot-vehicle performance through optimization of the display interface. Clearly, pilot-vehicle modeling plays a large part in this design. The details of the flight director design procedure used for this study are described in Subsection 3.2.

Note that there is a tradeoff between Steps 2 and 3, i.e., between control and display automation. A flight director might significantly improve performance of a partially automated system, but would probably be unnecessary in a fully automated context where the pilot is not actively involved in control.

Step 4. Select Display Information

This is the key step in the information requirements category. In selecting display elements we choose from among the measurable state variables $x_i(t)$ and the flight director signals of Step 3. In accordance with human response theory, it is assumed that if a variable $x(t)$ is displayed to the pilot then he also derives explicitly the rate $\dot{x}(t)$. Thus, each display element, or indicator y_i provides two independent observations, y_i and $y_{i+1} = \dot{y}_i$. The full set of observations $y(t) = [y_1, y_2, \cdots y_{NY}]$ consists of (combinations of) vehicle states and possibly control inputs, and is conveniently written in the form

$$y(t) = C_0 x(t) + D_0 u(t) \tag{2}$$

At this point, there is no apparent need for a separate indicator of rate information, if position is already displayed. However, as shown in Figure 1, the selection of the $y_i(t)$ is part of an iterative design loop. The subsequent display system evaluation is used to evaluate the utility and importance of the existing information, and to indicate the usefulness of additional displays. The decision to add or delete an indicator is based on control and monitoring performance.

If the subsequent model-based predictions of control and monitoring performance are to be realistic, indifference thresholds† must be included on the displayed variables.

†These are not to be confused with visual thresholds, which presume a given display format. However, for well-designed displays, visual threshold $\ll$ indifference threshold.

The threshold a_i describes the range of values for $| y_i(t) | \leq a_i$ within which the pilot is less likely to apply corrective action. The a_i are selected as

$$a_i = \frac{1}{k} y_{i,max} \quad , \quad 2 \leq k \leq 4 \tag{3}$$

where, excepting the flight director signals, $D_o = 0$

$$y_{i,max} = \sum_j | c_{ij} | x_{j,max} \tag{4}$$

In Equation (3) we choose $k = 4$. Thus, the indifference threshold corresponds to approximately 25 percent of the desired standard deviation of the displayed variable.

2.1.2 CONTROL AND MONITORING PERFORMANCE

The previous phase dealt primarily with the control/display system definition. Once a system is defined, pilot-modeling techniques are applied to evaluate its performance. Regardless of the form of the pilot/vehicle model used to carry out the control/display design, it is essential that it have realistic and quantitative metrics for the following:

- Control performance, P_c
- Workload for control, f_c
- Monitoring performance, P_m
- Workload for monitoring, f_m

With measures for these four quantities, one can explore the tradeoffs between control and monitoring functions, and between augmentation systems and displays.

Step 5. Predict Control Performance

The control performance metric selected for this study is

$$P_c = \frac{1}{NX} \sum_i \sigma_{x_i}^2 / x_{i,max}^2 \qquad (5)$$

where σ_{x_i} is the standard deviation of state x_i, and the summation is taken over those states for which $x_{i,max} < \infty$. NX is the number of such states. Equation (5) is a relative weighting of the variances of individual components of the state vector, normalized by their desired maximum values. Thus, a system that is operating with each $\sigma_{x_i} \approx x_{i,max}$ will have a control performance $P_c \approx 1$. The scalar P_c provides a handy and useful measure of performance. However, when evaluating competing systems in greater depth, one ultimately compares each of the state components on a one-to-one basis, in addition to the measure P_c.†

The control workload metric is based on the fractional attention the pilot allocates among the various display indicators. It is assumed that a pilot distributes a total amount of attention, or workload;

$$f_T \approx 0.8 < 1.0 \qquad (6)$$

between the tasks of control and monitoring leaving about 20 percent of his capacity for other duties (e.g., communications). Let f_c and f_m denote, respectively, the control and monitoring attentions, or workloads. Thus,

$$f_c + f_m = f_T \qquad (7)$$

The attention allocated for control, f_c, is distributed among all of the display variables $y_1, y_2, \cdots y_{NY}$, where y_i and $y_{i+1} = \dot{y}_i$ (i = odd) are obtained from the same display indicator. If $f_{c_i} > 0$ is the attention allocated to y_i for control purposes, then

†A well-designed system will not allow some $x_i(t) \gg x_{i,max}$ while other states $x_j(t) \ll x_{j,max}$.

$$\sum_{i=odd} f_{c_i} = f_c \tag{8a}$$

$$f_{c_{i+1}} = f_{c_i} \qquad i = 1, 3, 5, \ldots \tag{8b}$$

The pilot allocates his attention among the displays, spending the larger f_{c_i} on displays that are most useful for control.

A pilot-vehicle model for predicting f_{c_i}, given a control workload level f_c, was one of the major undertakings in this study. The model is described briefly in Subsection 2.2; the details may be found in References 4 and 5. With f_{c_i} selected, the pilot-vehicle model yields predictions of closed-loop performance $\sigma^2_{x_i}$, $\sigma^2_{y_i}$ and the control performance metric, P_c. Using these model predictions, we can study the tradeoffs between f_c and P_c for any given automation level/display system. Figure 2 is a typical performance/workload curve. It shows the performance attained for a given workload, as well as the workload required to obtain a given performance level.

Step 6. Predict Monitoring Performance

This step applies the pilot-vehicle model for simultaneous monitoring and control to determine the monitoring workload, f_m, and monitoring performance, P_m. In the hierarchy of control and monitoring the pilot will first attend to the control task, and with any available attention remaining, will then attend to the monitoring task. To determine the control workload requirements, we must specify a maximum level of control performance, $P_{c,max}$, consistent with the mission objectives. We choose

$$P_{c,max} = 1.0 \tag{9}$$

which corresponds (approximately) to the limiting case $\sigma_{x_i} \approx x_{i,max}$. In Figure 2, the intersection of the line $P_c = P_{c,max}$ with the P_c versus f_c curve gives the minimum

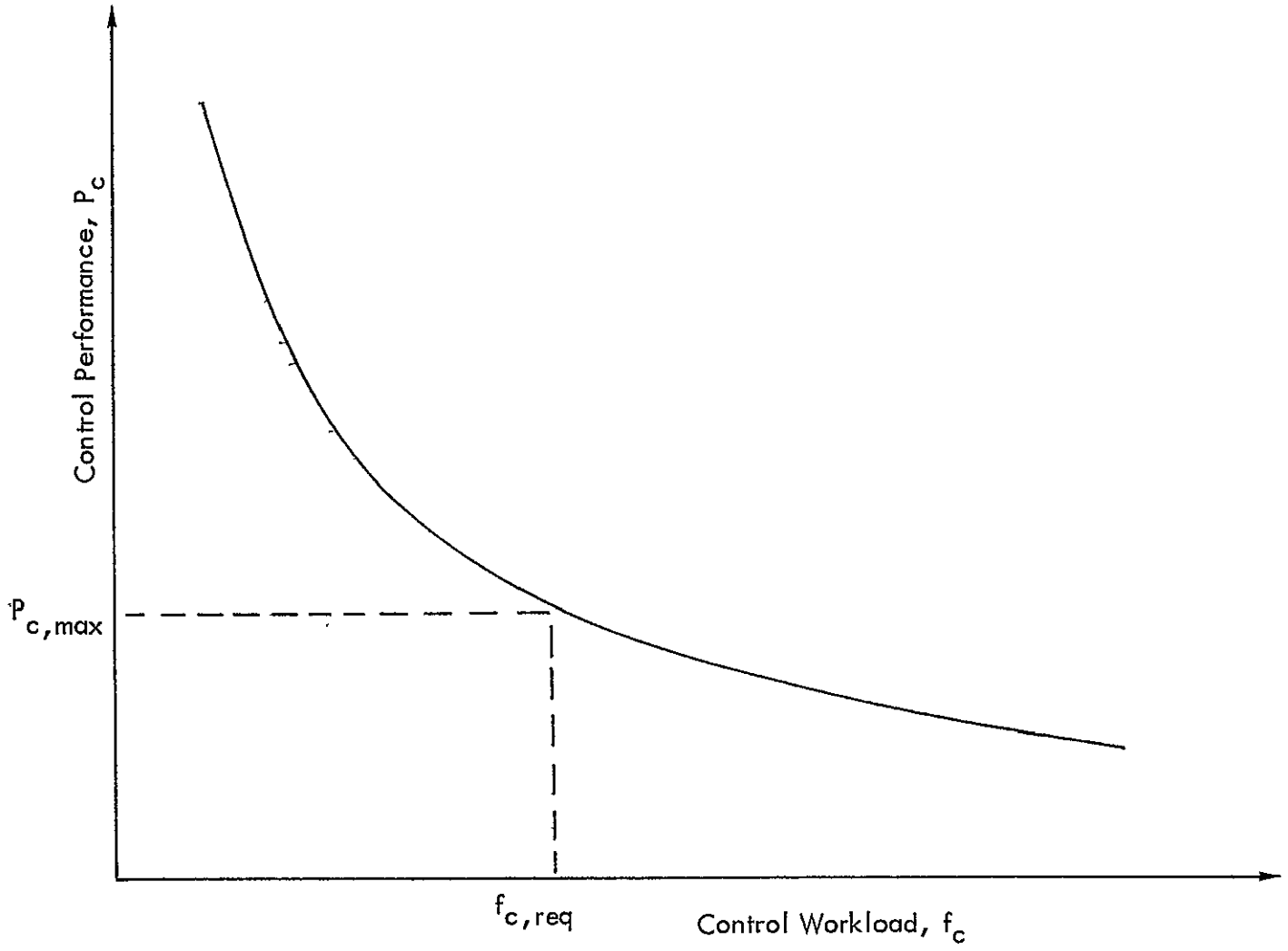

Figure 2. Conceptual Control Performance Versus Workload Curve.

amount of control attention required, $f_{c,req}$, for the given system to meet P_c specifications.† The difference between this amount of attention, and the total available for the entire task is the residual workload available for monitoring

$$f_{m,avail} = f_T - f_{c,req} \tag{10}$$

The fraction of attention f_m, available for monitoring is next applied as an input parameter to the model for pilot display monitoring (Subsection 2.3). This model assumes that the pilot distributes f_m among a subset of the display variables that excludes the flight director signals. Thus, only primary status instruments are explicitly monitored. If $f_{m_i} \geq 0$ is the attention allocated to y_i for monitoring purposes

$$\sum_{i=odd} f_{m_i} = f_m \tag{11a}$$

$$f_{m_{i+1}} = f_{m_i} \qquad i = 1, 3, \ldots \tag{11b}$$

and $f_{m_i} = 0$ for flight director signals.

The process by which a pilot selects the allocations f_{m_i} is not fully understood at present. While it is recognized that monitoring serves the dual role of status determination and failure detection, the relative weighting of these factors is unknown, and probably highly subjective. These issues are investigated from a modeling viewpoint in References 4 and 6. The model we are presently using to give predictions for f_{m_i} is based on status determination criteria, and is discussed in Subsection 2.3.

The monitoring performance metric P_m that has been selected is

$$P_m = \left(\frac{1}{NI} \sum_{i=odd} \frac{\sigma_{e_i}^2}{\sigma_{y_i}^2} \right)^{1/2} \tag{12}$$

†A slight modification of this approach would be to find $f_{c,req}$ such that $\underline{\text{all}}\ \sigma_{x_i} \leq x_{i,max}$.

where σ_{e_i} = standard deviation in the pilot's estimation error for signal y_i. The summation in Equation (12) is taken only over the NI displacements of status variables (i.e., indicator positions) and not their rates. Thus, with the help of the monitoring model, the results of this step are the monitoring workload f_m and the value of P_m that results from the model's choice of f_{m_i}. In the process of computing either the f_{c_i} or the f_{m_i}, a rank-ordering of the relative importance of each display variable will be obtained. This information is used in an iterative manner to add and/or delete display indicators in Step 4, as shown in Figure 1.

2.1.3 PILOT VERSUS AUTOMATIC TASK ALLOCATION

The process of selecting control/display configurations from among the candidate systems is based on the results of Steps 5 and 6. There are as many candidate systems as there are levels of automation times the number of flight director options. For each of these systems the J_c versus f_c trade-off curve is plotted and used to determine

1. $f_{c,req}$ to achieve $P_{c,max} = 1$
2. $f_{m,avail} = f_T - f_{c,req}$
3. P_m for cases in which $f_{m,avail} > 0$

This information is used in Step 7 of the procedure.

Step 7. Select Control/Display System

Criteria for choosing one or more systems, and thus allocating tasks between the pilot and automation should be based on the following criteria.

- The workload required for control, $f_{c,req} \leq 0.8$. Thus, all systems will be compared at the same level of control performance. This is in accordance with the basic assumption that pilot workload is first allocated to meet control specifications.

- Low sensitivity of performance to changes in f_c. To minimize the effects of pilot modeling errors on the performance predictions, the curves of P_c versus f_c should exhibit low sensitivity for $f_c \approx f_{c,req}$. Large changes in performance for common small changes in attention allocation (i.e., pilot variability) are undesirable.

- Effects of selected failure modes. A brief examination of certain system failure modes provides an indication of whether or not the system can continue to be controlled if either the display and/or control automation fails. We simply consider the change in $f_{c,req}$ in going from the given system to one of lower display automation (i.e., no flight directors), or less control automation.

- Monitoring performance. The monitoring metric, J_m, and the individual components σ_e/σ_y, can be used to give a comparison of monitoring performance for the proposed systems. Candidate systems are compared on a relative basis, and on an absolute scale with

$$J_{m,des} = 0.4 \tag{13}$$

  This corresponds, on the average, to $|e(t)| < 0.5\,|y(t)|$ for 80 percent of the time. (See Section 2.3.3.)

- Cost versus complexity. With a variety of systems compared on a common basis, the effects of additional levels of automation become evident vis-a-vis system performance. In some cases increased automation may yield only minor improvement over a less automated system. Thus, points of diminishing return might be identified.

The output of this step is the end result of the modeling process. Any further studies of the one or more selected systems become the objective of ground-based and/or flight tests.

2.1.4 DISPLAY FORMAT DESIGN

Step 8. Suggest Display Format

The process of going from the analytic design of a control/display system to its implementation for simulation tests requires the selection of a display panel that contains the information base y(t). The choice of display format is really an art, combining separated displays, perspective displays, clustered displays, analog versus digital

displays, etc., in a manner that provides maximum information to the pilot. There are, however, several guidelines for this process. The display should have the following attributes:

- Operator centered and oriented cues
- Geometric "real-world" compatibility
- Naturalness (for high stress situations)
- "Status at a glance" for situation displays
- Predictive capability for situation displays
- Compactness
- Lack of clutter

In addition to these considerations, operational guidelines should be used that include failure mode considerations, display operations (e.g., change in scale), and flexibility in trajectory selection.

The display format that is selected and ultimately mechanized must be consistent with the assumptions in the modeling phase if experimental results are to be comparable with the model predictions. For example, display visual thresholds should not exceed the assumed indifference thresholds of Equation (3). Naturally, one should expect control performance to degrade somewhat due to the practical aspects of implementing the display information. These would include display markings, display bandwidth and filtering, acuity and resolution, quantization, refresh rate, etc. These factors tend to increase information uncertainty, and can be counteracted somewhat by increased pilot attention or workload. If the control/display system selected in Step 7 exhibits low sensitivity to changes in f_c, one might conjecture that slight degradations in display quality should have only a minor effect upon P_c.

A decision whether or not to include an automatic performance assessment and failure monitor for a given operational scenario could be made at this step. If $f_{c,req} \approx f_T$, then little if any margin is available for unexpected distractions or for monitoring, and an independent monitoring system might be necessary to achieve a desired degree of pilot acceptance and confidence.

2.2 OPTIMAL CONTROL MODEL OF PILOT RESPONSE

Pilot modeling techniques are central to our analytical approach for system evaluation. A pilot model is needed to give predictions of closed-loop pilot/vehicle performance for a given workload, f_c, and to rank-order the usefulness of the displayed information. We have selected the optimal control model (OCM) of human response for use in the evaluation process. This model, shown in Figure 3, is perhaps the most general and most versatile representation of human response that has been developed to date. It has been applied across a variety of manual control tasks, and is capable of treating single-axis and multi-variable systems within a single conceptual framework using modern control-theoretic techniques. The modeling approach is based on the assumption that the well-trained pilot behaves in an optimal manner subject to his inherent limitations and the task requirements. As the OCM is well documented in the literature (References 7 - 10), only the primary features of the model are presented below.

2.2.1 VEHICLE/DISPLAY DYNAMICS

The system dynamics, which also include any augmented modeling or noise shaping states, are assumed to be described by the linearized equations

$$\dot{x}(t) = A_0 x(t) + B_0 u(t) + E_0 w(t) \qquad (14)$$

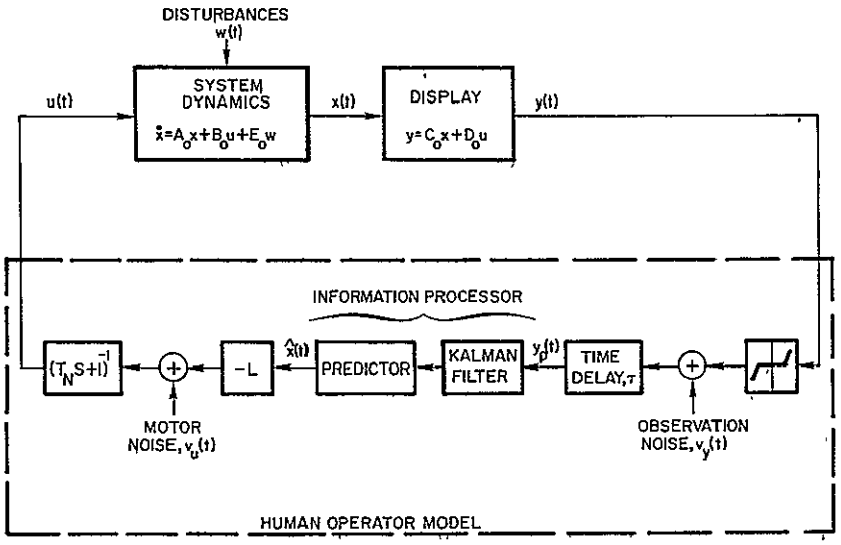

Figure 3. Optimal Control Model of Human Response.

Here, x(t) is the system state vector, u(t) are the NU pilot-generated corrective control inputs, and w(t) is a Gaussian white-noise process for modeling external disturbances (e.g., wind) and has covariance

$$E\{w(t)w'(\sigma)\} = W\delta(t-\sigma) \tag{15}$$

The pilot observes a set of NY displayed outputs that is related linearly to the system state and control,

$$y(t) = C_0x(t) + D_0u(t) \tag{16}$$

The usual assumption in the OCM is that y(t) contains both the position and velocity information of each displayed signal, but no higher derivative information. Thus, for convenience, we assume y(t) is ordered in position-velocity pairs with

$$y_{i+1}(t) = \dot{y}_i(t) \qquad i = 1, 3, \ldots NY-1 \tag{17}$$

2.2.2 HUMAN LIMITATIONS

The detailed description of the human's inherent psychophysical limitations,

and his resulting compensation or equalization is the essence of the OCM. The major performance degrading limitations are the following.

1. Time-delay: The various internal delays associated with visual, control processing and neuromotor pathways are combined into an "equivalent" perceptual time-delay τ. Nominally, $\tau = 0.2 \pm 0.05$sec.

2. Randomness: "Observation" noise and "motor" noise are lumped representations of controller central processing and sensory randomness. These noises represent the combined effects of random perturbations in human response characteristics, time variations in response parameters, and random errors in observing system outputs and generating system inputs.

   In the optimal control model an equivalent "observation" noise $v_{y_i}(t)$ is associated with each display variable $y_i(t)$. These noises are independent, Gaussian white-noise processes with covariances

$$E\{v_{y_i}(t)\, v_{y_i}(\tau)\} = V_{y_i}\delta(t-\tau) \tag{18}$$

   It has been determined (Reference 11) that the covariance V_{y_i} scales with the variance of the signal to which it is associated, i.e.,

$$V_{y_i} = \rho^{o}_{y_i}\sigma^{2}_{y_i} \tag{19}$$

   The noise/signal ratios $\rho^{o}_{y_i}$ depend on the relevant features of the display, the external environment, and the level of human training, among numerous other factors. However, the $\rho^{o}_{y_i}$ are generally independent of the system dynamics being controlled and for single high resolution displays

$$\rho^{o}_{y_i} \approx 0.01\pi \text{ (i.e., -20.dB noise/signal ratio)}$$

3. Attentional Allocation: When there is more than one display indicator, the human must allocate his attention among the various displays. If there are NY sources of information, and f_c denotes the total attention to the control task, then, since position-velocity pairs are obtained with no interference,

$$\frac{1}{2}\sum_{i=1}^{NY} f_{c_i} = f_c\,;\ 0 \le f_{c_i} \le f_c \tag{20}$$

where f_{c_i} denotes the pilot's attentional allocation to output i. In the optimal control model, the effect of attention sharing is to increase the noise/signal ratio from $\rho^o_{y_i}$ to

$$\rho_{y_i} = \rho^o_{y_i}/f_{c_i} \tag{21}$$

where $\rho^o_{y_i}$ is the noise/signal ratio that corresponds to full attention (References 12 and 13). The human is assumed to choose the f_{c_i} to "optimize" his information base vis-a-vis the control requirements. This attentional allocation problem has been solved as part of the present research effort.

4. Nonlinear Effects: If a particular signal y_i is very small in magnitude, a human may not be capable of detecting its non-zero value (visual threshold). Alternatively, and more importantly, he may choose not to react to small perturbations (indifference threshold). These threshold phenomena represent human nonlinear small signal characteristics. Specifically, if a signal y is displayed, the human will react to a signal y' given by

$$y' = f[y] = \begin{cases} y - a & y \geq a \\ 0 & |y| < a \\ y + a & y \leq -a \end{cases} \tag{22}$$

where a is the threshold level. Values for indifference thresholds are selected on the basis of the task requirements.

The total signal y_p that is perceived by the human must reflect the time-delay and observation noise limitations discussed above. Thus, the human perceives the delayed, noisy quantities,

$$y_{p_i}(t) = f[y_i(t - \tau)] + v_{y_i}(t - \tau) \tag{23}$$

As shown in Figure 3, it is the signal y_p that is "processed" internally by the human to yield a commanded control u_c. Random input describing function theory is used to model the effect of the nonlinearity as an increase in the observation noise according to

$$V_{y_i} = \frac{\rho_{y_i}}{N_i^2}\sigma^2_{y_i} \tag{24}$$

The "gain" $N_i(\sigma_{y_i}, a_i)$ is a function of a_i and σ_{y_i} (Reference 9).

5. Neuromotor Dynamics: Because of central processing and neuromuscular dynamics there is a lag between the internally generated "commanded" control and the actual control input generated by the human. The neuromotor dynamics are modeled† by a first order system

$$T_N \dot{u} + u = u_c \tag{25}$$

with minimum time-constants $(\tau_N)_{ii} \approx 0.1 \pm 0.02$ sec.

6. Motor Noise: The motor noise $v_u(t)$ is the second component of modeled human randomness. This noise is used to represent the effects of random errors in executing intended control movements (e.g., tremor) or the fact that the human does not have perfect knowledge of the system input u(t) because of "noisy" proprioceptive feedback channels. The motor noise is added to $u_c(t)$. Thus

$$T_N \dot{u} + u = u_c(t) + v_u(t) \tag{26}$$

The noises $v_u(t)$ are assumed to be white Gaussian processes with covariances V_{u_i} that scale with the control variances,

$$V_{u_i} = \rho^o_{u_i} \cdot \sigma^2_{u_i} \tag{27}$$

In most applications of the optimal control model to date, $\rho^o_{u_i} \approx 0.003\pi$ (i.e., -25 dB noise/signal ratio).

2.2.3 CONTROL TASK REPRESENTATION

In the optimal control model it is assumed that the control task is adequately reflected in the human's choice of control input and attention allocation that minimizes the quadratic cost functional

$$J_c(u, f) = \sum_{i=1}^{NY} q_{y_i} \sigma^2_{y_i} + \sum_{i=1}^{NU} q_{\dot{u}_i} \sigma^2_{\dot{u}_i} \tag{28}$$

conditioned on the perceived information y_p. The cost functional weighting parameters q_{y_i} and $q_{\dot{u}_i}$ may be either objective (specified by the experimenter or designer) or

†The modeling is not done directly, but rather indirectly via cost functional weightings on control rate (see Subsection 2.2.3).

subjective (adopted by the human in performing and relating to the task). Clearly, the selection of any subjective weightings is a non-trivial matter and is tantamount to mathematically quantifying the human's objective task requirements and his subjective performance criteria. One intuitively appealing method that has been found useful for selecting estimates for q_{y_i} is

$$q_{y_i} = \left| \frac{1}{y_{i,max}} \right|^2 \tag{29}$$

where $y_{i,max}$ is the (maximum or) desired value of y_i. Values of $y_{i,max}$ can be obtained most easily from the system specifications $x_{i,max}$ as in Equation (4), or could be elicited by pilot questionnaire. The values $y_{i,max}$ are also used to establish indifference thresholds a_i according to Equation (3).

The control rate weightings $q_{\dot{u}_i}$ are used to account for the pilot's limitation on the rate of control motion, and introduce first-order "neuromotor" dynamics in the OCM. The time constants $(\tau_N)_{ii}$ vary monotonically with the control rate weightings $q_{\dot{u}_i}$. The process of selecting values for $q_{\dot{u}_i}$ follows that for q_{y_i}, viz,

$$q_{\dot{u}_i} = \left| \frac{1}{\dot{u}_{i,max}} \right|^2 \tag{30}$$

where $\dot{u}_{i,max}$ is the (maximum or) desired rate that a human can or will manipulate control u_i. A lower bound to $q_{\dot{u}_i}$ is provided by the lower bound on $(\tau_N)_{ii} > 0.1 \pm 0.02$ sec, to be consistent with observed human limitations.

2.2.4 HUMAN EQUALIZATION

Within the postulated framework, the human's control characteristics are determined by minimizing $J_c(u, f_c)$ with respect to u (or u_c) and f_c. The commanded control that minimizes J_c is generated by the feedback law

$$u_c(t) = -L\hat{x}(t) \tag{31}$$

where $\hat{x}(t)$ is the "human's" best estimate of the system state $x(t)$ based on the perceived information $y_p(\sigma)$, $\sigma \leq t$. The gains L (and time constants T_N) are functions of only the system/display dynamics and the weightings q_{y_i} and $q_{\dot{u}_i}$. These gains are not dependent on the f_{c_i}.

The best estimate of $x(t)$ is generated in the OCM by the cascade combination of a Kalman filter and a least-mean-squared error predictor. The Kalman filter compensates optimally for the human's observation noise to generate a best estimate $p(t)$ of the delayed state $x(t - \tau)$ and control $u(t - \tau)$, via,

$$\dot{p}(t) = Ap(t) + Bu_c(t) + G[y_p(t) - C(t)] \tag{32}$$

The augmented matrices A, B are

$$A = \left[\begin{array}{c|c} A_0 & B_0 \\ \hline 0 & -T_N^{-1} \end{array}\right] ; \quad B = \begin{bmatrix} 0 \\ \hline T_N^{-1} \end{bmatrix} \tag{33}$$

and $C = [C_0 \mid D_0]$. The filter gain $G = \Sigma C' V_y^{-1}$, where Σ is the estimation error covariance matrix.

The predictor compensates optimally for the human's inherent time delay τ and generates from $p(t)$ the prediction of $x(t)$:

$$\begin{bmatrix} \hat{x}(t) \\ \hat{u}(t) \end{bmatrix} = e^{A\tau} p(t) + \int_{t-\tau}^{t} e^{A(t-\sigma)} B u_c(\sigma)\, d\sigma \tag{34}$$

Thus, the human's equalization, as shown in Figure 3, is modeled as consisting of an optimal filter-predictor combination (information processor), followed by a set of optimal gains. The detailed equations for the OCM sub-blocks may be found in References 4 - 11.

2.2.5 ATTENTION ALLOCATION USING THE OCM

The choice of f_{c_i} to minimize the cost functional $J_c(u, f_c)$ is the optimal attention allocation problem in manual control. In the OCM, the f_{c_i} affect the state estimate $\hat{x}(t)$. Thus, the attentional allocation problem may be viewed as optimizing the information base via-a-vis the control requirements. The solution of this problem was part of the research effort, and represented an important extension to the optimal control model. There are three steps in the solution process.

1. Obtain an expression for

$$J_c^*(f_c) = \min_u J_c(u, f_c) \tag{35}$$

that shows explicitly how the f_{c_i} affect the various cost functional terms.

2. Obtain an expression for the gradient terms $\partial J_c^*/\partial f_{c_i}$.
3. Develop a gradient algorithm to minimize J_c^*, subject to the total workload constraints on f_{c_i}.

In the OCM, the fractional attentions f_{c_i} modify the observation noise covariances according to

$$V_{y_i} = \frac{\rho_i^o}{f_{c_i}} \left[\frac{\sigma_{y_i}}{N(a_i, \sigma_{y_i})} \right]^2 \tag{36}$$

Note that this equation represents an implicit relationship for the actual noise variance since σ_{y_i} is itself a function of V_{y_i}, $i = 1, \ldots, NY$. Thus, since changes in f_{c_i} are reflected as changes in the observation noises, we first obtain an expression for J_c^* that isolates the V_y terms. From Reference 4 the result is

$$J_c^*(V_y) = \text{tr}[L_e \Sigma(V_y) L_e'] + \text{terms independent of } V_y \tag{37}$$

where L_e is an "equivalent" gain and Σ is the error covariance matrix for the estimate p(t). Σ is functionally dependent on the noise covariance V_y through the solution of a matrix Riccati equation.

Minimizing J_c^* with respect to f_{c_i} is a difficult nonlinear optimization problem. The difficulty is two-fold. First, f_{c_i} affects V_y in an implicit manner, and second, V_y affects J_c^* through the Riccati solution Σ. In order that the numerical process of minimizing J_c^* proceed efficiently, it is desirable to obtain closed-form expressions for the gradients $\partial J_c^*/\partial f_{c_i}$ and $\partial J_c^*/\partial V_{y_i}$. Thus, the time-consuming process of numerically evaluating these derivatives can be avoided. In References 4 and 5 it is shown that

$$g_f = \frac{\partial J_c^*}{\partial f_c} = \Gamma' \frac{\partial J^*}{\partial V_y} \tag{38}$$

where Γ is a "transformation" matrix with elements

$$(\Gamma)_{ij} = \frac{\partial V_{y_i}}{\partial f_{c_j}} \tag{39}$$

It is approximately diagonal with $(\Gamma)_{ii} = \dfrac{\partial V_{y_i}}{\partial f_{c_i}}$

The gradient vector $\partial J_c^*/\partial V_y$ is given by

$$\frac{\partial J_c^*}{\partial V_{y_i}} = \left(G' \int_0^\infty e^{\hat{A}'\sigma} L_e' L_e e^{\hat{A}\sigma} \, d\sigma \, G \right)_{ii} \tag{40}$$

where G is the Kalman filter gain matrix, and $\hat{A} = A - GC$ is the "closed-loop" filter matrix.

The gradient g_f in Equation (38) is the unconstrained gradient vector. However, the attentional allocations are not free but are constrained by

$$\frac{1}{2}\sum_{i=1}^{NY} f_{c_i} = f_c \tag{41a}$$

$$f_{c_{i+1}} = f_{c_i} \qquad i = 1, 3, \ldots, NY - 1 \tag{41b}$$

The projection of g_f on the constraint surface, Equation (41a), is given by

$$(g_f^p)_i = (g_f)_i - \frac{1}{NY}\sum_{i=1}^{NY} (g_f)_i$$

In other words, g_f^p is obtained by subtracting the average of $(g_f)_i$ from each element. The secondary projection of g_f^p on the constraints, Equation (41b), is accomplished by the replacements

$$(g_f^p)_i = (g_f^p)_{i+1} \leftarrow \frac{1}{2}\left[(g_f^p)_i + (g_f^p)_{i+1}\right] \tag{42}$$

This final gradient vector can be used in any standard gradient optimization algorithm, with the assurance that successive iterates f_c^n, f_c^{n+1}, etc., will satisfy the constraint Equation (41). One final constraint

$$f_{c_i} \geq 0.01 \tag{43}$$

is added to avoid numerical problems, and to assure that no display indicator goes without attention. The resulting extremal point f_c^* gives a prediction of the pilot's attentional allocation, and in turn is used to obtain the performance predictions σ_{y_i}.

The OCM, with the above attention allocation scheme, was applied to study the hover control of the CH-46C. The details of this effort, which served to validate the model, are given in References 4 and 5. Briefly, the automation levels were pitch and roll commands and heading hold. Pilot performance was studied with and without flight director signals. The conclusions of the modeling effort indicated that:

- Hovering over a 25 ft radius pad could not be accomplished satisfactorily using the status displays only.
- The flight directors make hovering possible with high workload. Levels of $f_c \approx 0.7 - 0.8$ are required to maintain the aircraft over the pad 80 - 85 percent of the time.
- Virtually full control attention f_{c_i} is given to the flight director instruments.
- There is little or no remaining pilot capacity $f_m = f_T - f_{c,req}$ with which to monitor the status instruments.

These conclusions, derived via an analytic modeling approach, are in general agreement with those from the flight tests reported in References 14 and 15.

2.2.6 USE OF THE OCM

In order to use the optimal control model to predict closed-loop performance for a given system, it is necessary to first specify the cost functional weightings q_{y_i} in terms of the task requirements. Values for q_{u_i} are next estimated from maximum human control rates, but such that $(\tau_N)_{ii}$ is not less than 0.1 ± 0.02 sec. Reasonable a priori values for the human response parameters τ, $\rho^o_{y_i}$, $\rho^o_{u_i}$ are available from data in the manual control literature, and from past experience using the OCM. For prediction purposes $\tau = 0.2$ sec, $\rho^o_{y_i} = -20$ dB, $\rho^o_{u_i} = -25$ dB. Values for the indifference thresholds are selected according to

$$a_i = \frac{1}{4} \left| y_{i,max} \right| \tag{44}$$

Once the model inputs are chosen, and a value for f_c is picked, numerous quantities can be obtained from the OCM that predict different facets of pilot response. These include

1. rms statistical measures. The closed-loop σ_{x_i}, σ_{u_i}, and σ_{y_i} are primary model results and are needed to evaluate the pilot/vehicle control performance P_c. The covariance matrix X of the augmented state $\chi = [x, u]'$ is computed, as is the output covariance matrix $Y = CXC'$. Finally we obtain a prediction of the optimal (pilot) cost functional J_c, and the part $tr(L_e \Sigma L_e')$ due to the human's own randomness.

2. Attention allocation measures. The optimized f_{c_i} give the attention allocation to each of the NY observed outputs, and the various display indicators. The elements $(g_f)_i$ of the unconstrained gradient give the relative incremental importance of each y_i. This shows whether position or rate information is of primary use from a given indicator.

3. Frequency domain measures. In time-invariant situations, model outputs include the power spectral density, PSD, of any system variables that show both input and pilot "remnant" related portions. Vehicle transfer functions and pilot describing functions give an indication of the form of human compensation, and can be used to compute crossover frequencies and phase margins.

2.3 CONTROL THEORETIC MODELS FOR DISPLAY MONITORING

The application of the optimal control model of human response yields predictions of pilot-vehicle control performance. The second step in the evaluation of a control/display system is the prediction of pilot monitoring response, and the use of a metric for assessing monitoring performance. In References 4 and 6 control theoretic models for pilot monitoring in the context of a fully automatic system were studied. The major conclusions of those efforts are summarized below. The extension of these ideas to the situation of simultaneous control and monitoring is presented in Subsection 2.4.

The pilot is assumed to monitor the automatic system

$$\dot{x}(t) = \bar{A}x(t) + Ew(t) \tag{45}$$

$$y(t) = Cx(t) \tag{46}$$

where $\bar{A}$ is the closed-loop matrix, containing the various feedback gains, etc. Following the assumptions as set forth in the OCM of human response, the pilot perceives the delayed, noisy signals

$$y_p(t) = y(t - \tau) + v_y(t - \tau) \tag{47}$$

The covariance V_{y_i} associated with $y_{p_i}(t)$ is

$$V_{y_i} = \frac{\rho_i^o}{f_{m_i}} \left[\frac{\sigma_{y_i}}{N(\sigma_{y_i}, a_i)} \right]^2 \tag{48}$$

where f_{m_i} is the fraction of monitoring attention allocated to y_i, and σ_{y_i} = rms value of y_i. Note that unlike the control case, σ_{y_i} is independent of V_{y_i} and/or f_{m_i}. The f_{m_i} are constrained by

$$\frac{1}{2} \sum_{i=1}^{NY} f_{m_i} = f_m = \text{monitoring workload} \tag{49a}$$

$$f_{m_{i+1}} = f_{m_i} \quad , \quad i = 1, 3, \ldots, NY - 1 \tag{49b}$$

The two major components of a monitoring model are the attentional allocation scheme (i.e., the manner in which the model allocates f_{m_i} among the various displays), and the monitoring performance metric J_m (i.e., the method by which monitoring performance is evaluated). A major conclusion of References 4 and 6 is that the two components should be combined by requiring that the f_{m_i} be chosen to minimize J_m subject to the constraints of Equation (49), and that each f_{m_i} be bounded away from zero to assure monitoring of all displays.

To establish suitable metrics for monitoring performance, we consider the basic role of the pilot as a display monitor. The monitoring task can be interpreted as having the two primary goals of 1) failure detection, and 2) status determination. The first goal is that of detecting automatic control system and/or instrument failures by cross-checking displays for consistency. The second goal is a statement of the

well-known fact that a pilot desires situation information to assess system status with respect to mission requirements. These goals provide two possible choices for a monitoring metric.

2.3.1 FAILURE DETECTION METRIC BASED MODEL

A general approach to failure detection is prohibitive due to the large numbers of failure possibilities. However, Gai and Curry (References 16 and 17) recently found that a decision model based on the residual of a Kalman filter provided an excellent descriptive model of the human's ability to detect additive (bias) failures in observed signals. In Reference 6 it is shown that the mean time to detect an additive failure on instrument i is

$$t_{D_i} = \gamma_i \frac{\sigma^2_{r_i}}{\sigma^2_{y_i}} \quad ; \quad i = 1, 3, \ldots, NY - 1 \tag{50}$$

where $\sigma^2_{r_i}$ is the unfailed residual covariance and γ_i is a constant that relates to the probability and magnitude of the failure. Consequently, minimizing the quantity

$$J_{m1} = \frac{2}{NY} \sum_{i=odd} t_{D_i} = \frac{2}{NY} \sum_{i=odd} \gamma_i \frac{\sigma^2_{r_i}}{\sigma^2_{y_i}} \tag{51}$$

with respect to f_{m_i} minimizes the average mean time to detect bias failures. Since $\sigma^2_{r_i} = V_{y_i}$ for an optimal Kalman filter, and V_{y_i} is given by Equation (48),

$$J_{m1} = \frac{2}{NY} \sum_{i=odd} \frac{\rho_i^o \gamma_i}{N^2(\sigma_{y_i}, a_i)} \cdot \frac{1}{f_{m_i}} \tag{52}$$

The optimum f_{m_i} are obviously

$$f_{m_i} = f_m/NY \qquad i = 1, 3, \ldots, NY - 1 \tag{53}$$

for cases in which $\gamma_i \approx \gamma_j$ and thresholds $a_i \approx 0$. This simple result has intuitive appeal: if each display is subject to the same type of failure, the best detection policy is to allocate attention equally.

2.3.2 ESTIMATION ERROR METRIC BASED MODEL

This approach suggests that a pilot's monitoring strategy is to pick the f_{m_i} to minimize some norm of the estimation error

$$e(t) = y(t) - C\hat{x}(t) \tag{54}$$

The monitoring metric suggested is

$$J_{m2} = \frac{2}{NY} \sum_{i=1}^{NY} \gamma_i \frac{\sigma^2_{e_i}}{\sigma^2_{y_i}} \tag{55}$$

where

$$\gamma_i = \begin{cases} 1 & i = \text{odd} \\ 0 & i = \text{even} \end{cases}$$

Thus only the position information on an instrument is of monitoring concern. We assume that the implicitly derived rates are not themselves monitored, but that their information is used to obtain better estimates of the explicitly presented display variables. In Reference 6 it was shown that in the special case of independent observations y_1, y_3, etc., the minimizing f_{m_i} agree precisely with the results of the Sender's sampling model, Reference 18, wherein f_{m_i} are proportional to signal bandwidth.

In the general case, minimizing J_{m2} with respect to f_{m_i} is similar to the control problem of minimizing J_c with respect to f_{c_i}. Noting that

$$J_{m2} = \frac{2}{NY} \text{ tr } (C_e \Sigma C_e') \tag{56}$$

where Σ = Kalman filter estimation error covariance matrix and

$$C_e = \text{diag}\left[\frac{\gamma_i}{\sigma_{y_i}}\right] \cdot C e^{A\tau} \tag{57}$$

the gradient terms are

$$(g_{fm})_i = \frac{\partial J_m 2}{\partial f_{m_i}} = -\frac{V_{y_i}}{f_{m_i}} \left[G' \int_0^\infty e^{\hat{A}'\sigma} C_e' C_e e^{\hat{A}\sigma} \, d\sigma \, G \right]_{ii} \tag{58}$$

where G is the filter gain and $\hat{A} = A - GC$ is the closed-loop filter matrix. Thus, the same gradient algorithm used to optimize J_c is easily applied to the monitoring problem. Note the similarity of Equation (56) with Equation (38). In the control case we seek to optimize the information base relative to L_e; in the monitoring case the weighting factor becomes C_e.

2.3.3 CHOICE OF MONITORING MODEL

It is likely that a pilot's monitoring strategy is a combination of the above two approaches. Thus, it might seem logical to consider a monitoring cost functional

$$J_m = c_1 J_{m1} + c_2 J_{m2} \tag{59}$$

where c_1 and c_2 are chosen to reflect the relative importance of estimation and (instrument) failure detection goals. However, there are no data presently available to help

make this choice, nor are there likely to be any soon. Consequently, recognizing that the first term prevents any $f_{m_i} \to 0$ because of terms proportional to $1/f_{m_i}$, we have selected to minimize

$$J_m = J_{m2} \tag{60}$$

subject to the constraints of Equation (49) and the additional constraint

$$f_{m_i} \geq 0.01 \tag{61}$$

Further interpretation of J_m as a monitoring cost functional is obtained by defining

$$k_i = \frac{\sigma_{e_i}}{\sigma_{y_i}} = \text{error fraction for variable } y_i \tag{62}$$

The error fractions are useful vis-a-vis the probabilities associated with estimation error criteria. If we define

$$E(\beta) = \Pr\{|e(t)| > \beta\sigma_y\} \tag{63}$$

as the probability that the estimation error exceeds a given fraction β of the signal rms then

$$E(\beta) = \frac{2}{\sqrt{\pi}} \int_{\beta/k\sqrt{2}}^{\infty} e^{-w^2}\, dw = \text{erfc}\left[\frac{\beta}{k\sqrt{2}}\right] \tag{64}$$

A reasonable performance level to expect in monitoring is $\beta = 1/2$, i.e., the estimation error should not exceed 0.5σ of the monitored variable. The probability (or percent of time) that this criterion is exceeded is $E(1/2)$, and varies monotonically with k. Figure 4 shows this relation. Note that in order for $E(1/2) < 0.2$ we require $k < 0.4$.

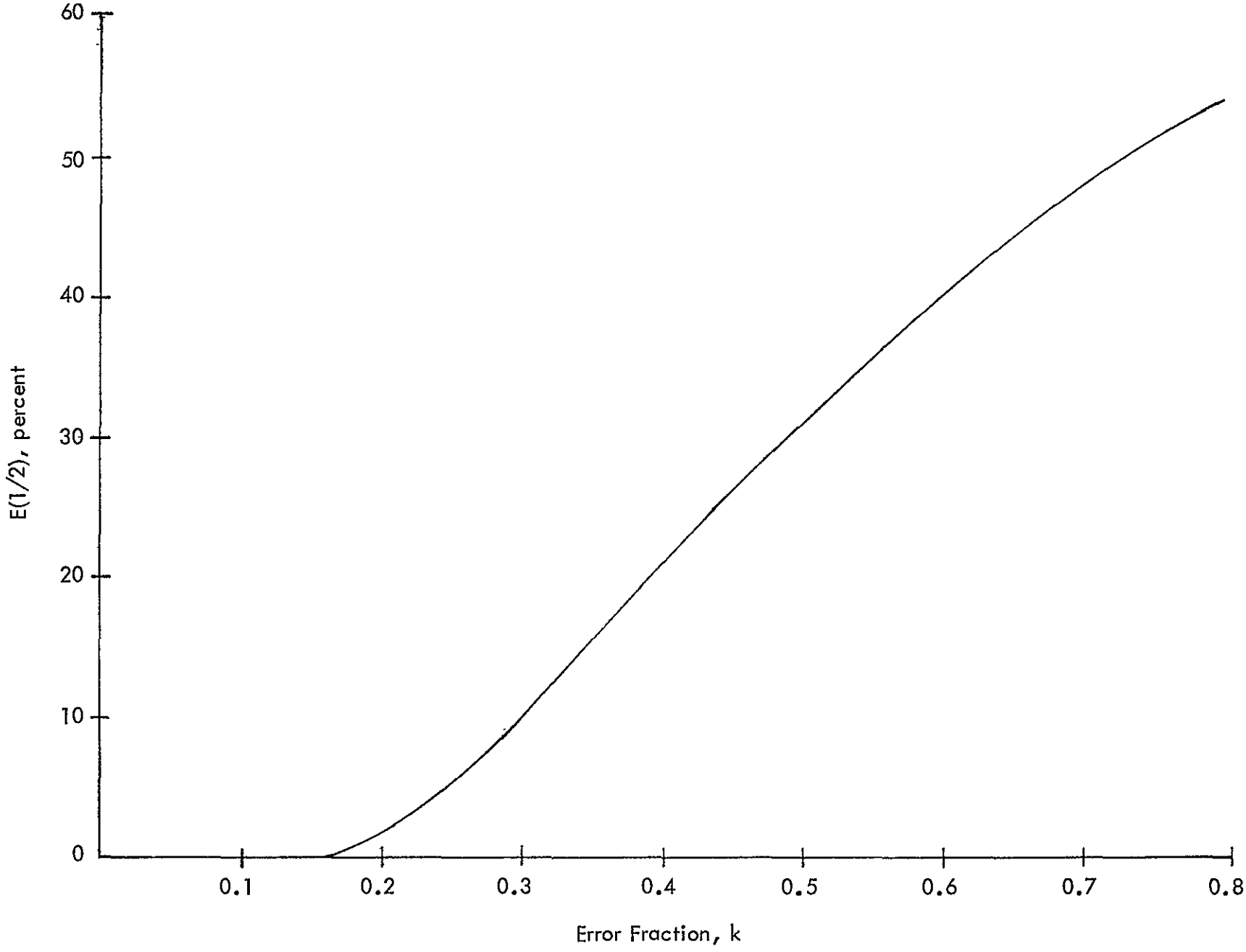

Figure 4. E(1/2) Dependence on Error Fraction.

The cost functional J_m is associated with the pilot's choice of f_{m_i}. There remains to be chosen a monitoring performance metric P_m as described in Step 5 of the design/evaluation process. In view of the above discussion, we select

$$P_m = \sqrt{J_m} = \text{rms error fraction} \tag{65}$$

with $P_{m,des} \leq 0.4$, although a complete evaluation of monitoring performance must ultimately consider each k_i.

2.4 SIMULTANEOUS MONITORING AND CONTROL

The above discussion is relevant to pilot monitoring for a completely automatic system. For the situation of semi-automatic control, our approach for determining control/display requirements was described in Subsection 2.1. For a given system configuration we determine the fraction of control attention $f_c \leq f_T$ that is required to achieve a desired performance level P_c. The excess capacity $f_m = f_T - f_c$ is then available for display monitoring. We prefer to follow this approach, in which control performance is established first, since it will limit our considerations to those systems that have realistic requirements at the initial stages of investigation. Thus, for systems in which $f_m > 0$, the objective is to determine how this monitoring workload is allocated, i.e., the f_{m_i} $i = 1, \ldots, NY$. Note that in this process, the f_{m_i} will depend on f_c (and the f_{c_i}), whereas the f_{c_i} are independent of f_m.

The constraints on the f_{m_i} are given by Equation (49). In the situation of simultaneous monitoring and control we assume no monitoring of flight directors, or other combined state information that is geared specifically to aircraft control.† Thus, for these instruments, $f_{m_i} = 0$, and for the other primary status displays we require $f_{m_i} \geq 0.01$.

†Of course this does not rule out cross-checking the flight director signals via monitoring of the status instruments.

The total attention that is allocated to a given displayed quantity is the sum of control and monitoring fractions,

$$f_{T_i} = f_{c_i} + f_{m_i} \tag{66}$$

However, in formulating a monitoring model it is necessary to decide what part of f_{T_i} is actually used for monitoring. This is equivalent to deciding whether or not f_{c_i} is used for monitoring, i.e., whether a display is implicitly monitored in the course of its use for vehicle control. This is not an easy decision, inasmuch as data to answer the questions are lacking. In fact, there are heuristic arguments to support either assumption 1) no f_{c_i} used for monitoring or 2) all f_{c_i} used for monitoring. We will let α (to be determined) be the fraction of f_{c_i} that is used implicitly for monitoring. Thus, the total attention to a display for monitoring is $\alpha f_{c_i} + f_{m_i}$, i.e., the sum of implicit plus explicit contributions.

The resulting monitoring model for the combined control/monitoring case now follows directly from Subsection 2.3 with the replacement $f_{m_i} \rightarrow \alpha f_{c_i} + f_{m_i}$. The f_{c_i} are fixed from the control allocation problem. The f_{m_i} are thus found by minimizing

$$J_m = \frac{\sum_i \gamma_i \sigma_{e_i}^2 / \sigma_{y_i}^2}{\sum_i \gamma_i} \tag{67}$$

where

$$\gamma_i = \begin{cases} 1 & i = \text{odd and a status instrument} \\ 0 & \text{if } y_i \text{ is a flight director signal} \\ 0 & i = \text{even} \end{cases}$$

The pilot monitoring observations for all instruments are

$$y_p(t) = C x(t - \tau) + \quad y(t - \tau) \tag{68}$$

where the observation noise covariances are

$$V_{y_i} = \frac{\rho_i^o}{\alpha f_{c_i} + f_{m_i}} \left[\frac{\sigma_{y_i}}{N(\sigma_{y_i}, a_i)} \right]^2 \quad ; \quad i = 1, 2, \ldots, NY \tag{69}$$

The gradient algorithm for optimizing J_m follows directly from the results of Subsection 2.3.

The value of α remains to be chosen. The choice $\alpha = 1$ is optimistic in the sense that all available control-directed information is used simultaneously for monitoring. This means that even if all $f_{m_i} = 0$, we would still have $\sigma_{e_i} < \sigma_{y_i}$, i.e., $k_i \leq 1$. The choice $\alpha = 1$ also implies use of the flight director signals for situation assessment. This may be an unrealistic conclusion. Furthermore, the choice $\alpha = 1$ may result in a low sensitivity of J_m with respect to f_{m_i}. The contribution of f_{m_i}, when added to f_{c_i}, may be "lost" if f_{c_i} is large. As a result, almost any reasonable monitoring strategy is likely to yield similar values for J_m.

On the other hand, the choice $\alpha = 0$ is pessimistic in that no implicit monitoring is assumed while controlling. In addition, no flight director information is used since $V_{y_i} \rightarrow \infty$ for these signals. Clearly, this is a worst-case design, and can result in $\sigma_{e_i} > \sigma_{y_i}$, i.e., larger errors than the signal itself! However, with $\alpha = 0$, J_m will show the greatest sensitivity to f_{m_i}, and thus might better establish the relative importance of the y_i for monitoring.

To explore this issue further, we consider the case of simultaneous monitoring and control of the CH-47 longitudinal dynamics at hover, with control system F and full flight directors.† Values $f_c = 0.4$ and $f_m = 0.3$ are chosen arbitrarily. The

†See Section 3.

Table 2. CH-47 Control Results, System F, $f_c = 0.4$.

Output	σ_{y_i}	f_{c_i}	a_i
x	2.9'	0.01	1.25
z	1.0'	0.01	1.25
θ	0.5°	0.03	0.25
FD_1	0.16	0.2	0.13
FD_2	0.18	0.15	0.11

optimal f_{c_i} and the resulting σ_{y_i} for the positional quantities only are given in Table 2. Also shown are the indifference thresholds. To see the effects of α, the monitoring model is exercised for several values of α between 0.0 and 1.0. Table 3 gives the results of this study.

Table 3. Monitoring Case Study Results.

$$J_m = \frac{1}{3}(k^2 + k_z^2 + k_\theta^2)$$

	$\alpha = 1.0$	$\alpha = 0.5$	$\alpha = 0.2$	$\alpha = 0.1$	$\alpha = 0.0$
$(J_m^*)^{1/2}$	0.404	0.476	0.55	0.583	0.625
$(J_m^\circ)^{1/2}$	0.407	0.492	0.59	0.647	0.726
$f_{m,x}$	0.09	0.08	0.08	0.075	0.075
$f_{m,z}$	0.15	0.18	0.19	0.20	0.20
$f_{m,\theta}$	0.06	0.04	0.03	0.025	0.025
k_x	0.28	0.33	0.39	0.42	0.45
k_z	0.50	0.59	0.68	0.72	0.77
k_θ	0.40	0.47	0.54	0.57	0.61
$k_{FD\theta}$	0.85	0.99	1.13	1.21	1.31
k_{FDz}	0.75	0.84	0.94	0.98	1.03

In view of the above comments, the results in Table 3 are as expected. Consider first the cost functional values J_m. The minimum value $(J_m^*)^{1/2}$ and the value $(J_m^o)^{1/2}$, corresponding to the initial (naive) guess $f_{m_i} = f_m/NY = 0.1$, are shown in Table 3. Optimizing J_m with respect to the f_{m_i} yields a mere 1 percent improvement with $\alpha = 1$. On the other hand, the greater sensitivity with respect to f_{m_i} is clear for $\alpha = 0$, where a 15 percent cost improvement is realized. The optimal monitoring attentions f_{m_i} show a surprising indifference to α. Over the range $0 < \alpha < 0.5$, the resulting f_{m_i} are well within limits that might be expected from intersubject differences.

All error fractions k_i increase with decreasing α. The relatively large k_i for z and θ is a reflection of the fact that σ_z and σ_θ are on the order of their indifference thresholds. No explicit monitoring attention f_{m_i} is placed on the two flight director signals FD_θ and FD_z. The k_i associated with these signals for $\alpha = 0$ is the error in estimating FD_θ and FD_z from the monitored status information x, z, θ. Thus, for this case, there is no effective crosschecking of the flight director signals and E(1/2) > 60 percent.

On the basis of the above discussion and test results, we have selected $\alpha = 0$ for use in the monitoring model. This represents a conservative worst case analysis, wherein J_m shows maximum sensitivity to f_{m_i}. Moreover, the results in Table 3 show that the optimal f_{m_i} for $\alpha = 0$ are not significantly different from those with $\alpha > 0$. Thus, we could place reasonable faith in the predictions of f_{m_i}, although monitoring performance $P_m = J_m^{1/2}$ may be pessimistic.

The one remaining aspect of the monitoring model is a scheme for finding the optimal f_{m_i} for the full aircraft system. To find the optimal f_{m_i} one could write a high-order state equation for combined lateral and longitudinal dynamics, and use the previous algorithm. But since these dynamics are independent, it is easier to treat the two axes separately and allocate the f_{m_i} by considering two "independent" monitoring

tasks. Let f_{mA} and J_{mA} denote the fractional monitoring attention, and monitoring cost, respectively, for the longitudinal axes. A similar definition is made for f_{mB} and J_{mB} for the lateral axes. Clearly,

$$f_{mA} + f_{mB} = f_{m,avail} \tag{70}$$

and if both axes have the same number of instruments to be monitored†,

$$J_m = \frac{1}{2}(J_{mA} + J_{mB}) \tag{71}$$

A one-dimensional search technique for optimizing J_m is suggested, as shown in Figure 5.

In the present effort we first specify reasonable f_{mA} and f_{mB}, and then omit the iterative search procedure. This reduces considerably the computational burden. The motivation for this approach is that the optimal J_m, arrived at via the scheme of Figure 5, is very insensitive to a f_{mA} versus f_{mB} inter-axis split. Increases in J_{mA} tend to be balanced by decreases in J_{mB} as f_{mA} and f_{mB} are varied. This same interaxis broadness was observed in the CH-46 control attentional allocation results reported in Reference 4. Thus, we can expect that a reasonable choice of f_{mA} and f_{mB} will give "near optimal" results for J_m and f_{m_i}. Furthermore, intersubject differences would tend to run high when sensitivity is low; thus, tracking down the true "optimal" f_{mA} may be of limited value. If N_A and N_B are the number of longitudinal axis and lateral axis instruments to be monitored, the logical choice is

$$f_{mA} = \frac{N_A}{N_A + N_B} f_{m,avail} \tag{72a}$$

$$f_{mB} = f_m - f_{mA} = \frac{N_B}{N_A + N_B} f_{m,avail} \tag{72b}$$

†The general case presents an easy modification that depends on the number of instruments in A versus B.

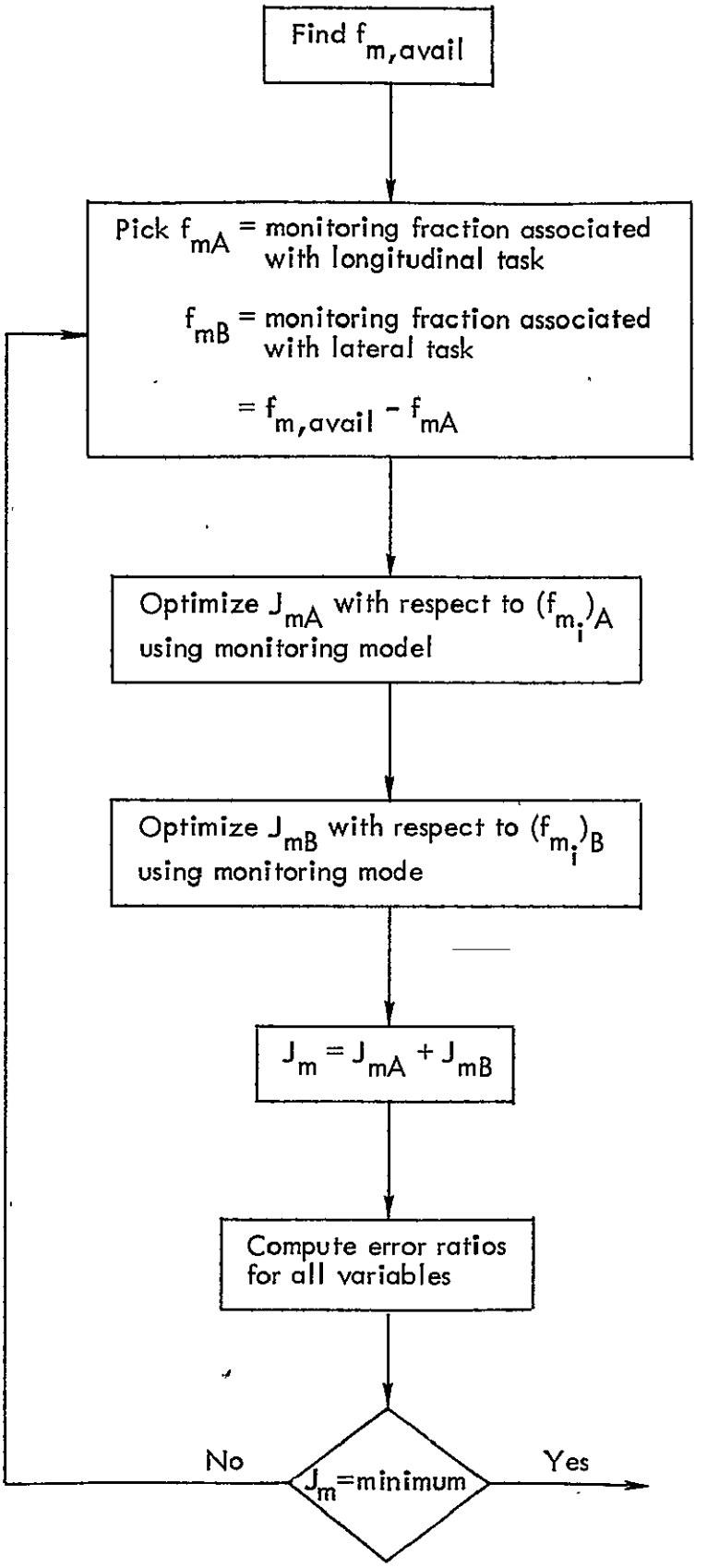

Figure 5. Flow Diagram for Dual Axis Monitoring Scheme.

SECTION 3

CONTROL/DISPLAY CONFIGURATIONS

The application of the design methodology presented in the previous section requires the specification of candidate control/display configurations. These can be either obtained independently from some other source, or defined through a systematic procedure as a corollary to the main analysis. This section describes the procedures used to develop the candidate control/display configurations in the present study, and presents the numerical application to the CH-47 helicopter.

3.1 CONTROL SYSTEM DESIGN PROCESS

A systematic design process has been developed to formulate a series of control system automation levels for the CH-47 helicopter ranging from fully manual to automatic with complete position feedback.

3.1.1 METHODOLOGY REVIEW

The control design methodology was presented in detail in References 4 and Basically, the Quadratic Synthesis technique was used to generate the linear feedback control laws and closed-loop dynamics for a series of quadratic performance measures. Increasing stages of automation were obtained by consecutively including higher level state variable terms in the performance measure. Table 4 shows the possible automation levels in each of the four control channels for the helicopter. The longitudinal axes (forward and vertical) and the lateral axes (lateral and directional) were analyzed separately since there is effectively very little coupling between these, although there is considerable coupling between the forward and vertical channels and between the lateral and directional channels.

Table 4. Levels of Control Channel Automation.

Automation Level	Control Channel			
	Forward	Vertical	Lateral	Directional
Manual	δ_e	δ_c	δ_a	δ_r
Attitude Rate	q		p	r
Attitude	θ		ϕ	ψ
Velocity	V_x	V_z	V_y	
Position	x	h	y	

Ideally, each control input should provide a completely uncoupled response at the desired automation level in a single channel only. However, there are insufficient degrees of freedom to accomplish this goal, and one objective of the control design is to minimize these undesired cross-coupling effects. In addition, a desirable uncoupled, closed-loop response for a given level of automation is often specified in terms of bandwidth and damping. These response criteria and physical vehicle constraints have been used to establish the weightings used in the quadratic performance measure.

3.1.2 CONTROL FEEDBACK GAINS AND CLOSED-LOOP RESPONSE

Figure 6 illustrates the loop structure for the pilot-vehicle-controller-display system. The feedback gains L_{cs} are selected to give some desirable closed-loop response characteristics (e.g., decoupling, stability, etc.) at a given level of automation. These feedbacks are assumed to be implemented by an automatic, optimally designed controller. The resulting closed-loop system is to be controlled by the human.

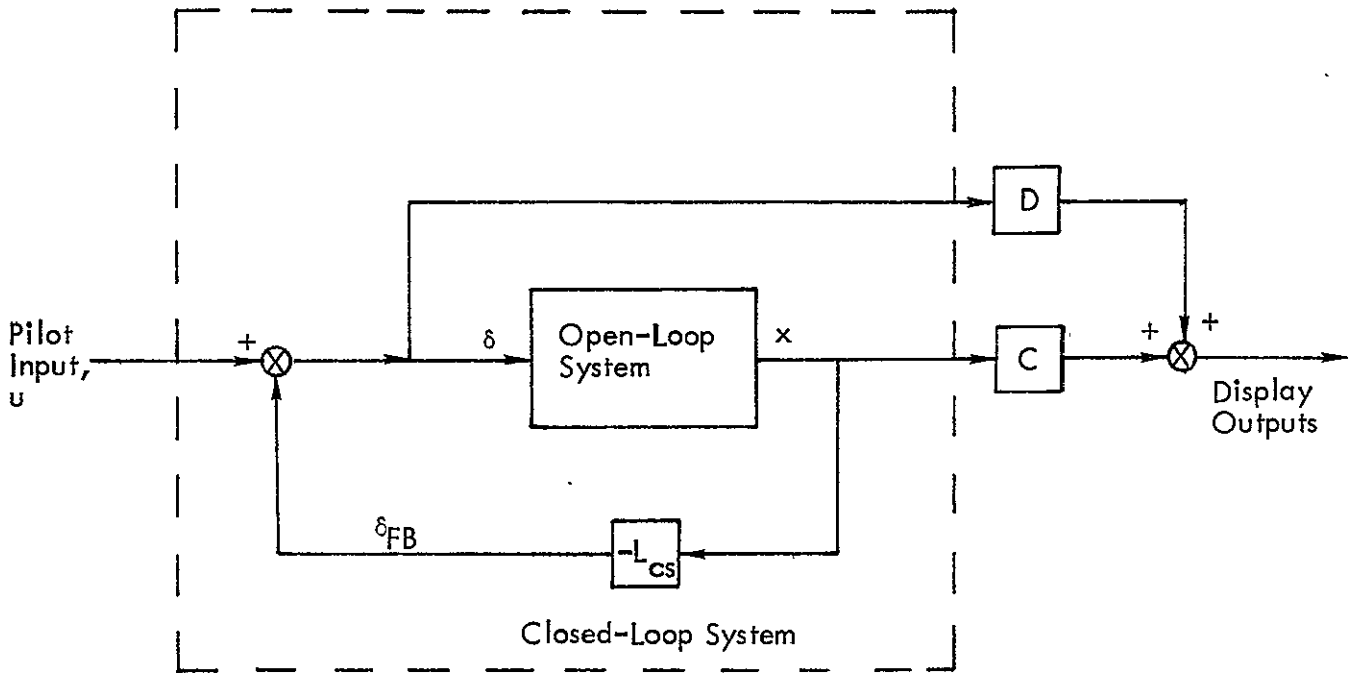

Figure 6. Closed-Loop VTOL System for Control Synthesis.

The open-loop system dynamics are:

$$\dot{x}(t) = A_{0L}x(t) + B_0\delta(t) + E_0w(t) \tag{73}$$

The display outputs are:

$$y = C_{0L}x + D_0\delta \tag{74}$$

The first n_{x1} states of the n_x state vector x(t) are assumed to be noise-shaping states. Feedbacks from these states are zeroed out in L_{cs}. The feedback signal

$$\delta_{FB} = -L_{cs}x(t) \tag{75}$$

is chosen to minimize the quadratic cost functional

$$J(u) = E\{x'Q_xx + u'Q_uu\} \tag{76}$$

Solving for L_{cs} yields

$$L_{cs} = Q_u^{-1} B_0' P \tag{77}$$

The matrix P satisfies the Riccati equation

$$PA_{0L} + A_{0L}' P + Q_x - PB_0 Q_u^{-1} B_0' P = 0 \tag{78}$$

Once having computed L_{cs}, the first n_{x1} columns are set to zero.† The closed-loop system dynamics are thus

$$\dot{x}(t) = A_0 x(t) + B_0 u(t) + E_0 w(t) \tag{79}$$

$$y = C_0 x + D_0 u \tag{80}$$

with $A_0 = A_{0L} - B_0 L_{cs}$, $C_0 = C_{0L} - D_0 L_{cs}$.

It is also useful to determine the open-loop transfer functions between pilot input δ and the outputs y. These enable the analyst to

a. test the degree of control decoupling of the automatic feedbacks

b. compare the effective closed-loop control/vehicle dynamics with the desired model (e.g., bandwidth and damping).

The transfer function matrix from u(s) to y(s) is

$$y(s) = [C_0' (sI - A_0)^{-1} B_0 + D_0] u(s) \tag{81}$$

3.1.3 CONTROL PERFORMANCE WEIGHTINGS

The performance measure weightings (Q_x, Q_u) in Equation (76) are diagonal matrices which determine the closed-loop system dynamics. They must be selected to provide the desired system response without excessive control activity. Experience has

†This has no effect on closed-loop poles.

shown that reasonable preliminary values for these can be determined from the largest desirable variations in the states and controls, i.e.,

$$Q_{x_{ii}} = (p_{x_i})^{-2} \tag{82}$$

$$Q_{u_{ii}} = (p_{u_i})^{-2} \tag{83}$$

where the weighting parameters p_{x_i} and p_{u_i} depend upon the level of automation desired.†

Reference 19 describes a design procedure that was developed to provide a systematic method of selecting these parameters for various levels of control automation. Simple dynamic models were developed to approximate the desired closed-loop response for each automation level in each control channel. These uncoupled models, examples of which are presented in Subsection 3.3 for the CH-47, were used to determine the appropriate values for the state variable weightings in Equation (82). For each successive level of control automation, the state weighting corresponding to the outermost feedback variable (i.e., the lowest element in the appropriate column of Table 4) is added to the nonzero values of Q_x. As an example, at the velocity level in the forward channel, a nonzero weight in Q_x would be specified for V_x as well as for the "inner loop" states θ and q. This differs slightly from the previous effort (Reference 4) wherein only the weighting for the outermost loop was used. However, the revised procedure is more harmonious with classical design methods in which outer feedback loops are consecutively added to the previous closed-loop system.

The control input limits p_{u_i} can be determined approximately for each flight condition from the constraints on vehicle angular and vertical accelerations, using the principal stability derivatives. For example, the maximum limit for δ_e is

†Note that a zero entry for $Q_{x_{ii}}$ implies that the corresponding state variable x_i is unconstrained insofar as the automatic control system is concerned.

$$P_{u_{\delta_e}} \approx \frac{\dot{q}_{max}}{(M_{\delta_e}/I_{yy})}$$

where $\dot{q}_{max}$ is the pitch acceleration limit, and M_{δ_e}/I_{yy} is the pitch acceleration due to δ_e.

3.2 FLIGHT DIRECTOR DESIGN PROCESS

The previous subsection described the first of two aspects of system automation. The second aspect deals with display automation, via the design and use of augmented flight director signals. The basic concept behind the flight director is to provide to the pilot (synthesized) information that is useful for control, thus rendering the piloting task easier in some sense. This section describes a flight director design process using the quadratic synthesis techniques of the optimal control model.

3.2.1 PRELIMINARY DESIGN APPROACH

Figure 7 shows the structure of the feedback loop under consideration. The state equations of the unaugmented vehicle were given by Equation (73). $\delta(t)$ are the control inputs and the feedback signals δ_{FB} are assumed to be implemented by an automatic control system as described in Subsection 3.1. Thus, $u(t)$ are the pilot's command inputs, and the augmented dynamics as "seen" by the pilot are given by Equation (79).

The status information that is observed by the pilot is

$$y_s(t) = C_s x(t) + D_s u(t) \tag{84}$$

where $y_s(t)$ contains both the position and rate of an explicitly displayed quantity. For the longitudinal axis

$$y_s = [x, V_x, z, V_z, \theta, q]' \tag{85}$$

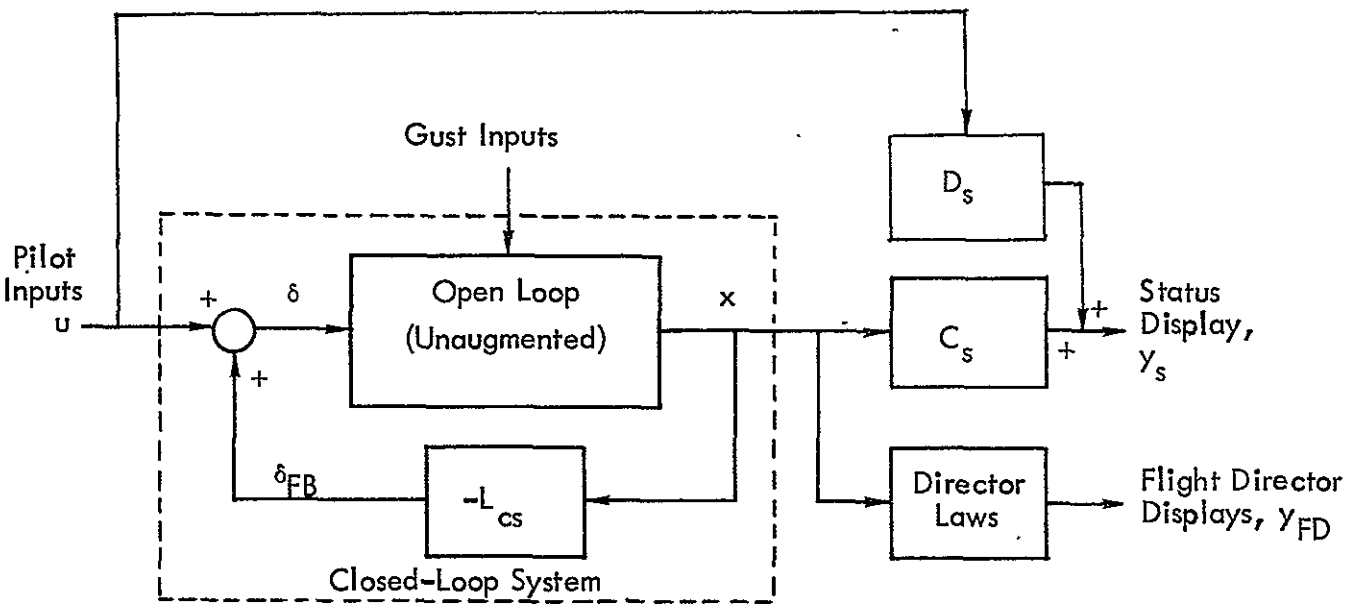

Figure 7. VTOL System Structure for Display Design.

while for the lateral axis,

$$y_s = [y, V_y, \phi, \dot{\phi}, \psi, \dot{\psi}]' \tag{86}$$

Defining status outputs that are the same as basic aircraft states eliminated the D_s matrix, and greatly simplifies the form of the C_s matrix and the selection of the design parameters $y_{i,max}$.

The flight director display information

$$y_{FD} = [FD_1, \dot{FD}_1, FD_2, \dot{FD}_2 \ldots FD_{Nu}, \dot{FD}_{Nu}] \tag{87}$$

also includes the implicitly derived indicator rates. In general, there can be as many FD_i as there are control inputs. Each flight director signal FD_i is assumed to be a linear combination of primary vehicle states,†

†i.e., measurable quantities and excluding wind-shaping states, etc.

$$FD_i = h_i' x(t) \tag{88}$$

with possibly some filtering to remove noise or high frequency components. Thus, the total information base displayed to the pilot is

$$y(t) = \begin{bmatrix} y_s(t) \\ y_{FD}(t) \end{bmatrix} \tag{89}$$

The flight director gains h_i are chosen so that if $FD_i(t)$ is kept "small" by the pilot, the resulting aircraft motion will be desirable. Since the pilot is in control of the (augmented) vehicle, there are two issues that relate to the harmony between FD(t) and pilot response. The first concerns the nature of the control task as viewed by the pilot. Thus, the task of keeping $FD_i(t)$ small should not conflict with the overall pilot-control task requirements. The second issue relates to the required form of the pilot compensation, as the FD_i and u_i are in one-to-one correspondence. From a reduced workload point of view, one should design a flight director signal $FD_i(t)$ such that the transfer function from input $u_i(t)$ to $FD_i(t)$ is approximately k/s. The required pilot compensation then be simple proportional feedback

$$u_i(t) \approx k \cdot FD_i(t) \tag{90}$$

In the first phase of this effort (Reference 4) an OCM based flight director design procedure was proposed, and validated by application to the CH-46 in hover flight. From the OCM, the pilot's control strategy is given by

$$T_N \dot{u} + u = -L \hat{x}(t) \tag{91}$$

The gains L (and T_N) are obtained by minimizing the cost functional

$$J_c(u) = E\left\{y_s' Q_{ys} y_s + \dot{u}' Q_{\dot{u}} \dot{u}\right\} \tag{92}$$

where the weighting matrices are assumed diagonal with

$$(Q_{ys})_{ii} = \frac{1}{|y_{si,max}|^2} \tag{93}$$

$$(Q_{\dot{u}})_{ii} = \frac{1}{|\dot{u}_{i,max}|^2} \tag{94}$$

The suggested design procedure was simply

$$FD_i(t) = \hat{\ell}_i' x(t) \quad ; \quad i = 1, 2, \ldots, Nu \tag{95}$$

where $\hat{\ell}_i'$ is the i^{th} row of $\hat{L}$; and $\hat{L}$ is equal to L but with gains on the unmeasurable noise shaping states set to zero. In addition, to simplify implementation, only the important gains in $\hat{\ell}_i$ would normally be retained.

3.2.2 MODIFIED DESIGN PROCEDURE

The design approach outlined above is simple, is related to the pilot's interpretation of the control task, and considers the form of pilot compensation. However, it does not consider the possibility that the flight directors, once added to the display panel, modify the pilot's control task and hence change the cost functional $J_c(u)$. Excluding FD_i from the cost functional implies that the pilot's control objectives are basically the same as before introducing these signals. Thus, the situation or status variables y_s remain only of concern, and the flight directors provide only enhanced state information. Including the FD_i within $J_c(u)$, in addition to the other terms, implies that one of the pilot's direct control objectives is to keep the FD_i small. We assume the latter, i.e., the director signals y_{FD} are explicitly controlled.†

†Sometimes this is done to the exclusion of the $y_s(t)$!

The control cost functional, modified to weight deviations of $FD_i(t)$, and possibly the rates $\dot{FD}_i(t)$, is

$$J_c(u) = E\left\{y_s' Q_{ys} y_s + \dot{u}' Q_{\dot{u}} \dot{u}\right\} + \sum_{i=1}^{Nu} M_i E\left\{FD_i^2\right\} + N_i E\left\{\dot{FD}_i^2\right\} \qquad (96)$$

The weighting terms M_i are selected as

$$M_i = \frac{1}{|FD_{i,max}|^2} \qquad (97)$$

to be consistent with the choice of the Q_{ys} and $Q_{\dot{u}}$ terms. The maximum flight director excursions are computed according to the rule

$$|FD_{i,max}| = \sum_j \gamma_j \left|\hat{\ell}_{ij}\right| \cdot |x_{j,max}| \qquad (98)$$

where γ_j are 0 or 1 to indicate which variables are of concern in forming $FD_{i,max}$. We select

$$\gamma_j = \begin{cases} 1 \text{ if } x_j \text{ is a positional variable} \\ 0 \text{ if } x_j \text{ is a rate variable} \end{cases} \qquad (99)$$

Thus, the flight director signal is at its maximum value when all error displacements are at their design limits. We set the weights $N_i = 0$ in the present approach, to indicate that flight director rates are not explicitly controlled. This modeling assumption is justified by the analogy between reducing $FD_i(t)$ to zero, and human tracking in simple (k/s) compensatory systems (References 7 and 8), where error rate terms need not be included in J_c.

With the pilot cost functional modified as in Equation (96), the pilot model control is now obtained by minimizing

$$J_c(u) = E\left\{y' Q_y y + \dot{u}' Q_{\dot{u}} \dot{u}\right\} \qquad (100)$$

where $y(t)$ is given by Equation (89) and includes the rate terms $\dot{FD}_i$ as in Equation (89).† The matrix Q_y is diagonal with

$$Q_y = \text{diag}\,(Q_{y_s}, M_1, 0, M_2, \ldots, M_{Nu}, 0) \tag{101}$$

The display information y may be written as a linear combination of vehicle states,

$$y(t) = C_0 x(t) + D_0 u(t) = \begin{bmatrix} C_s \\ \hline C_{FD} \end{bmatrix} x(t) + \begin{bmatrix} D_s \\ \hline D_{FD} \end{bmatrix} u(t) \tag{102}$$

where

$$C_{FD} = \begin{bmatrix} \hat{\ell}_1' \\ g_1' \\ \vdots \\ \hat{\ell}_{Nu}' \\ g_{Nu}' \end{bmatrix} \qquad D_{FD} = \begin{bmatrix} 0 \\ h_1' \\ \vdots \\ 0 \\ h_{Nu}' \end{bmatrix}$$

Each g_i and h_i is obtained (for $\dot{FD}_i$) from the corresponding $\hat{\ell}_i'$ via

$$\begin{aligned} \dot{FD}_i &= \hat{\ell}_i' \dot{x}(t) = \hat{\ell}_i' A_0 x(t) + \hat{\ell}_i' B_0 u(t) \\ &= g_i x(t) + h_i' u(t) \end{aligned} \tag{103}$$

Since $w(t)$ drives only the noise shaping states, $\hat{\ell}_i' E_0 = 0$.

The result of minimizing Equation (100) is the control strategy

$$T_N \dot{u} + u = -L\hat{x}(t) \tag{104}$$

†The rate terms have no effect on the control strategy. They are included to be compatible with the structure of the OCM. They do have minor influence on the model's information processor.

But since the cost functionals of Equations (92) and (100) are not the same, the gains L in Equation (104) differ from those in Equation (91). Hence, the flight director signals of Equation (95) and the required pilot control gains in Equation (104) are no longer in harmony. This mismatch can be corrected via the iterative process of computing feedback gains and flight director signals as shown in Figure 8.

The proposed algorithm has given rapid convergence in all of the examples tested. Generally 2 to 5 iterations have been needed, and in many cases the resulting converged gains were within 10 percent of the initial values $\hat{L}^{(0)}$ obtained from Equation (92). The flight director signals must be included in the pilot's information base for subsequent modeling in the OCM. The display information y(t) is already in the required form $C_o x + D_o u$ via Equation (102). Values for the observation noise/signal ratios ρ_i^o and thresholds a_i remain to be selected for y_{FD}. The ρ_i^o are set to -20 dB nominal values. The thresholds on the positional displacements FD_i are chosen in the same manner as those for y_s, (see Subsection 2.1),

$$a_{FD_i} = \frac{1}{4} |FD_{i,max}| \tag{105}$$

Since the maximum deviations of $\dot{FD}_i$ are not defined (i.e., ∞), we select thresholds for $\dot{FD}_i$ on the basis of those for FD_i. Maintaining consistency with previous work, we pick

$$a_{\dot{FD}_i} = \frac{1}{2} a_{FD_i} \tag{106}$$

With the computation of the flight director gains $\hat{L}$, we can examine the transfer functions between pilot inputs u and the flight director signals y_{FD}. These will test whether the composite vehicle-flight director dynamics are similar to k/s as anticipated, and will show the (presumably small) degree of cross-coupling between u_i and FD_j, $j \neq i$. The transfer function from u_i (s) to FD_j(s) is simply

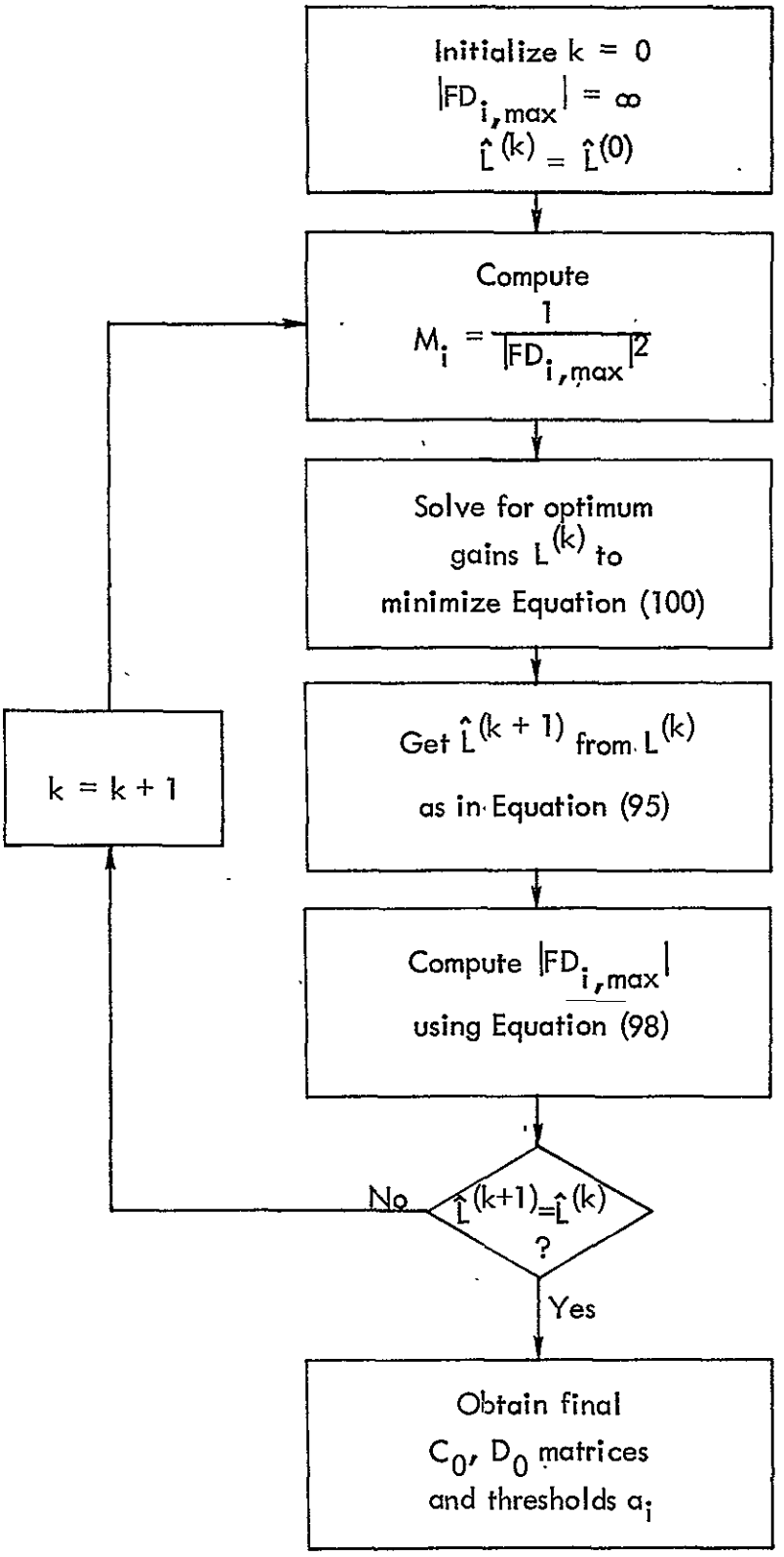

Figure 8. Flow Diagram for Computing Flight Director Gains.

$$\frac{FD_i(s)}{u_i(s)} = \hat{\ell}_i^T (sI - A_0)^{-1} b_i \; ; \; i, j = 1, \ldots, Nu$$

$$= \frac{\det [sI - A_0 + b_i \hat{\ell}_i^T]}{\det [sI - A_0]} - 1 \qquad (107)$$

Example transfer functions given in Subsection 3.3.4 show that in most, but not all, cases FD_i/u_i is "similar" to k/s. This does not appear to be a drawback with the above design process, however. Even in cases where the k/s criterion is not met, the OCM predicts that the flight directors will significantly improve system performance. Further research is warranted in this matter.

3.3 CH-47 APPLICATION

The control/display design processes described in the previous two subsections were applied to the CH-47 helicopter to obtain a matrix of control automation/display sophistication configurations for subsequent analysis using the methodology of Section 2.

3.3.1 FLIGHT CONDITIONS

A set of six flight conditions was selected for conducting the CH-47 control/display tradeoff evaluations. As shown in Table 5, these include hover, cruise, and four approach conditions. The three straight-in approaches range from the 3° glide slope of a conventional ILS approach to a fairly steep 15° descent at 45 knots. The spiral approach was originally developed by ASI in an earlier study of the guidance and control requirements for such a maneuver (Reference 19).

3.3.2 SYSTEM DYNAMICS

Vehicle Perturbation Equation

The linearized equations of motion used in the analysis were developed in Reference 4. These were modified slightly to include the non-zero bank angle and

Table 5. Flight Conditions for CH-47 Analysis.

Flight Condition	V_x (kt)	V_y	V_z (ft/min)	h (ft)	ϕ (deg)
Hover	0	0	0	0	0
Cruise	130	0	0	3000	0
Straight Approach at 3°	120	0	636	~500	0
Straight Approach at 9°	59.3	0	951	~500	0
Straight Approach at 15°	43.5	0	1180	~500	0
Spiral Approach	60	0	500	1000	9.05

consequent steady turn rate for the spiral approach. The resulting perturbation equations, in terms of the inertial velocity components, are given below

$$\Delta\dot{V}_x = \left(\frac{X_u}{m} + \left(\frac{X_w}{m} - Q_0\right)\tan\theta_0\right)\Delta V_x + (\tan\theta_0)\Delta\dot{V}_z - \left(\frac{X_u}{m}\tan\theta_0 - \left(\frac{X_w}{m} - Q_0\right)\right)\Delta V_z + \left(\frac{R_0}{\cos\theta_0}\right)\Delta V_y + \frac{1}{\cos\theta_0}\left(\frac{X_q}{m}\dot{\theta} - \left(\frac{X_u}{m}W_0 - \left(\frac{X_w}{m} - Q_0\right)U_0 + g\cos\theta_0\cos\phi_0\right)\theta + W_0\phi - (U_0 + W_0\tan\theta_0 - g\cos\theta_0\sin\phi_0)\psi + \frac{X_\delta}{m}\delta\right) \quad (108a)$$

$$\Delta\dot{V}_y = (P_0\sin\theta_0 - R_0\cos\theta_0)\Delta V_x + (R_0\sin\theta_0 + P_0\cos\theta_0)\Delta V_z + \left(\frac{Y_v}{m}\right)\Delta V_y + \frac{Y_p}{m}\dot{\phi} + \left(P_0 \cdot U_0 + \left(\frac{Y_v}{m} + R_0\right)W_0 + g\cos\theta_0\cos\phi_0\right)\phi - \left(\frac{Y_p}{m}\sin\theta_0 - \frac{Y_r}{m}\cos\theta_0\right)\dot{\psi} - \left(\frac{Y_v}{m}(U_0\cos\theta_0 + W_0\sin\theta_0) + g\sin\theta_0\right)\psi + \frac{Y_\delta}{m}\cdot\delta \quad (108b)$$

$$\Delta\dot{V}_z = -(\tan\theta_0)\,\Delta\dot{V}_x + \left(\frac{Z_u}{m} + Q_0 + \frac{Z_w}{m}\tan\theta_0\right)\Delta V_x - \left(\left(\frac{Z_u}{m} + Q_0\right)\tan\theta_0 - \frac{Z_w}{m}\right)\Delta V_z$$
$$- \left(\frac{P_0}{\cos\theta_0}\right)\Delta V_y + \frac{1}{\cos\theta_0}\left(\frac{Z_q}{m}\dot{\theta} - \left(\left(\frac{Z_u}{m} + Q_0\right)W_0 - \frac{Z_w}{m}U_0 + g\sin\theta_0\right)\theta\right.$$
$$\left. - (g\cos\theta_0\sin\phi_0 + P_0 \cdot W_0)\phi + (P_0 \cdot U_0 + P_0 \cdot W_0\tan\theta_0)\psi + \frac{Z_\delta}{m}\cdot\delta\right) \qquad (108c)$$

$$\ddot{\theta} = \left(\frac{M_u}{I_{yy}}\cos\theta_0 + \frac{M_u}{I_{yy}}\sin\theta_0\right)\Delta V_x - \left(\frac{M_u}{I_{yy}}\sin\theta_0 - \frac{M_w}{I_{yy}}\cos\theta_0\right)\Delta V_z + \frac{M_q}{I_{yy}}\dot{\theta}$$
$$- \left(\frac{M_u}{I_{yy}}W_0 - \frac{M_w}{I_{yy}}U_0\right)\theta - \left(\frac{R_0(I_{xx} - I_{zz})}{I_{yy}} + \frac{2P_0 \cdot J_{xz}}{I_{yy}}\right)\dot{\phi}$$
$$+ \left(\left(\frac{R_0(I_{xx} - I_{zz})}{I_{yy}} + \frac{2P_0 \cdot J_{xz}}{I_{yy}}\right)\sin\theta_0 - \left(\frac{P_0(I_{xx} - I_{zz})}{I_{yy}} + \frac{2R_0 \cdot J_{xz}}{I_{yy}}\right)\cos\theta_0\right)\dot{\psi}$$
$$+ \frac{M_\delta}{I_{yy}}\delta \qquad (108d)$$

$$\ddot{\phi} = \frac{L_y}{I_{xy}}\Delta V_y + \left(\frac{L_p}{I_{xx}} + \frac{Q_0 \cdot J_{xz}}{I_{xx}}\right)\dot{\theta} + \left(\frac{L_p}{I_{xx}} + \frac{Q_0 \cdot J_{xz}}{I_{xx}}\right)\dot{\phi} + \left(\frac{L_v}{I_{xy}}W_0\right)\phi$$
$$+ \left(\frac{J_{xz}}{I_{xx}}\cos\theta_0 + \sin\theta_0\right)\ddot{\psi} - \left(\left(\frac{L_p}{I_{xx}} + \frac{Q_0 \cdot J_{xz}}{I_{xx}}\right)\sin\theta_0\right.$$
$$\left. - \left(\frac{L_r}{I_{xx}} - \frac{Q_0(I_{zz} - I_{yy})}{I_{xy}}\right)\cos\theta_0\right)\dot{\psi} - \frac{L_v}{I_{xx}}(U_0\cos\theta_0 + W_0\sin\theta_0)\psi + \frac{L_\delta}{I_{xx}}\delta \qquad (108e)$$

$$\ddot{\psi} = \frac{1}{B}\left[N_v \Delta V_y - (P_0(I_{yy} - I_{xx}) + R_0 J_{xz})\dot{\theta} + J_{xz}\ddot{\phi} + (N_p - Q_0(I_{yy} - I_{xx}))\dot{\phi} \right.$$

$$+ (N_v \cdot W_0)\phi - ((N_p - Q_0(I_{yy} - I_{xx})) \sin\theta_0 - (N_r - Q_0 J_{xz}) \cos\theta_0)\dot{\psi}$$

$$\left. - N_v(U_0 \cos\theta_0 + W_0 \sin\theta_0)\psi + N_\delta \delta \right] \qquad (108f)$$

where $B \triangleq I_{zz} \cos\theta_0 + J_{xz} \sin\theta_0$, and where $(\ )_\delta \delta$ indicates the summation over the four control inputs.

As mentioned previously, the longitudinal axes and the lateral axes were analyzed separately to reduce the computation time and complexity. Thus the dynamic coupling between these axes in the spiral approach was also neglected, but this does not jeopardize the results since the steady-bank angle is small (9^o). Moreover, this entire analysis is a conceptual one which involves other assumptions of the same order of magnitude.

Atmospheric Turbulence Model

The single first-order disturbance inputs used in each axis during the previous analysis (Reference 4) has been replaced with a more realistic turbulence model based on the Military Specification 8785B. The translational and rotational gusts are generated by the following equations:

- Longitudinal Disturbances

$$\dot{u}_g = -\frac{V}{L_u} u_g + \sigma_u \sqrt{\frac{2V}{L_u}}\ \eta_u \qquad (109)$$

$$\dot{w}_g = -\frac{2V}{L_w} w_g + \frac{V}{L_w} w_{g1} + \sigma_w \sqrt{\frac{3V}{L_w}}\ \eta_w \qquad (110)$$

$$\dot{w}_{g1} = -\frac{V}{L_w} w_{g1} + \sigma_w \sqrt{\frac{V}{L_w}}\, \eta_w \tag{111}$$

$$\dot{q}_g = -\frac{\pi V}{4b} q_g + \frac{\pi}{4b} \dot{w}_g \tag{112}$$

- Lateral Disturbances

$$\dot{v}_g = -\frac{2V}{L_v} v_g + \frac{V}{L_v} v_{g1} + \sigma_v \sqrt{\frac{3V}{L_v}}\, \eta_v \tag{113}$$

$$\dot{v}_{g1} = -\frac{V}{L_v} v_g + \sigma_v \sqrt{\frac{V}{L_v}}\, \eta_v \tag{114}$$

$$\dot{p}_g = -\frac{\pi V}{4b} p_g + \sigma_w \frac{\pi}{2b} \sqrt{\frac{\pi V}{5L_w} \frac{\pi L_w}{4b}}^{1/3} \eta_p \tag{115}$$

$$\dot{r}_g = -\frac{\pi V}{3b} r_g - \frac{\pi}{3b} \dot{v}_g \tag{116}$$

In the above equations, $(\,)_g$ refers to a gust disturbance variable, and the η_i are Gaussian white driving noises with zero mean and unity variance.

The scale distances L_u, L_v, L_w are functions of altitude, as shown in Table 6.

Table 6. Scale Distances Versus Altitude.

Altitude (ft)	L_u	L_v	L_w
$h < 100$	$145h^{1/3}$	$145h^{1/3}$	100
$100 \leq h \leq 1750$	$145h^{1/3}$	$145h^{1/3}$	h
$h > 1750$	1750	1750	1750

The rms gust intensities σ_u, σ_v, σ_w are related as follows:

$$\frac{\sigma_u^2}{L_u} = \frac{\sigma_v^2}{L_v} = \frac{\sigma_w^2}{L_w} \tag{117}$$

For moderate turbulence, the vertical intensity varies with altitude. We assume Mil Spec 8785B is a 3σ model, which gives

$$\sigma_w = 3.42 - 0.42 \log_{10} h \tag{118}$$

The horizontal intensities can then be obtained from Equation (117).

The only remaining parameters needed in Equations (109 through 11) and Table 6 are the airspeed V, the altitude h, and span b. The equivalent span from the helicopter is taken as the combined span of the two overlapped rotors, which is 99 feet from the CH-47.

Augmented Systems

As discussed in Section 2, the wind disturbance equations must be augmented to the vehicle dynamics to obtain the complete system dynamics in the form of Equation (73). This was performed separately for the longitudinal and the lateral axes. The resulting state, control and noise vectors are defined below.

- Longitudinal Dynamics

$$x = [u_g, w_g, w_{gl}, q_g, x, V_x, z, V_z, \theta, \dot{\theta}]' \tag{119a}$$

$$u = [\delta_e, \delta_c]' \tag{119b}$$

$$w = [\eta_u, \eta_w]' \tag{119c}$$

- Lateral Dynamics

$$x = [v_g, v_{gl}, p_g, r_g, y, V_y, \phi, \dot{\phi}, \psi, \dot{\psi}]' \quad (120a)$$

$$u = [\delta_a, \delta_r]' \quad (120b)$$

$$w = [\eta_v, \eta_p]' \quad (120c)$$

3.3.3 CONTROL SYSTEM DESIGN RESULTS

Control Automation Levels

As shown in Table 4, there are three or five levels of automation possible in each of the control channels of the helicopter. Thus, the number of possible combinations is $5 \times 5 \times 3 \times 3 = 225$. However, many of these combinations are not practical systems for normal operations. A series of eight systems were selected to represent the full range of automation for the CH-47 helicopter ranging from purely manual with direct actuator commands to full position control. These are shown in Table 7.

Table 7. CH-47 Control Automation Levels.

System	Control Channel Command			
	Pitch or Forward	Collective or Vertical	Roll or Lateral	Yaw or Directional
A	δ_e	δ_c	δ_a	δ_r
B	q	δ_c	ϕ	Ψ
C	θ	δ_c	ϕ	Ψ
D	θ	δ_c	y	Ψ
E	θ	$\dot{h}$	ϕ	Ψ
F	V_x	V_z	V_y	Ψ
G	x	$\dot{h}$	ϕ	Ψ
H	x	$\dot{h}$	y	Ψ

The system automation levels in Table 6 differ from those used in the first phase of the study (Reference 4). The eight configurations used previously were reevaluated, along with a series of systems postulated by the LaRC Flight Research Division for a split-axis control investigation, before defining the resulting levels of control automation selected for the present study. In Table 7, the two extreme systems (A and H) are the same as in Reference 4, and the revised system E is the same as the previous system F. The remaining five systems have been redefined. The systems in Table 7 are presented in their approximate order of increasing automation. System A is a fully manual system with no stability augmentation in any channel.

In the longitudinal axes, System B has only pitch rate feedback added to the manual system, while systems C, D, and E are pitch attitude command systems. System E also has altitude command in the vertical channel. System F is a velocity-command system, and systems G and H both have forward and vertical position feedback.

In the lateral-directional axes, all systems other than A assume heading hold or heading command. Systems B, C, E and G use roll attitude command, while systems D and H have lateral position feedback. As mentioned before, system F is a three-axis velocity command system.

Weighting Parameters

The procedure used to select the state variable weightings in the quadratic synthesis of the various automation levels has been modified slightly from the process discussed in Reference 4. The numerical values for the maximum state devisions are selected in the same manner as described in Reference 4. However, instead of weighting just the state variable for the outermost feedback loop alone, the weightings for each of the previously closed loops are also included. The resulting weighting parameters are shown in Table 8. This modified procedure corresponds to the normal control

Table 8. State Variable Weighting Parameters for CH-47 Automation Levels.

System	p_{x_i}											
	x (ft)	V_x (ft/sec)	z (ft)	V_z (ft/sec)	θ (rad)	$\dot{\theta}$ (rad/sec)	y (ft)	V_y (ft/sec)	ϕ (rad)	$\dot{\phi}$ (rad/sec)	ψ (rad)	$\dot{\psi}$ (rad/sec)
A	-	-	-	-	-	-	-	-	-	-	-	-
B						.435			.435	.435	.435	.435
C					.435	.435			.435	.435	.435	.435
D					.435	.435	84.0	28.0	.435	.435	.435	.435
E			30.0	7.5	.435	.435			.435	.435	.435	.435
F		28.0		7.5	.435	.435		28.0	.435	.435	.435	.435
G	84.0	28.0	30.0	7.5	.435	.435			.435	.435	.435	.435
H	84.0	28.0	30.0	7.5	.435	.435	84.0	28.0	.435	.435	.435	.435

system design process whereby outer loops are closed sequentially around the previous closed-loop system. The actual weighting terms are found by using the values from Table 8 in Equation (82).

As described in Subsection 3.1, the control variable limits used to define the control weighting terms can be determined approximately from the maximum vehicles angular and vertical accelerations as shown below:

$$\delta_{e,max} = \dot{q}_{max} \Big/ \left| \frac{M_{\delta_e}}{I_{yy}} \right| \tag{121}$$

$$\delta_{c,max} = \dot{w}_{max} \Big/ \left| \frac{Z_{\delta_c}}{m} \right| \tag{122}$$

$$\delta_{a,max} = \dot{p}_{max} \Big/ \left| \frac{L_{\delta_a}}{I_{xx}} \right| \tag{123}$$

$$\delta_{r,max} = \dot{r}_{max} \Big/ \left| \frac{N_{\delta_r}}{I_{zz}} \right| \tag{124}$$

The CH-47 stability derivative data (Reference 20) was interpolated for the six flight conditions of Table 5, and used to solve Equations (121 through 124). The following acceleration constraints used for these calculations were developed in Reference 4:

$$\dot{q}_{max} = 0.87 \text{ rad/sec}^2$$

$$\dot{w}_{max} = 3 \text{ ft/sec}^2$$

$$\dot{p}_{max} = 0.87 \text{ rad/sec}^2$$

$$\dot{r}_{max} = 0.87 \text{ rad/sec}^2$$

The resulting control limits are presented in Table 9. These were used with Equation (83) to define the control weighting matrices for the quadratic synthesis design application.

Table 9. CH-47 Control Variable Limits.

Flight Condition	P_{u_k}			
	δ_e(in.)	δ_c(in.)	δ_a(in.)	δ_r(in.)
Hover	2.643	0.372	2.0938	4.2685
Cruise	1.9741	0.2595	2.1303	4.3651
Spiral Approach	2.2112	0.3276	2.1584	4.461
3° Straight Approach	1.8547	0.2529	2.1731	4.5209
9° Straight Approach	2.2003	0.3362	2.169	4.4984
15° Straight Approach	2.313	0.3958	2.1298	4.4673

Closed-Loop Response

The above-mentioned state and control weights were used to generate the automatic feedback gains (Equation (77)) and closed-loop system response matrix (Equation (79)) for each automation level in Table 7. As discussed above, the longitudinal and lateral axes were analyzed separately for each of the flight conditions of Table 5. Since it would be impractical to present all of the numerical design results in this report, Appendix A contains detailed data for Configuration F at the hover flight condition as an example.

As mentioned in Subsection 3.1, the control system design process uses simple, uncoupled closed-loop response models to establish the performance weights in Equation (76). These models are presented in Table 10 for the CH-47 at hover. To

Table 10. Uncoupled Hover Control System Models.

Form of Transfer Function	ω (rad/sec)	ζ	τ (sec)
$\frac{p}{p_c}, \frac{q}{q_c} = \frac{k}{\tau s + 1}$			0.5
$\frac{\phi}{\phi_c}, \frac{\theta}{\theta_c} = \frac{k\omega^2}{s^2 + 2\zeta\omega s + \omega^2}$	1.0 - 1.4	1.0 - 0.7	
$\frac{V_y}{V_{y_c}}, \frac{V_x}{V_{x_c}} = \frac{k\omega^2/\tau}{s^3 + 2\zeta\omega s^2 + \omega^2 s + \omega^2/\tau} \approx \frac{k}{\tau s + 1}$	1.0 - 1.4	1.0 - 0.7	2.0
$\frac{y}{y_c}, \frac{x}{x_c} = \frac{k\omega^2}{s^2 + 2\zeta\omega s + \omega^2}$	0.35	0.7	4.0
$\frac{\psi}{\psi_c} = \frac{k\omega^2}{s^2 + 2\zeta\omega s + \omega^2}$	1.4	0.7	
$\frac{\dot{h}}{\dot{h}_c} = \frac{k}{\tau \cdot s + 1}$			2.5
$\frac{h}{h_c} = \frac{k\omega^2}{s^2 + 2\zeta\omega s + \omega^2}$	0.25	0.7	

verify the control design technique, the resulting closed-loop system frequency responses, Equation (81), were calculated and compared with the models in Table 10. Figures 9 and 10 illustrate the open-loop longitudinal frequency response for the unaugmented CH-47 (System A) at hover. Figures 11 through 16 present the resulting closed-loop system frequency response plots for each level of longitudinal control automation; the corresponding response plots are also shown for the uncoupled models of Table 10. Figures 11 through 16 typify the closed-loop system results obtained over all six flight conditions for the lateral axes as well as the longitudinal axes. These results show that the coupled closed-loop system response generally follows the corresponding uncoupled model response over the significant frequency range.

Another desirable characteristic of the closed-loop response is minimum coupling between control channels. Again, the frequency response provides a means of examining these coupling effects. This is illustrated in Figure 17, which compares the forward and vertical cross-coupling response for the velocity control system (System F) with the same response for the unaugmented CH-47 (System A). It is apparent from these results that the closed-loop system provides a significant attentuation of the cross-coupling gain. These results are also representative of those generally observed for the other flight conditions and control configurations.

3.3.4 FLIGHT DIRECTOR DESIGN RESULTS

Status Information

The flight director design procedure outlined in Subsection 3.2 was applied to the CH-47 for each of the six flight conditions shown in Table 5. The status information for the longitudinal and lateral axes was given in Equations (85) and (86), with the augmented state vectors of Equations (119a) and (120a), the status displays are defined by

- Longitudinal

$$C_s = \begin{bmatrix} 0 & 0 & 0 & 0 & 1 & 0 & 0 & 0 & 0 & 0 \\ 0 & 0 & 0 & 0 & 0 & 1 & 0 & 0 & 0 & 0 \\ 0 & 0 & 0 & 0 & 0 & 0 & 1 & 0 & 0 & 0 \\ 0 & 0 & 0 & 0 & 0 & 0 & 0 & 1 & 0 & 0 \\ 0 & 0 & 0 & 0 & 0 & 0 & 0 & 0 & 57.3 & 0 \\ 0 & 0 & 0 & 0 & 0 & 0 & 0 & 0 & 0 & 57.3 \end{bmatrix} \tag{125a}$$

$$D_s = 0 \tag{125b}$$

- Lateral

$$C_s = \begin{bmatrix} 0 & 0 & 0 & 0 & 1 & 0 & 0 & 0 & 0 & 0 \\ 0 & 0 & 0 & 0 & 0 & 1 & 0 & 0 & 0 & 0 \\ 0 & 0 & 0 & 0 & 0 & 0 & 57.3 & 0 & 0 & 0 \\ 0 & 0 & 0 & 0 & 0 & 0 & 0 & 57.3 & 0 & 0 \\ 0 & 0 & 0 & 0 & 0 & 0 & 0 & 0 & 57.3 & 0 \\ 0 & 0 & 0 & 0 & 0 & 0 & 0 & 0 & 0 & 57.3 \end{bmatrix} \tag{126a}$$

$$D_s = 0 \tag{126b}$$

In the C_s matrices, the parameter $57.3 = 180/\pi$ is used to convert the angular displacements and rates from radians to degrees.

Weighting Parameters

The parameters $y_{s_{i,max}}$ and $\dot{u}_{i,max}$ needed to define the weighting matrices in Equations (93) and (94) are selected to be consistent with mission requirements and physical capabilities. The status weightings reflect the pilot's attempted control

performance as a function of flight envelope. The values selected for the CH-47 are given in Table 11; as discussed in Section 2, these are presumed to represent 1σ perturbation levels. The "cruise/approach" values shown in Table 11 were used for all but the hover flight condition, since we are conducting a fixed-point analysis. However, in the non-stationary case, these would "funnel down" from the cruise values to the hover values as the pilot tightens his control in approaching the pad.

Table 11. Pilot Status Weighting Parameters.

Status Variable ($y_{s_{i,max}}$)	Units	Flight-Condition	
		Cruise/Approach	Hover
x	ft	25	5
V_x	ft/sec	2.5	1
z	ft	25	5
V_z	ft/sec	2.5	1
θ	deg	1	1
$\dot{\theta}$	deg/sec	0.5	0.5
y	ft	25	5
V_y	ft/sec	2.5	1
ϕ	deg	2	1
$\dot{\phi}$	deg/sec	1	0.5
ψ	deg	2	1
$\dot{\psi}$	deg/sec	1	0.5

The control rate weightings, as discussed earlier, are selected to achieve a reasonable value for the pilot's neuromuscular time delay in the model ($T_N \approx 0.1$ sec), or to satisfy his physical limitations in manipulating the controls. In the case of the CH-47, a constant value of $\dot{u}_{i,max} = 2.0$ in/sec was found to provide a reasonable T_N in each control channel over all of the flight conditions investigated.

Frequency Response

The design process produced two flight director signals and their rates for the lateral and the longitudinal axes of each control configuration and at each flight condition. In the longitudinal axes, these FD_i correspond to the forward and vertical control inputs (δ_e and δ_c), respectively; while in the lateral axes, they direct the bank and directional pilot controls (δ_a and δ_R).

- Longitudinal

$$y_{FD} = [FD_\theta, \dot{FD}_\theta, FD_z, \dot{FD}_z]' \tag{131}$$

- Lateral

$$y_{FD} = [FD_\phi, \dot{FD}_\phi, FD_\psi, \dot{FD}_\psi]' \tag{132}$$

As before, presentation of all the results is much too cumbersome for this report, and Appendix A provides more details for the CH-47 at hover.

The frequency response from each control input to the corresponding flight director signal was calculated to examine the open-loop dynamics observed by the pilot. Figure 18 presents examples of these results for the longitudinal axes at hover. These show that the composite vehicle-flight director dynamics for both the unaugmented vehicle (System A) and the velocity-command system (System F) are "similar" to k/s, especially in the vertical channel (FD_z/δ_c). In the forward control channel for

System F for example, the composite dynamics resemble k/s, but with a lead-lag filter centered at about 1 rad/sec. The results in Figure 18 are representative of many, but not all of the composite system dynamics. However, even when the k/s similarity does not exist the flight director signal does significantly improve system performance.

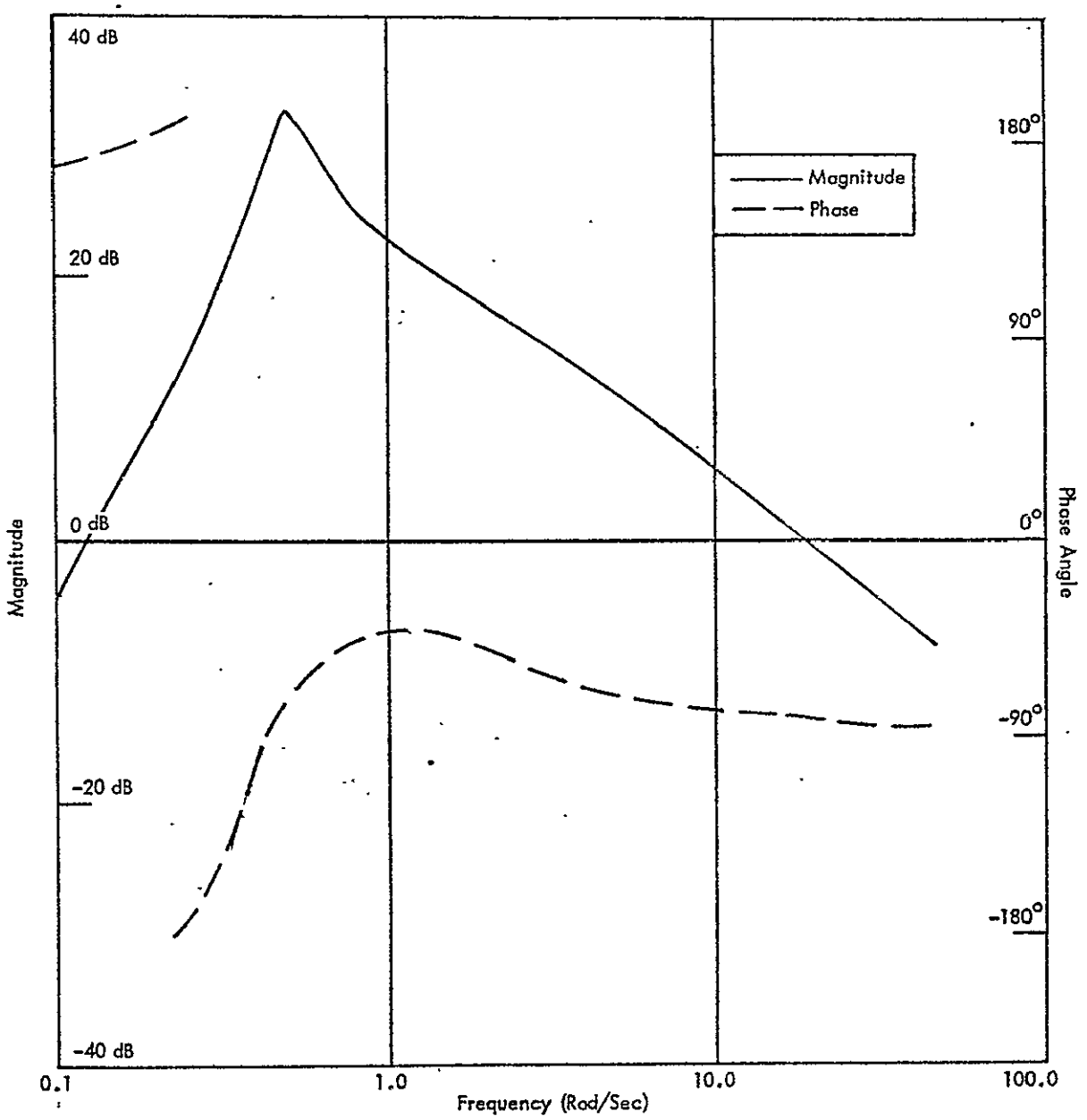

Figure 9. Open-Loop Frequency Response for Unaugmented Longitudinal Control - System A, Hover.

(a) q/δ_e.

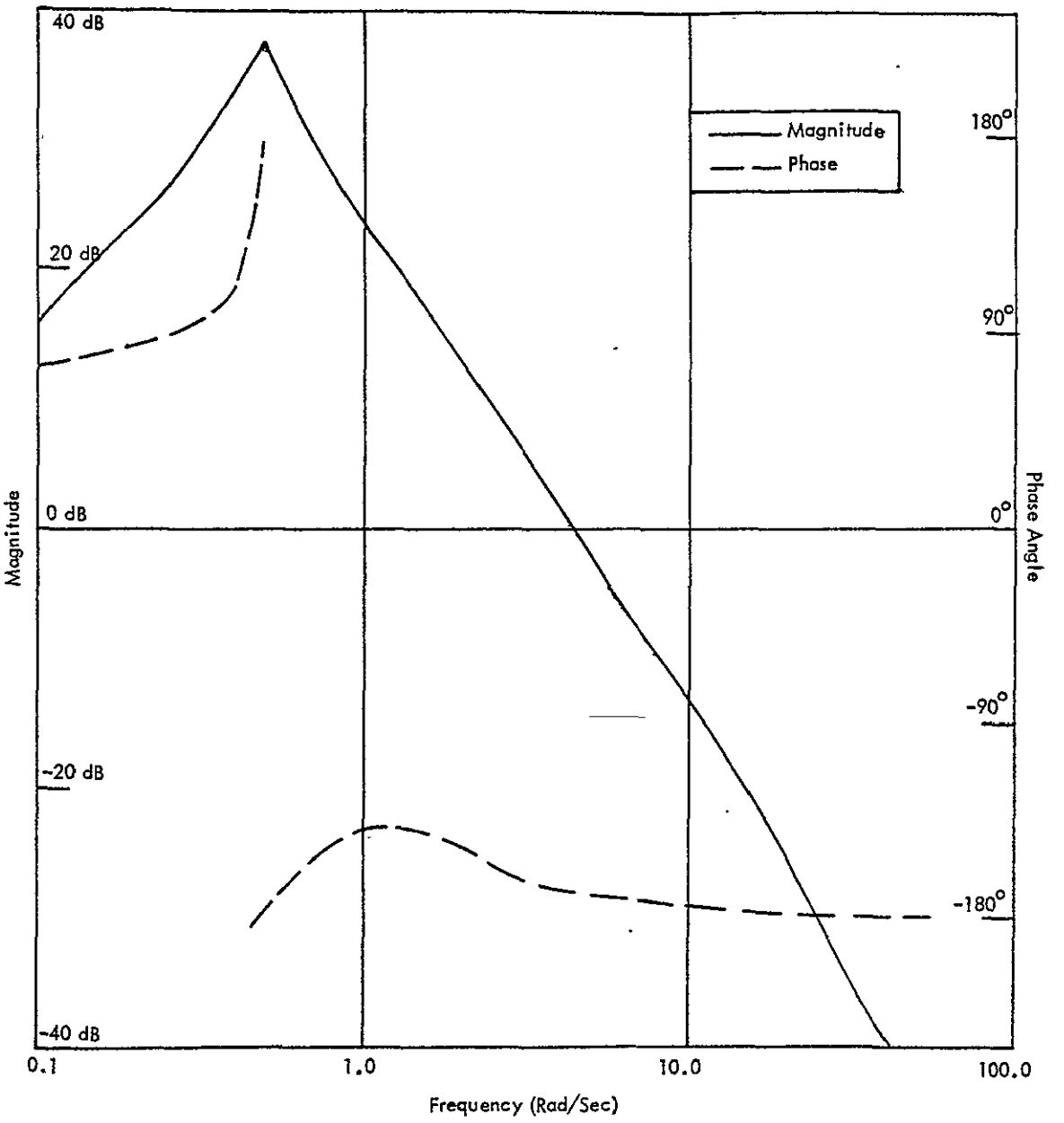

Figure 9. (b) θ/δ_e.

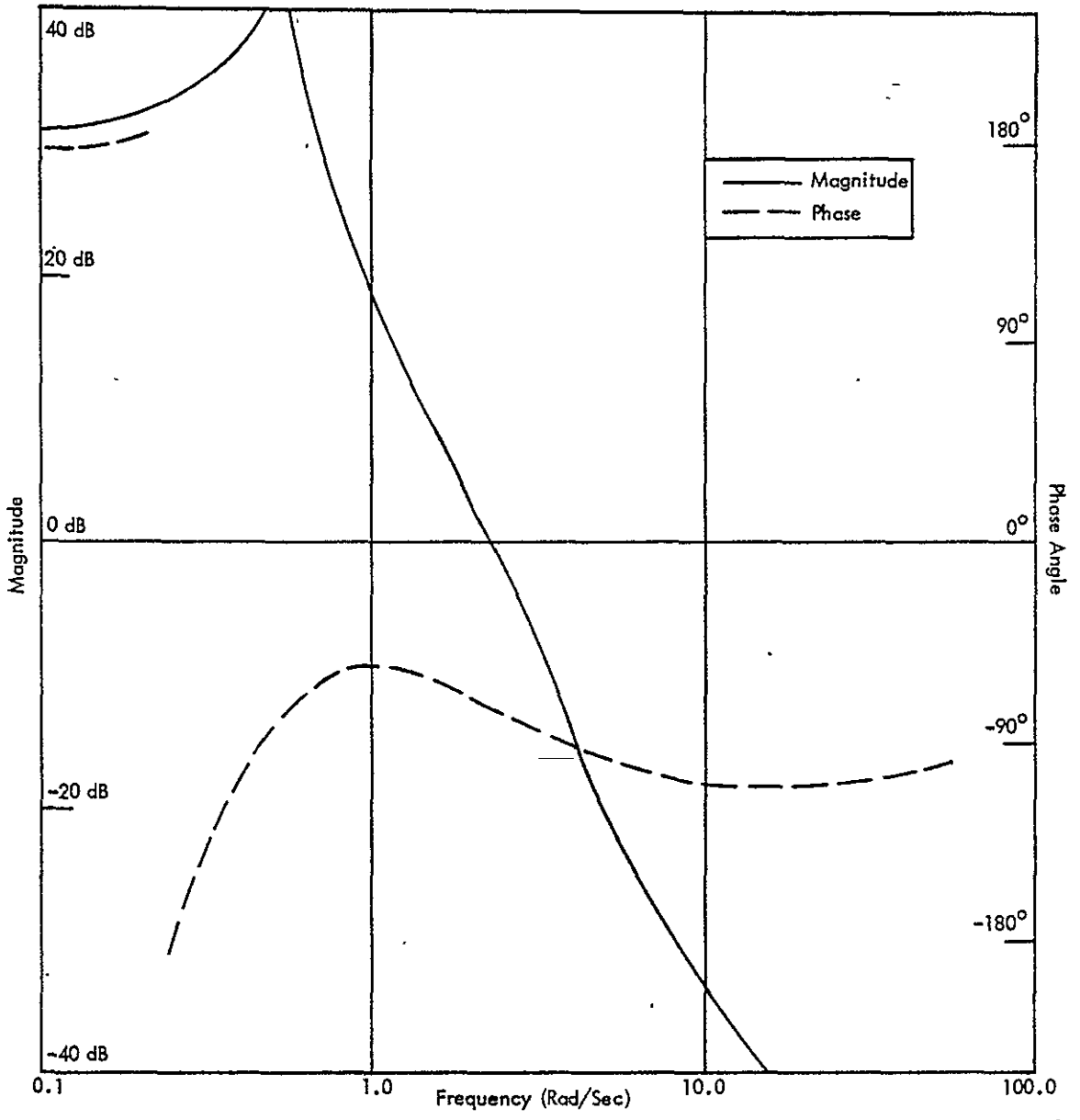

Figure 9. (c) V_x/δ_e.

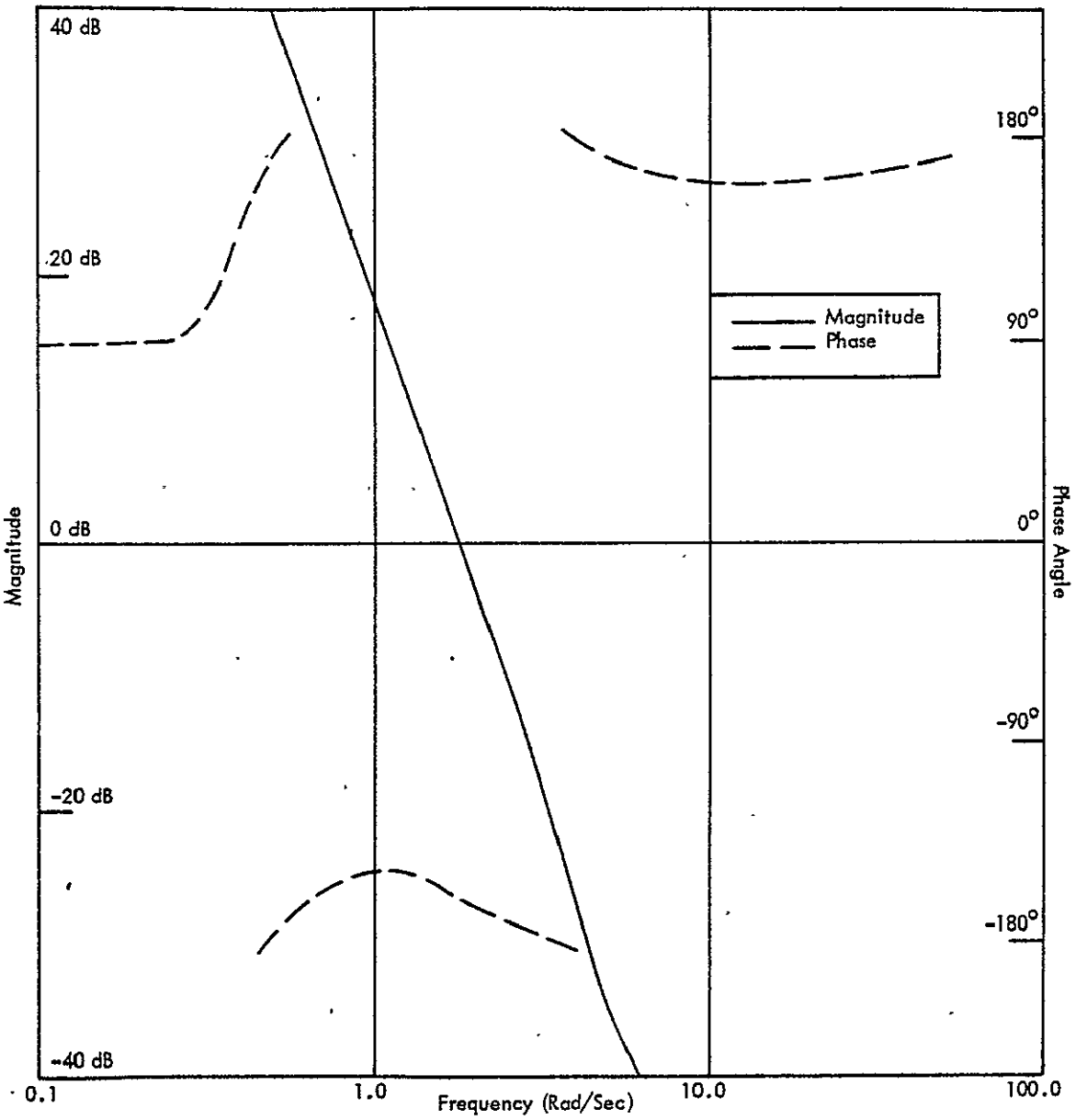

Figure 9. (d) x/δ_e.

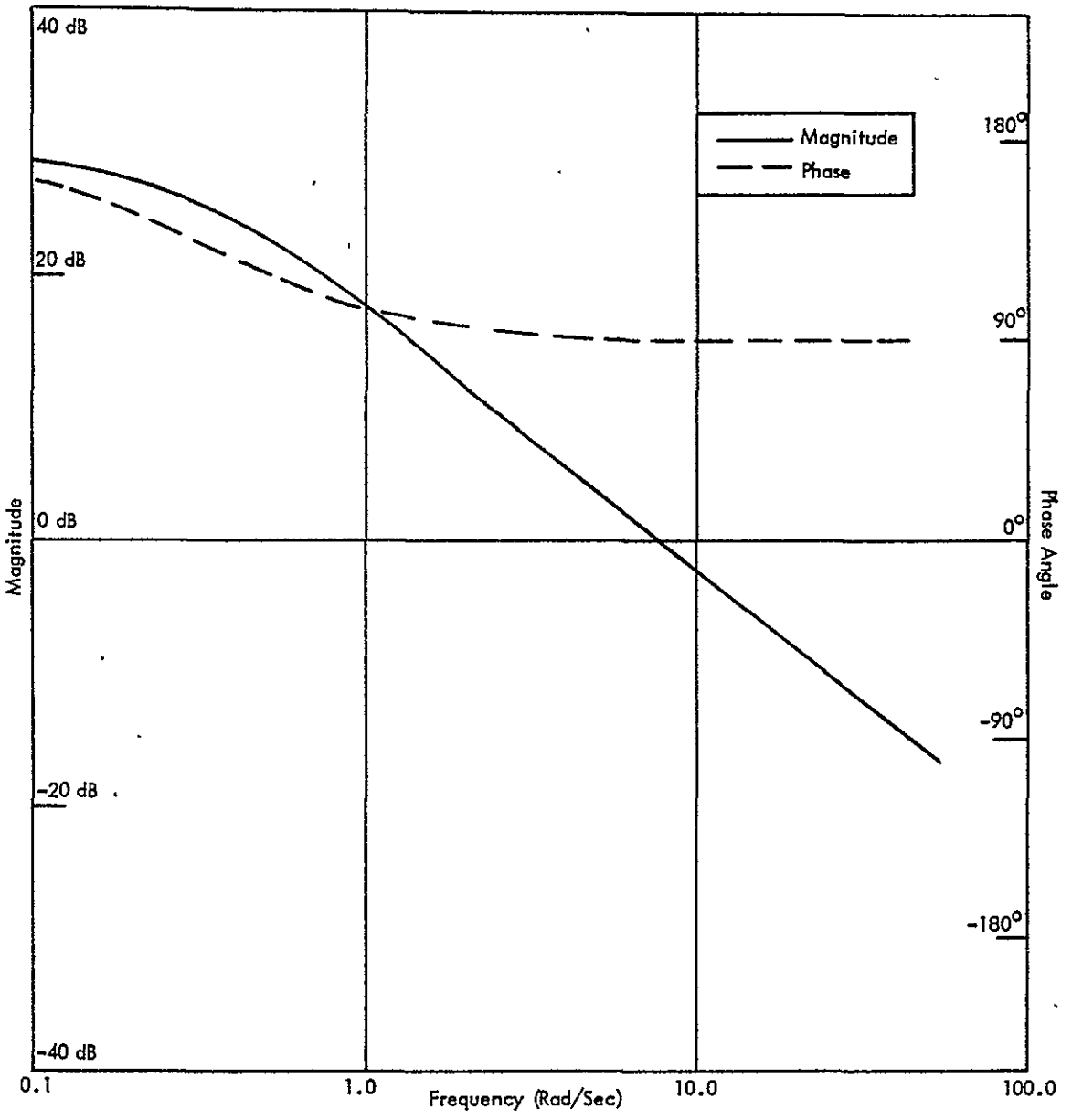

Figure 10. Open-Loop Frequency Response for Unaugmented CH-47 Vertical Control - System A, Hover.

(a) V_z/δ_c.

C-2

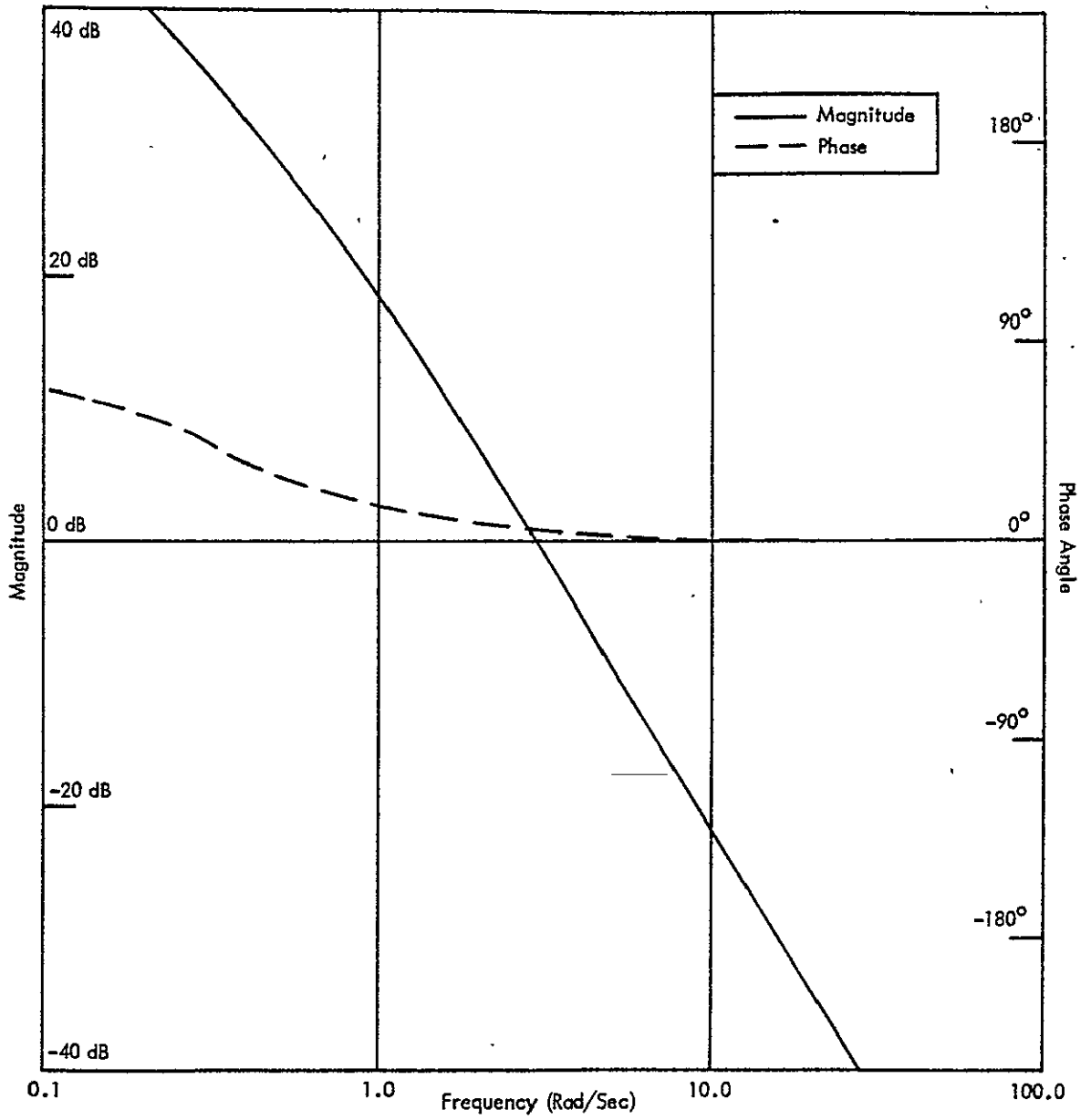

Figure 10. (b) z/δ_c.

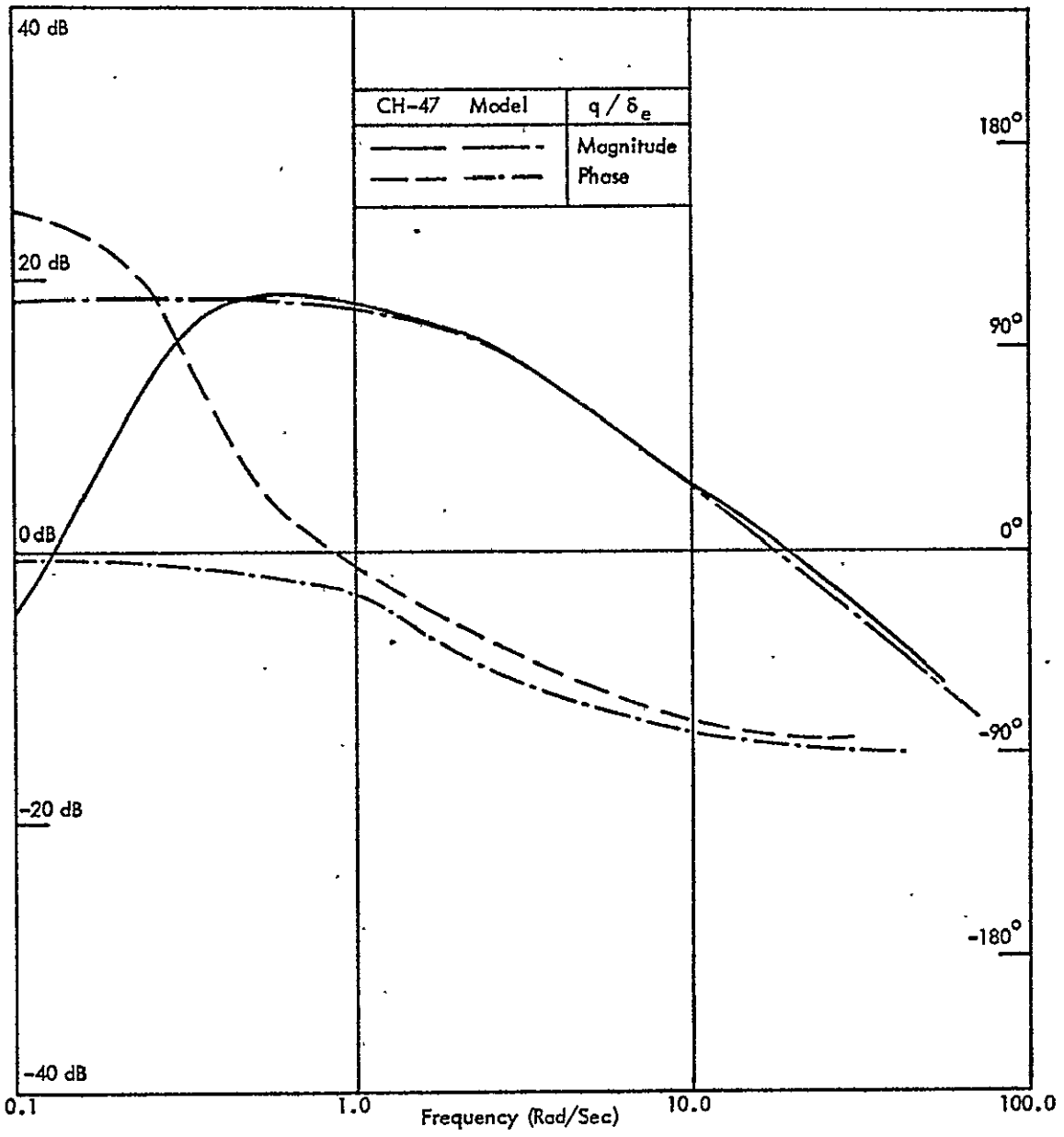

Figure 11. Closed-Loop Pitch Rate Control Response - System B; Hover.

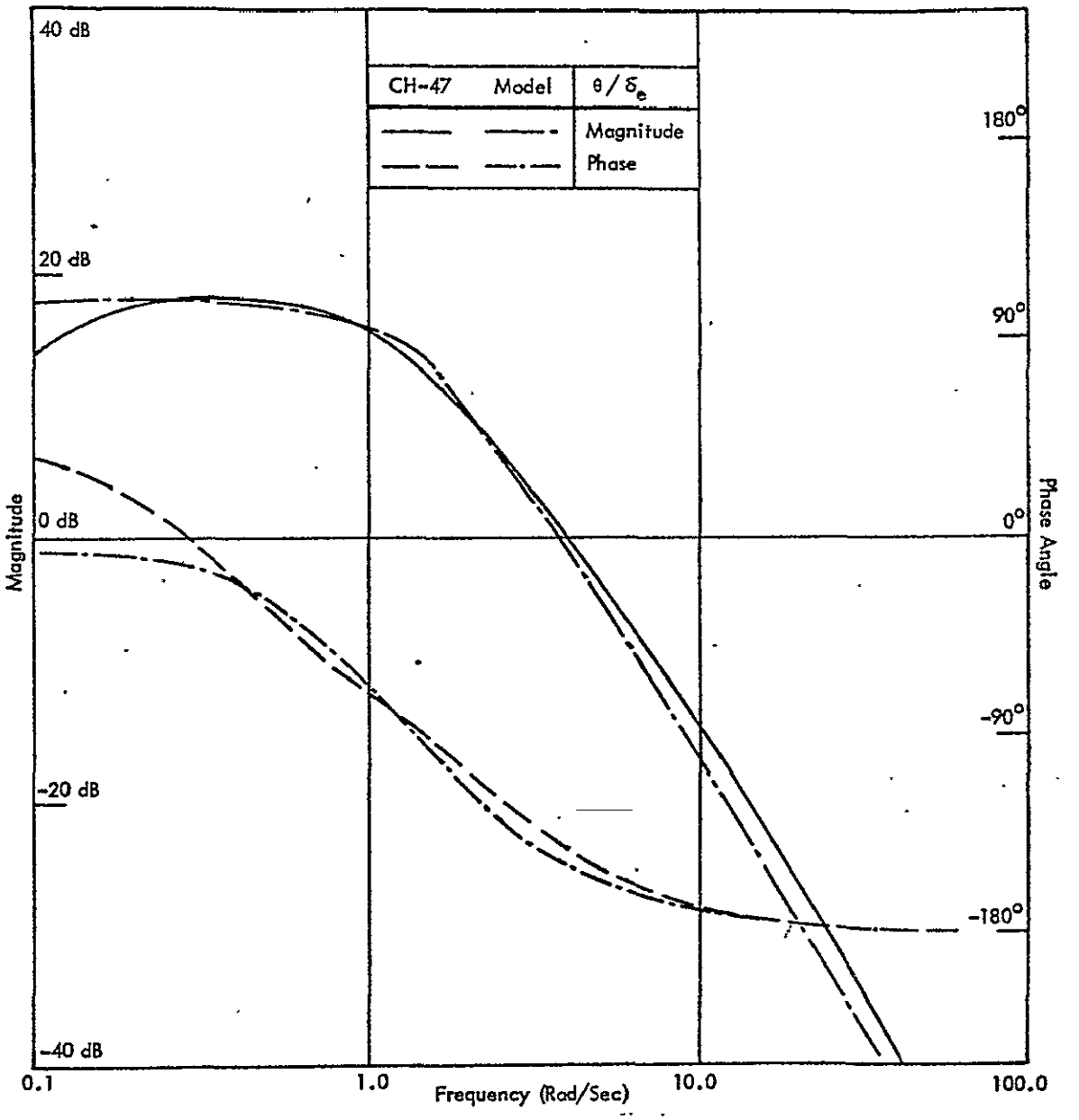

Figure 12. Closed-Loop Pitch Attitude Control Response - Systems C, D; Hover.

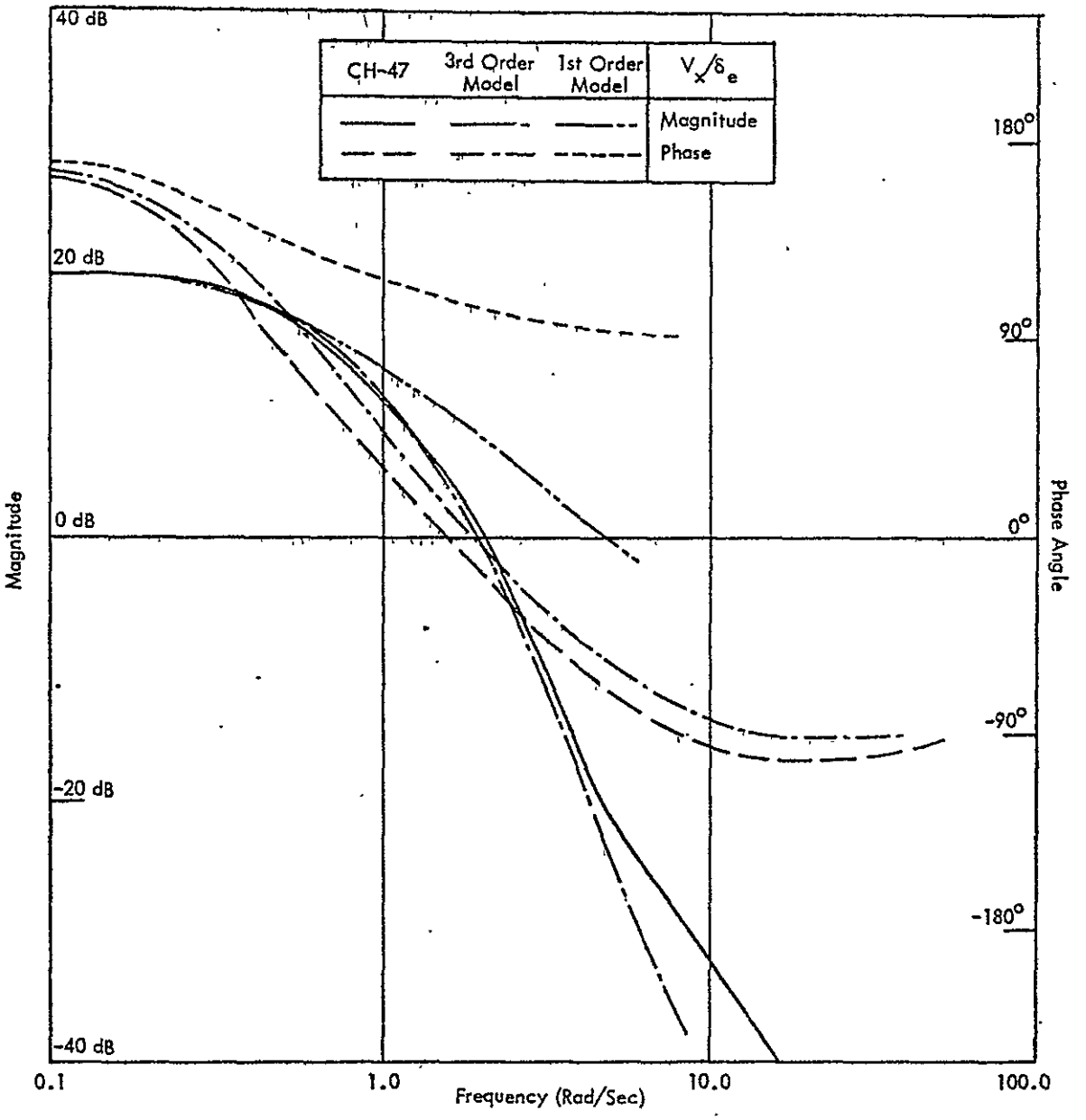

Figure 13. Closed-Loop Forward Velocity Control Response - System F; Hover.

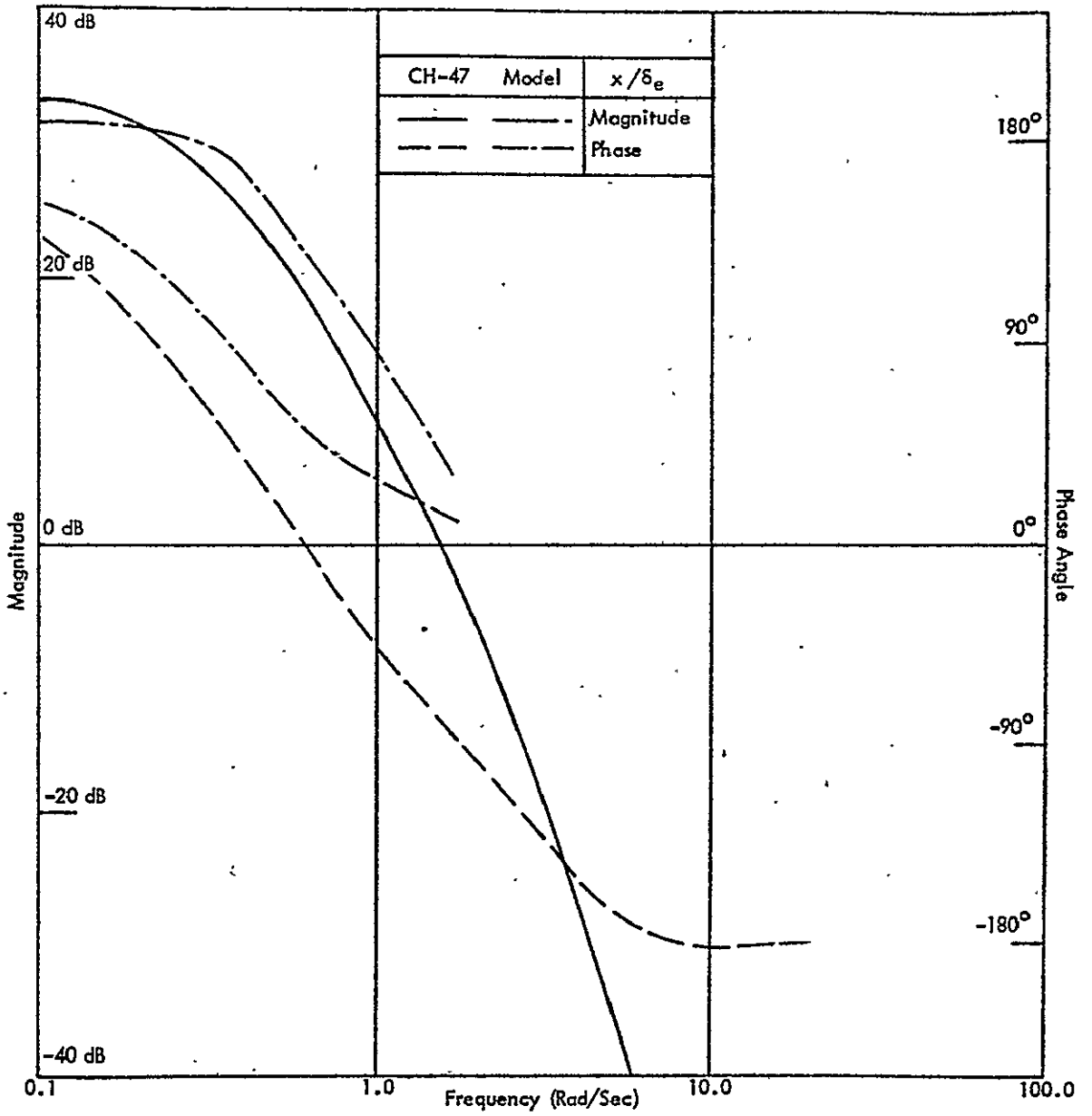

Figure 14. Closed-Loop Forward Position Control Response - Systems G, H; Hover.

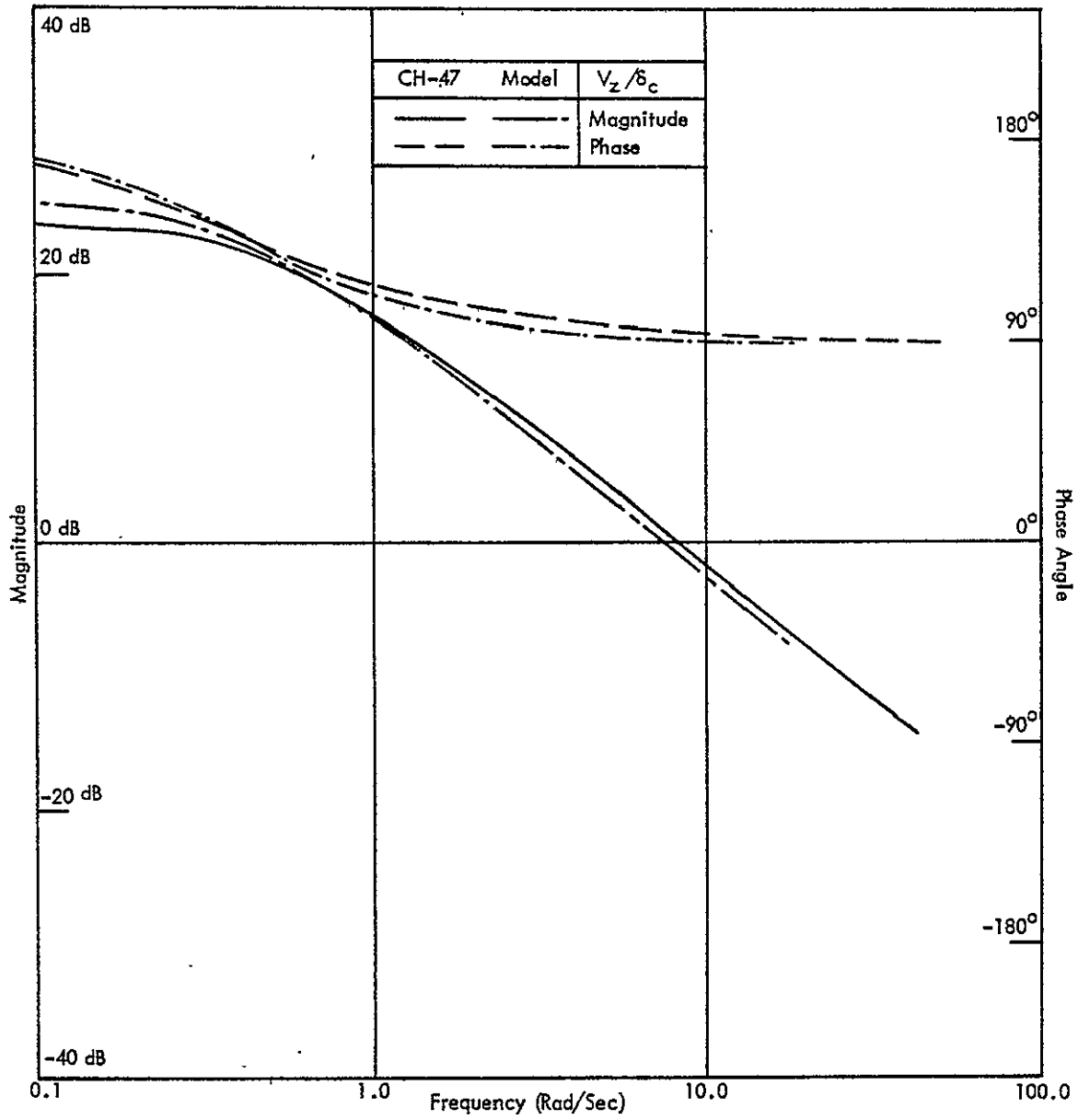

Figure 15. Closed-Loop Vertical Velocity Control Response - System F; Hover.

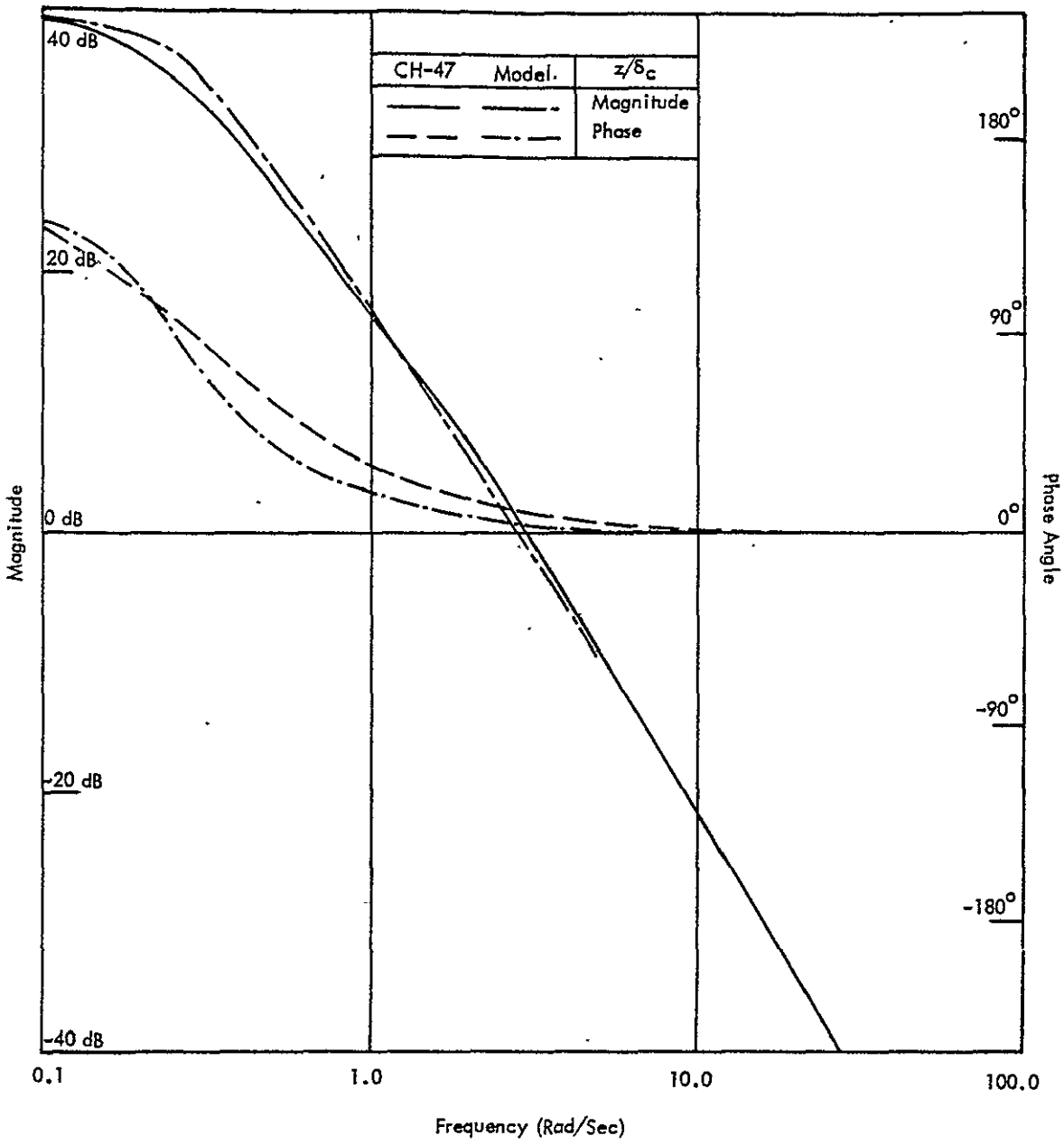

Figure 16. Closed-Loop Altitude Control Response - Systems E, G, H; Hover.

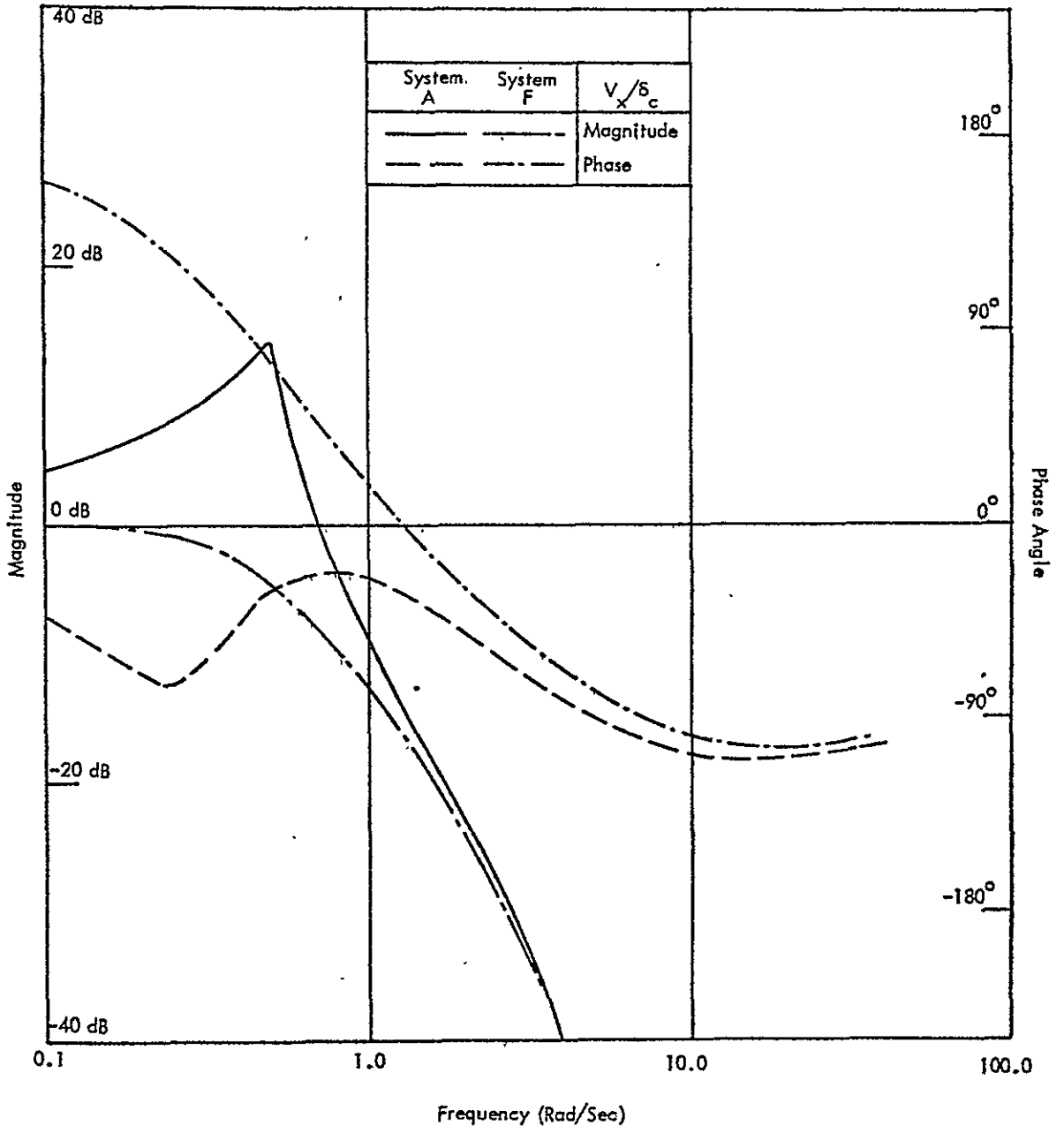

Figure 17. Closed-Loop Cross-Channel Control Coupling Response - System F, Hover. (a) V_x/δ_c.

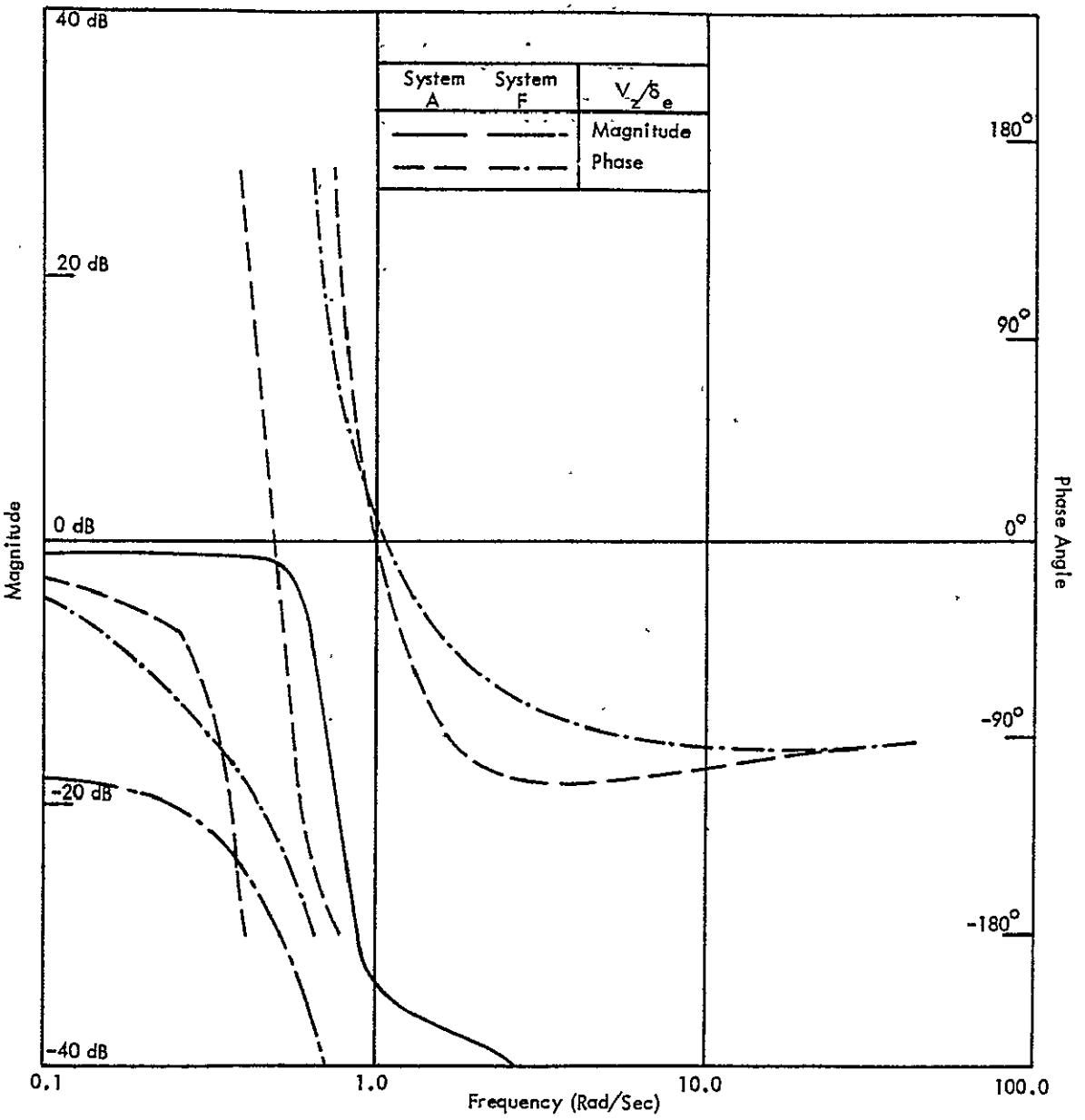

Figure 17. (b) V_z/δ_e.

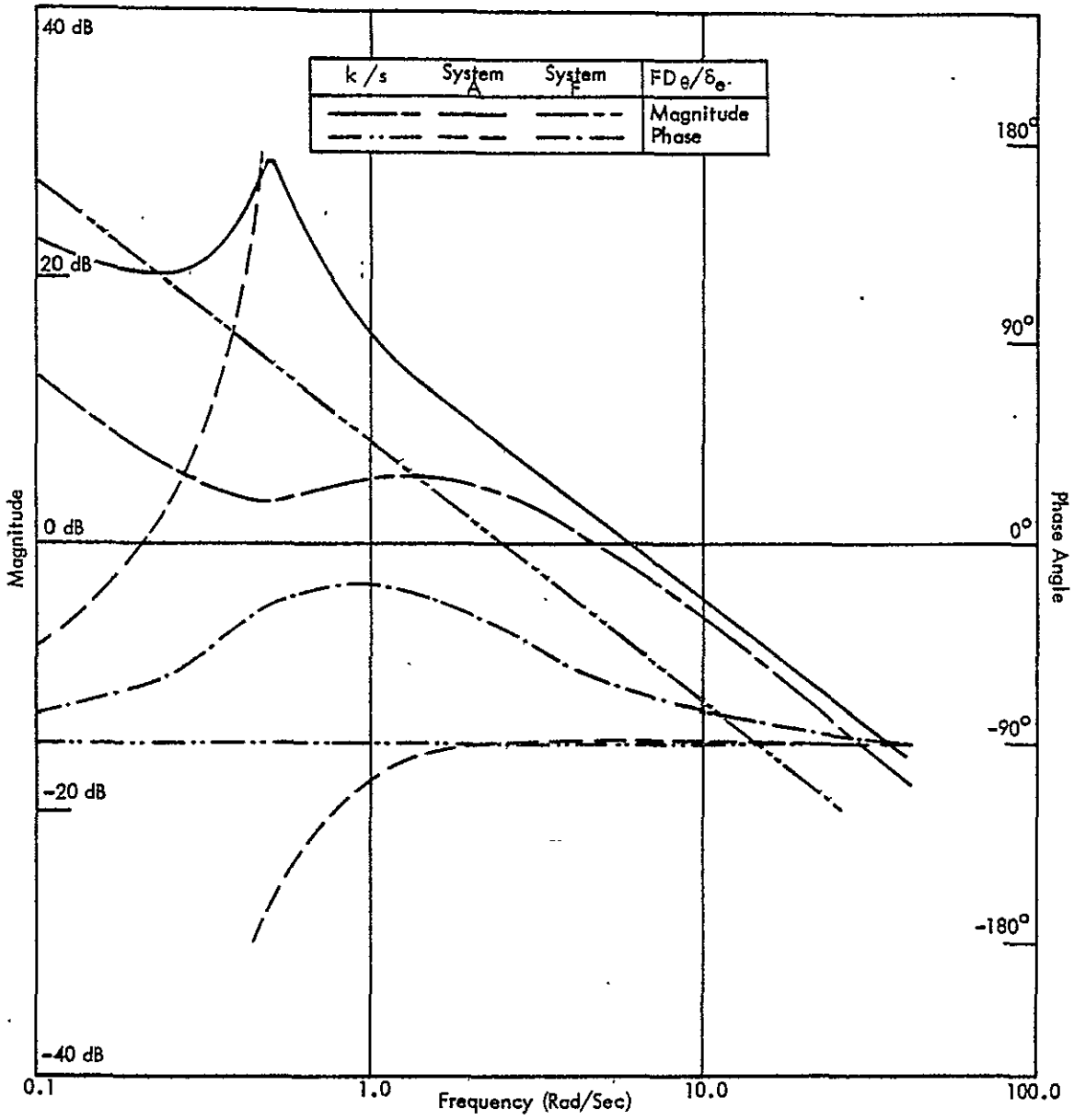

Figure 18. Composite Vehicle-Flight Director Longitudinal Response - Systems A, F; Hover.

(a) FD_θ/δ_e.

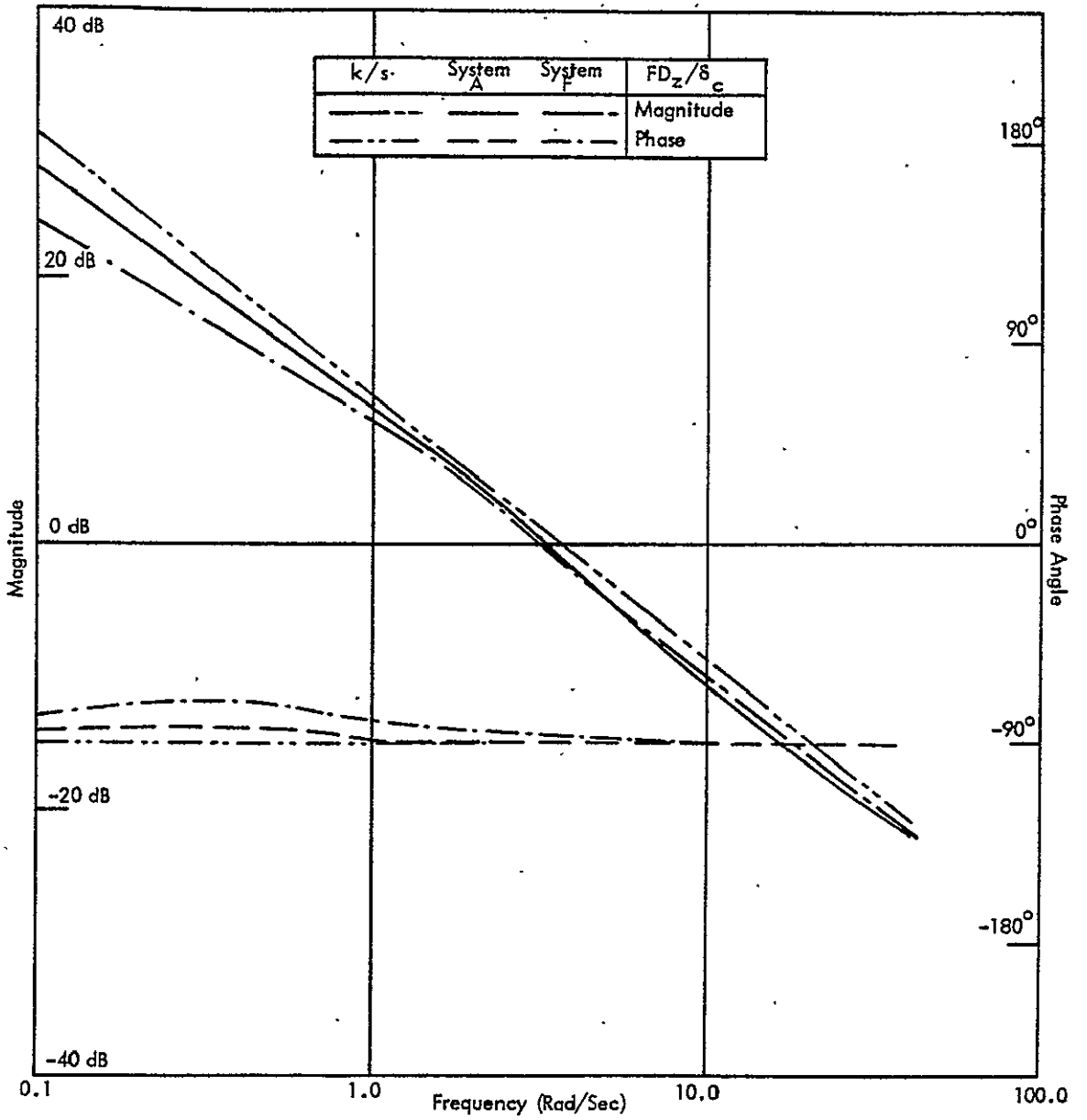

Figure 18. (b) FD_z/δ_c.

SECTION 4

CH-47 CONTROL/MONITORING APPLICATION

The previous sections described the modeling methodology that serves as the basis for a systematic procedure for evaluating competing VTOL control/display system configurations. In this section, these techniques are applied to the CH-47 helicopter in order to evaluate control and monitoring performance for candidate control systems. Our objective is to determine one or more control/display configurations that will provide acceptable performance over a range of flight conditions (see Table 5):

- Hover
- Straight Approach (3^{o}, 6^{o}, 9^{o})
- Spiral Approach
- Cruise

Our approach is to analyze first the most difficult piloting task, i.e., hover. Those configurations that are acceptable at hover will be studied further at the other flight conditions. The analysis will consider both longitudinal and lateral control in a decoupled manner, as in the previous section. The evaluation process will follow the procedure outlined in Subsection 2.1, specifically as shown in Figure 1 and Table 1.

4.1 FORMULATION AND INFORMATION REQUIREMENTS

The first phase of the evaluation process consists of several steps leading to the choice of a candidate control/display system. As noted earlier, this selection process may be conducted independent of the main thrust of the evaluation methodology. However, for completeness, a subset of design algorithms that can be used to develop candidate control/flight-director laws are included in Subsections 3.1 and 3.2. Their application to the CH-47 vehicle is presented in Subsection 3.3.

The control performance requirements of the pilot-vehicle combination are specified in terms of allowable RMS deviations, $x_{i,max}$, for the vehicle states. These design specifications are generally a function of mission requirements or flight conditions. Thus, Table 12 shows separate specifications for hover, approach and cruise. It should be noted that the design tolerances for approach are the same as those for cruise. In a more general analysis these tolerances would vary continuously from initial (cruise) values to final (hover) values. Our present analysis technique, being static in nature, does not allow for time-varying weightings. Thus, equating approach to cruise tolerances effectively means the results are applicable primarily to the first portion of the approach.† The values of $x_{i,max}$ in Table 12 are needed in various steps of the design process including flight director design, pilot modeling and performance evaluation.

Table 12. Performance Specifications for CH-47.

	Variable	Units	Desired RMS level; $x_{i,max}$		
			Hover	Approach	Cruise
Longitudinal	x	ft	5	25	25
	V_x	ft/sec	1	2.5	2.5
	z	ft	5	25	25
	V_z	ft/sec	1	2.5	2.5
	θ	deg	1	1	1
	q	deg/sec	0.5	0.5	0.5
Lateral	y	ft	5	25	25
	V_y	ft/sec	1	2.5	2.5
	ψ	deg	1	2	2
	$\dot{\psi}$	deg/sec	0.5	1	1
	ϕ	deg	1	2	2
	$\dot{\phi}$	deg/sec	0.5	1	1

†In retrospect, selecting (constant) approach weights as the average of hover and cruise values seems a more logical choice for the preliminary analysis. In any case, prior to simulator or flight tests, a more thorough evaluation should analyze a series of points along the approach path.

Eight levels of automation have been selected in Subsection 3.3 as candidates for the CH-47 helicopter (Table 7). These systems span a range from the unaugmented vehicle, through attitude and velocity command, to a fully automated (position command) system. The choices were motivated by past VTOL control system studies (References 14, 15, and 21), and via discussions with NASA personnel involved in the VALT program. They are listed in Table 7 in order of increasing control automation from A to H.

The design of candidate control systems that realize each of the automation levels B to H is developed in Subsection 3.3. Note that for a given automation level, the control system parameters will be a function of the flight conditions. Thus, some form of adaptation might be required to implement the control system design on the actual aircraft. Appendix A gives the control system feedback gains L_{cs} and closed-loop dynamics A_0 for system F at hover.

Flight director laws were not specified a priori for any of the systems A through H. Thus, it was necessary to apply the flight director design procedure developed in Subsection 3.2 to the CH-47. As noted earlier, the status information y_s that is assumed to be observed by the pilot is

$$y_s = [x, V_x, z, V_z, \theta, q]' \qquad \text{longitudinal axis}$$

$$y_s = [y, V_y, \phi, \dot{\phi}, \psi, \dot{\psi}]' \qquad \text{lateral axis}$$

It is convenient to order the vehicle states x_i on a one-to-one basis with the status variables y_{si}. Thus, the design parameters $y_{si,max}$ to be used in Equation (93) are simply those given in Table 12. The design values $\dot{u}_{i,max}$, needed in Equation (94), are selected on the basis of human response limitations as discussed in Subsection 2.2.3. For the CH-47, $\dot{u}_{i,max} = 2$ in/sec has been selected for all control inputs.

Application of the flight director design process to the CH-47 is described in Subsection 3.3. As is the case with the control system parameters, the flight director gains (for a given automation level) change with flight condition. The complete results for candidate System F, including the values for $|FD_{i,max}|$, and the indifference thresholds on $FD_i(t)$, are given in Appendix A.

The final step in the formulation and information requirements phase is the selection of display information. For each automation level we consider four possibilities:

1. Status information only with no flight director signals
2. Status information plus longitudinal flight directors only
3. Status information plus lateral flight directors only
4. Status information with both longitudinal and lateral flight directors.

In accordance with human response theory, explicit display indicators are not required for the status variable rates, V_x, q, etc.† Thus, the display indicators are:

x, z, θ for longitudinal axis

y, ϕ, ψ for lateral axis

plus any additional flight director signals as specified. The display information base is thus given in the requisite form:

$$y = C_0 x + D_0 u$$

along with the indifference thresholds a_i, as the outcome of the computational process of Figure 8.

4.2 PERFORMANCE COMPUTATIONS

For each flight condition, each level of automation and each display choice, it is necessary to apply the optimal control pilot model to obtain the tradeoff curve

†Recall that the rate information V_x, q, etc., is obtained from the positional variables x, θ, etc.

(Figure 2) for control performance P_c versus control workload f_c. For the CH-47 application, there is a maximum of 6 x 8 x 4 = 192 such curves that need to be obtained. Clearly this is an overwhelming amount of data to assimilate which, fortunately, can be significantly reduced. We will consider first the hover flight condition, as this represents the most difficult piloting task. Thus, only those control/display configurations that are acceptable at hover need to be analyzed further at the other flight conditions. We also note that by considering longitudinal and lateral control tasks separately the computational burdens are reduced further due to repetitions in the automation choices. The unique choices are:

Longitudinal Systems: A, B, C/D, E, F, G/H

Lateral Systems: A, B/C/E/G, D/H, F

For each of these control configurations we have two possible display configuration --- with or without flight director indicators. Thus, at hover we need to compute 6 x 2 = 12 tradeoff curves for the longitudinal axis; and 4 x 2 = 8 such curves for the lateral axis.

4.2.1 CONTROL PERFORMANCE RESULTS, HOVER CONDITION

Figures 19 through 22 are the pilot model predictions of control performance P_c versus control workload f_c. Predictions of RMS quantities, σ_{xi}, are obtained from straightforward application of the OCM computer programs using the nominal set of pilot parameters:

τ = time-delay = 0.2 sec

ρ_{yi} = observation noise ratios = -20 dB

ρ_{ui} = motor noise ratios = -25 dB

τ_{Ni} = "neuro-motor" time constants $\geq$ 0.1 sec[†]

[†]With the selected values $\dot{u}_{i,max} = 2$ in/sec, the values of τ_{Ni} were generally ≈ 0.2 sec.

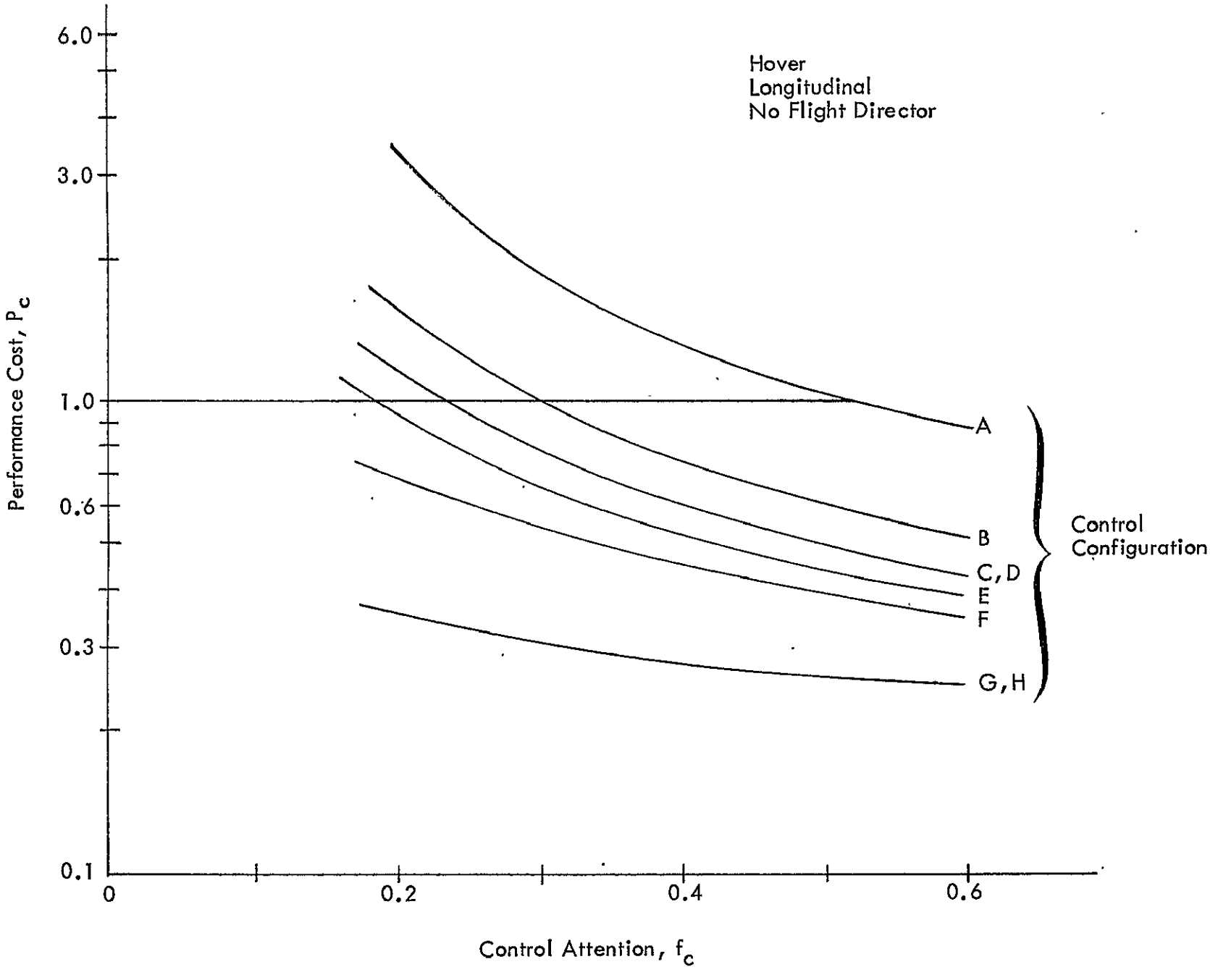

Figure 19. Control Performance Versus Control Attention - Hover, Longitudinal, No Flight Director.

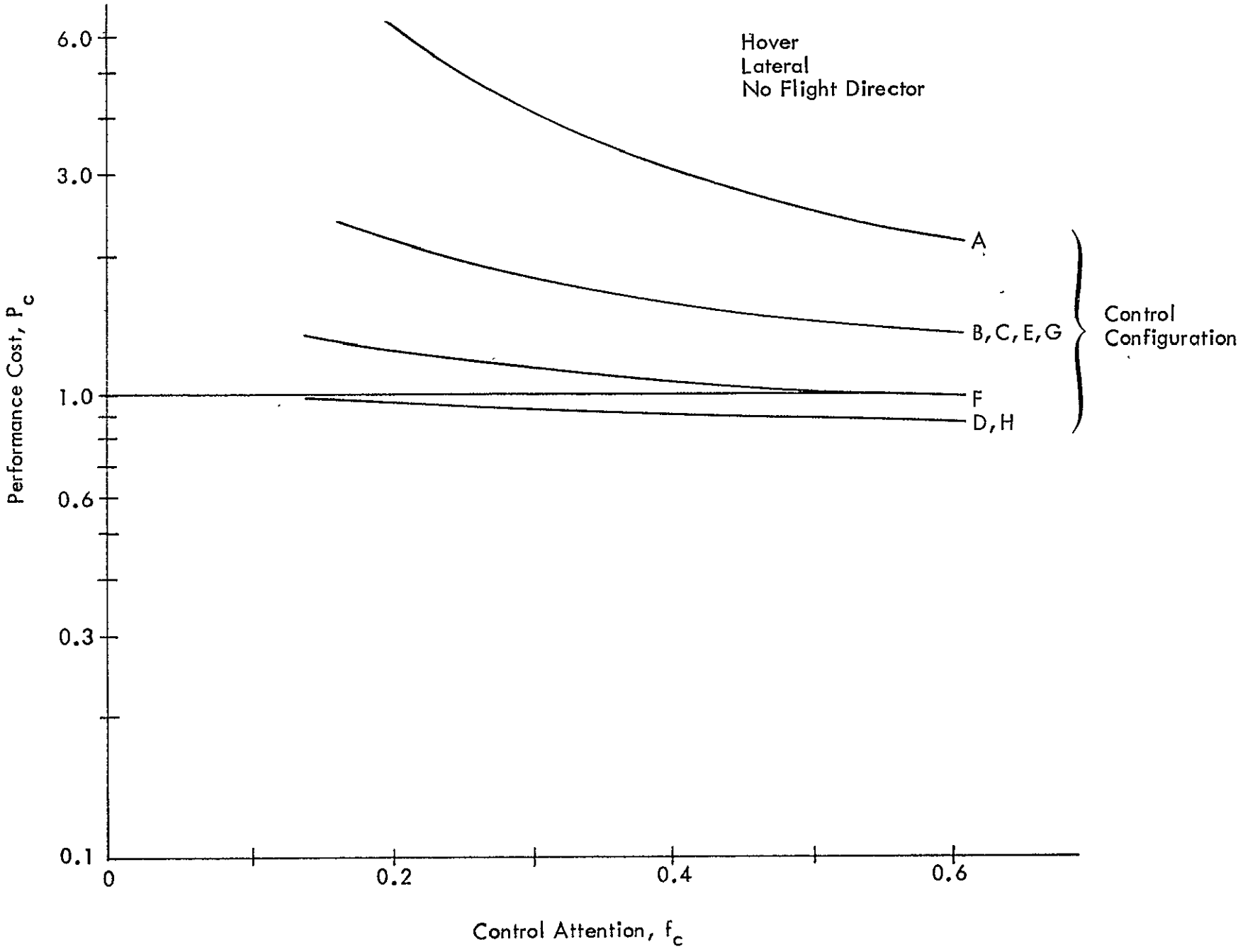

Figure 20. Control Performance Versus Control Attention - Hover, Lateral, No Flight Director.

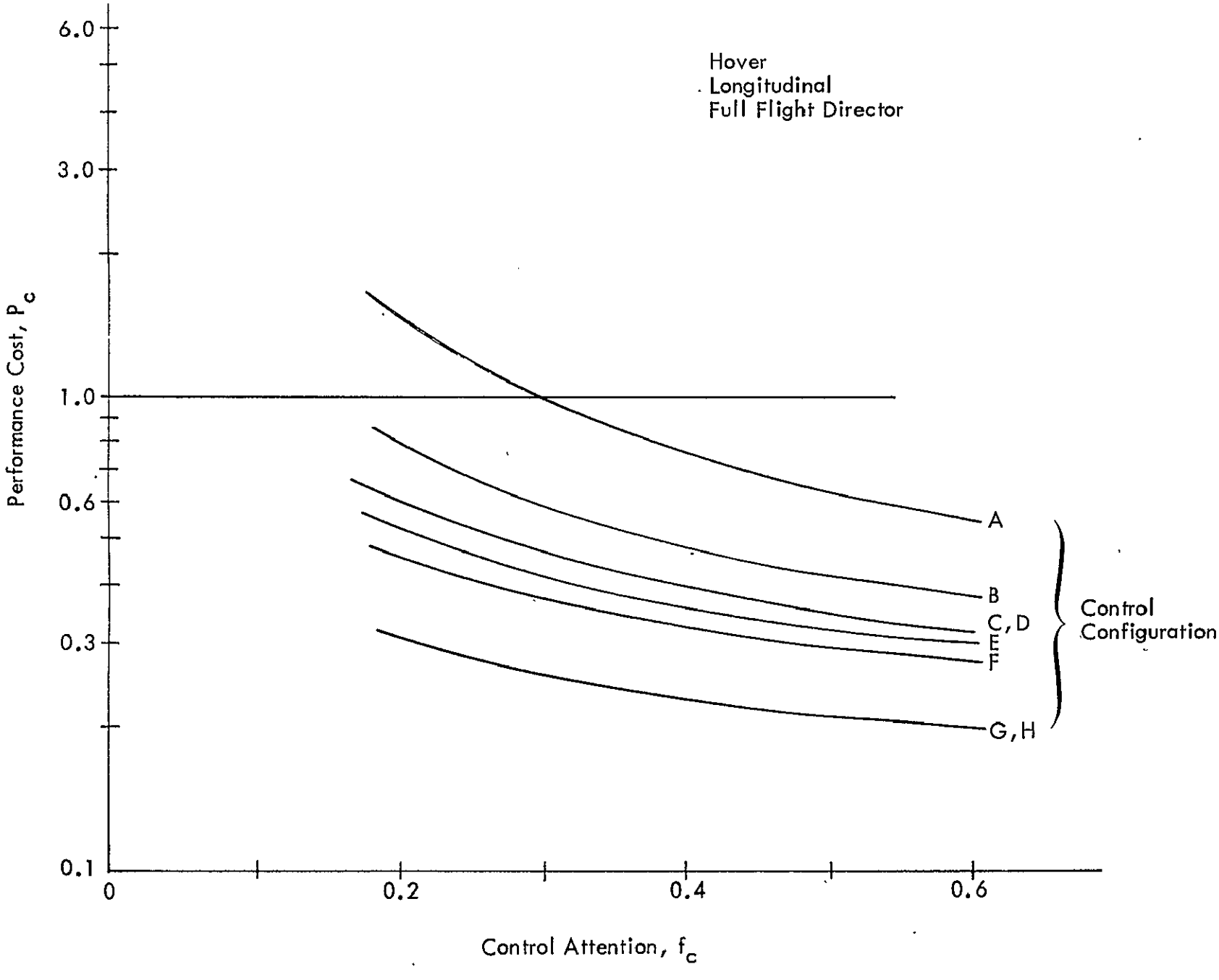

Figure 21. Control Performance Versus Control Attention - Hover, Longitudinal, Full Flight Director.

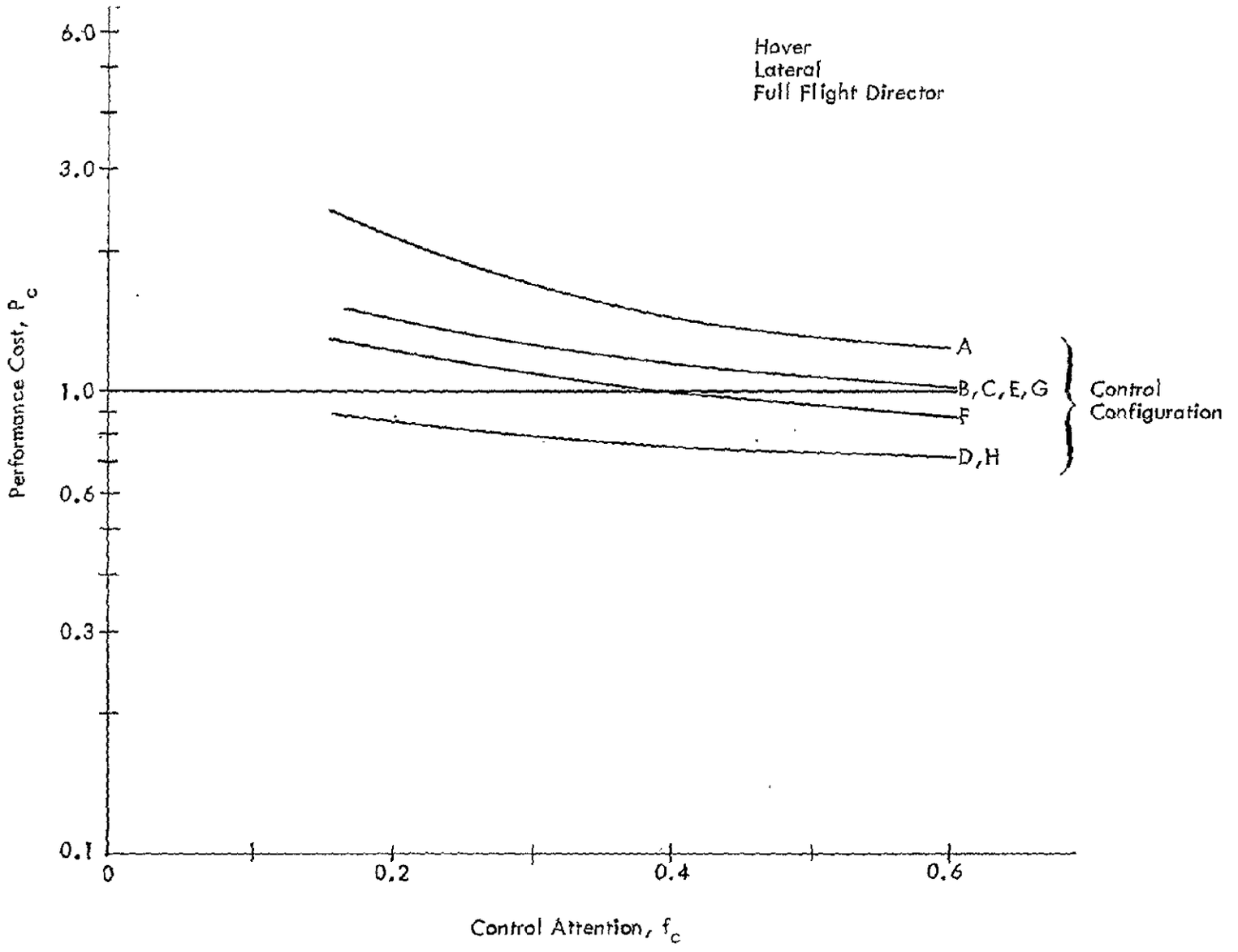

Figure 22. Control Performance Versus Control Attention - Hover, Lateral, Full Flight Director.

The control performance is then computed using Equation (5). For both longitudinal and lateral axes of control there are six terms that enter the summation, as specified in Table 12.

The performance curves have the shapes expected. P_c increases with decreasing control attention, although the rate of increase (i.e., sensitivity to f_c) is somewhat less for the more automated systems. The insensitivity is most evident for the lateral case in System F (velocity command) and Systems D and H (position command), where large changes in f_c have little effect on P_c.

As expected, P_c decreases with increasing automation at a fixed level of attention. This is also true with respect to increasing display automation, i.e., adding flight directors. In comparing Figure 19 and Figure 21 with Figure 20 and Figure 22, respectively, we see that the flight directors provide the most benefit to those systems with the least control automation. Very little benefit is provided to the full position command System H. Thus, there is a clear tradeoff between control and display automation, at the same performance level.

4.2.2 ESTABLISH WORKLOAD REQUIREMENTS, $f_{c,req}$

For each control/display configuration it is necessary to determine the workload required $f_{c,req}$ to achieve a performance level $P_{c,max} = 1.0$. Those systems for which $f_{c,req} < f_T = 0.8$ are candidates for further evaluation using the monitoring models with

$$f_{m,avail} = f_T - f_{c,req}$$

Values of f_c that yield $P_c = 1.0$ are read easily from Figures 19 through 22, for lateral and longitudinal axes separately. Thus, the total workload is

$$f_{c,req} = f_{c,req}\Big|_{\text{Longitudinal}} + f_{c,req}\Big|_{\text{Lateral}}$$

Table 13 presents the complete summary of control and monitoring workloads for the hover task. As can be seen, only the two Systems D and H convincingly meet the requirement $f_{m,avail} > 0$. A third System, F, is acceptable provided the lateral flight director is used. The reason that only three of eight possible control configurations are acceptable is due primarily to the lateral response characteristics of the CH-47. The highest levels of automation are required in the lateral axis to meet performance specifications. Thus, Systems D and H have full lateral position command, while System F requires a flight director in addition to its velocity command. The attitude (ϕ) command system in the lateral axis (Systems B, C, E and G), even with flight director augmentation, requires an excessive workload level (0.65).

Of the $8 \times 4 = 32$ possible combinations of control/display configurations, we have selected three as candidates for further evaluation. They are:

(I) System D with longitudinal flight directors only

(II) System F with lateral flight directors only

(III) System H with no flight directors

The decisions to omit various flight directors were based on the sensitivities of $f_{m,avail}$ in Table 13. Clearly, the flight directors provide little, if any, benefit in the highly automated System H. Their use would probably not outweigh the added complexity they require in implementation. This same reasoning was used to omit the longitudinal flight directors in System F and the lateral directors for System D. Lateral flight directors are essential in System F; the longitudinal directors in System D appear to be highly advantageous, increasing $f_{m,avail}$ from 0.41 to 0.57.

4.2.3 SYNTHESIS OF SYSTEM F1

From the results of Figures 19 through 22, and the composite summary of Table 13, several interesting facts are apparent.

Table 13. CH-47 Control and Monitoring Attention Summaries for Hover.

HOVER	Control System								Flight Director	
	A	B	C	D	E	F	G	H	Long	Lat
	δ_e, δ_c δ_a, δ_r	$\dot{\theta}$, δ_c ϕ, ψ	θ, δ_c ϕ, ψ	θ, δ_c y, ψ	θ, z ϕ, ψ	V_x, V_z V_y, ψ	x, z ϕ, ψ	x, z y, ψ	FD_θ, FD_z	FD_ϕ FD_ψ
$f_{c,long}$	0.52	0.31	0.24	0.24	0.19	0.10	0.03*	0.03*	None	None
$f_{c,lat}$	-	-	-	0.15	-	-	-	0.15		
$f_{c,req}$	-	-	-	0.39	-	-	-	0.18		
$f_{m,avail}$	-	-	-	0.41	-	-	-	0.62		
$f_{c,long}$	0.30	0.15	0.08	0.08	0.05*	0.05*	0.05*	0.05*	Full	None
$f_{c,lat}$	-	-	-	0.15	-	-	-	0.15		
$f_{c,req}$	-	-	-	0.23	-	-	-	0.20		
$f_{m,avail}$	-	-	-	0.57	-	-	-	0.60		
$f_{c,long}$	0.52	0.31	0.24	0.24	0.19	0.10	0.03*	0.03*	None	Full
$f_{c,lat}$	-	0.65	0.65	0.12	0.65	0.45	0.65	0.12		
$f_{c,req}$	-	0.96	0.89	0.36	0.84	0.55	0.68	0.15		
$f_{m,avail}$	-	-	-	0.44	-	0.25	0.12	0.65		
$f_{c,long}$	0.30	0.15	0.08	0.08	0.05*	0.05*	0.05*	0.05*	Full	Full
$f_{c,lat}$	-	0.65	0.65	0.12	0.65	0.45	0.65	0.12		
$f_{c,req}$	-	0.80	0.73	0.20	0.70	0.50	0.70	0.17		
$f_{m,avail}$	-	0.00	0.07	0.60	0.10	0.30	0.10	0.63		

*Minimum control attention of 0.01 on each instrument, see Equation (43).

- High levels of control/display automation are needed in the lateral axis, with Systems D/H requiring least workload.
- In the longitudinal axis, Systems B through H all provide acceptable performance with low workload requirements, provided flight directors are used.
- For the longitudinal axis, large increases in $f_{c,req}$ result for Systems B through E when the flight directors are removed. Systems F and H are indifferent to the use of longitudinal flight directors.
- System F (longitudinal) with no flight director performs comparably to Systems B through E with flight directors.

On the basis of these facts it appears that an attractive control configuration would be a full position command system in the lateral axis, with velocity command for the longitudinal axis (i.e., a combination of longitudinal System F and lateral System H). We will define this configuration as System F1. As seen in Table 14, no flight director is necessary for acceptable performance. This configuration provides acceptable performance using $\dot{f}_{c,req} = 0.25$, leaving $f_{m,avail} = 0.55$ for monitoring. We have,

Table 14. Control and Monitoring Attention for System F1 at Hover.

Hover	Control System F1 V_x, V_z, y, ψ	Flight Director
$f_{c,long}$	0.10	None
$f_{c,lat}$	0.15	
$f_{c,req}$	0.25	
$f_{m,avail}$	0.55	

therefore, synthesized a fourth candidate configuration for further evaluation:

(IV) System F1 with no flight directors

This choice provides slightly less $f_{m,avail}$ compared to System H, which is more automated. However, it provides more $f_{m,avail}$ than System F by using one more level of

control automation in lieu of display augmentation. Systems F1 and D are the two candidates for which the workload requirements $f_{c,req}$ are nearly equal (i.e., balanced) for both axes.

The System F1 was not one of the originally suggested control configurations. It is a hybrid system, pieced together from only the results of Table 13. No further computations using the OCM were necessary. Of course, this was possible only because lateral and longitudinal axes have been decoupled. Thus, there is an interesting sidelight to our design/evaluation technique—the ability to easily propose and evaluate alternate configurations, provided they are hybrid combinations of systems already under study.

4.2.4 PREDICTION OF MONITORING PERFORMANCE

Having determined those control/display configurations that yield acceptable performance with $f_{c,req} < 0.8$, the next step in the design process is to evaluate the monitoring performance that is achieved with the available f_m. Subsections 2.3 and 2.4 describe the monitoring model used in the present study. In addition to the monitoring performance metric P_m, the model generates the following predictions for each display indicator:

f_{m_i} = attention allocations for monitoring

$g_{f_{m_i}} = \partial J_m / \partial f_{m_i}$ = gradient components

k_i = monitoring error fractions

$E(1/2)$ = percentage estimation error

The total attention to display indicator i is obtained by combining the control and monitoring components, viz

$$f_{T_i} = f_{c_i} + f_{m_i}$$

Table 15 gives an overview that lists P_c, $f_{c,req}$, $f_{m,avail}$ and P_m for the four configurations under study. Tables 16 through 19 give the detailed results of applying the monitoring model to Configurations I through IV as specified above. These tables also contain a summary of the OCM control performance predictions.

Table 15. Performance Summary at Hover.

Configuration	Description	P_c	$f_{c,req}$	$f_{m,avail}$	P_m
I	D, Long. FD	1.0	0.23	0.57	0.40
II	F, Lateral FD	1.0	0.55	0.25	0.58
III	H, No FD	1.0	0.18	0.62	0.375
IV	F1, No FD	1.0	0.25	0.55	0.374

These results reveal that all configurations, with the exception of II (System F with lateral flight director), achieve $P_m \leq 0.4 = P_{m,des}$. For these cases, the average estimation errors are no greater than $\sigma_{y_i}/2$ for 20 percent of the time. Configuration II has $P_m = 0.58$. This is due, in part, to the low $f_{m,avail}$, which in the longitudinal axis results in each $k_i > 0.43$. For all configurations the error fraction k_ψ for monitoring heading exceeds 0.6. This does not imply poor performance, but rather is due to the heading hold augmentation keeping ψ errors to less than 0.1 deg — well below the visual/indifference threshold of 0.25 deg. None of the other vehicle states or outputs exhibit this phenomenon. Indeed, for most system variables we see that $\sigma_{x_i} \approx x_{i,max}$ as anticipated. This is a consequence of the selection $P_{c,max} = 1$, and the tendency of optimal LQG systems to distribute their errors inversely as $(Q_x)_{ii}$.

Configurations I and II use flight director augmentation to meet control requirements. As described in Subsections 2.3 and 2.4, these signals are not used for

Table 16. Configuration I, Model Predictions at Hover.

Output i	y_{RMS}	$-g_{f_{c_i}}$	f_{c_i}	f_{m_i}	f_{T_i}	$-g_{f_{m_i}}$	k_i	E(1/2)
x	5.61	0.8	0.01	0.04	0.10	0.56	0.320	11.8
V_x	1.14	18.6				0.68		
z	3.19	11.5	0.01	0.12	0.13	0.58	0.384	19.3
V_z	0.936	51.8				0.63		
θ	0.894	25.0	0.01	0.08	0.09	0.69	0.469	28.7
$\dot{\theta}$	0.710	12.5				0.55		
FD_θ	0.359	76.2	0.05	-	0.05	-	0.946	59.7
$\dot{FD}_\theta$	1.23	4.3						
FD_z	0.465	68.0	0.02	-	0.02	-	0.677	46.0
$\dot{FD}_z$	0.313	39.6						
y	5.12	0.16	0.125	0.27	0.40	0.17	0.192	1.0
V_y	1.03	3.5				0.71		
ϕ	1.55	0.12	0.015	0.01	0.02	0.13	0.195	1.0
$\dot{\phi}$	0.577	0.45				0.20		
ψ	0.0865	~ 0	0.01	0.01	0.02	~ 0	0.639	43.4
$\dot{\psi}$	0.0515	~ 0				~ 0		

Table 17. Configuration II, Model Predictions at Hover.

Output i	y_{RMS}	$-g_{f_{c_i}}$	f_{c_i}	f_{m_i}	f_{T_i}	$-g_{f_{m_i}}$	k_i	E(1/2)
x	6.15	4.8	0.053	0.044	0.097		0.431	24.6
V_x	1.11	29.1				2.0		
z	3.39	7.9	0.03	0.057	0.087	2.3	0.516	33.2
V_z	0.924	29.7				2.1		
θ	0.798	15.6	0.017	0.019	0.036	0.76	0.468	28.5
$\dot{\theta}$	0.564	6.0				0.76		
y	5.26	0.04	0.06	0.09	0.15	0.72	0.333	13.3
V_y	1.01	2.75				6.5		
ϕ	1.54	0.03	0.01	0.017	0.027	0.95	0.220	2.3
$\dot{\phi}$	0.672	0.46				1.1		
ψ	0.0576	~0	0.01	0.015	0.025	~0	1.12	65.6
$\dot{\psi}$	0.0487	~0				~0		
FD_ϕ	0.195	2.67	0.35	-	0.35	-	0.957	60.1
$\dot{FD}_\phi$	1.62	0.31						
FD_ψ	0.0443	~0	0.02	-	0.02	-	1.47	73.4
$\dot{FD}_\psi$	0.190	0.03						

Table 18. Configuration III, Model Predictions at Hover.

Output i	y_{RMS}	$-g_{f_{c_i}}$	f_{c_i}	f_{m_i}	f_{T_i}	$-g_{f_{m_i}}$	k_i	E(1/2)
x	4.81	12.5	0.01	0.1	0.11	0.40	0.272	6.65
V_x	0.763	15.2				0.45		
z	3.28	8.4	0.01	0.13	0.14	0.40	0.329	12.9
V_z	0.80	27.2				0.41		
θ	0.559	0.45	0.01	0.07	0.08	0.30	0.425	23.9
$\dot{\theta}$	0.369	0.87				0.53		
y	5.12	0.16	0.125	0.27	0.4	0.17	0.192	1.0
V_y	1.03	3.5				0.71		
ϕ	1.55	0.12	0.015	0.016	0.03	0.13	0.195	1.0
$\dot{\phi}$	0.577	0.45				0.20		
ψ	0.0865	~0	0.01	0.014--0.024		~0	0.639	43.4
$\dot{\psi}$	0.0515	~0				~0		

Table 19. Configuration IV, Model Predictions at Hover.

Output i	y_{RMS}	$-g_{f_{c_i}}$	f_{c_i}	f_{m_i}	f_{T_i}	$-g_{f_{m_i}}$	k_i	E(1/2)
x	6.15	4.8	0.053	0.1	0.153	0.39	0.284	7.85
V_x	1.11	29.1				0.44		
z	3.39	7.9	0.03	0.14	0.17	0.38	0.335	13.5
V_z	0.924	29.7				0.41		
θ	0.798	15.6	0.017	0.05	0.067	0.37	0.410	22.3
$\dot{\theta}$	0.564	6.0				0.44		
y	5.12	0.16	0.125	0.27	0.4	0.17	0.192	1.0
V_y	1.03	3.5				0.71		
ϕ	1.55	0.12	0.015	0.01	0.02	0.13	0.195	1.0
$\dot{\phi}$	0.577	0.45				0.20		
ψ	0.0865	~ 0	0.01	0.01	0.02	~ 0	0.639	43.4
$\dot{\psi}$	0.0515	~ 0				~ 0		

monitoring. However, it is often suggested that one purpose of monitoring the status variables is to crosscheck the flight director signals. The error fractions k_{FD} in Tables 16 and 17 show that it is quite difficult to estimate FD(t) from the status variables x, V_x, z, etc. The values $k_{FD} \approx 1$, which gives $E(1/2) \approx 60$ percent. This poses a potential problem for flight director use, namely that it may be very difficult to detect certain failures or malfunctions in the Systems D and F.

The attention allocations f_{c_i} and f_{m_i} show the relative importance of each display indicator to the control and monitoring tasks, respectively. In the OCM it is assumed that position and rate information are obtained simultaneously from a single indicator. We can determine which type (i.e., position or rate) of information is most important via the gradient terms $\partial J_c/\partial f_{c_i}$ and $\partial J_m/\partial f_{m_i}$. This gives additional insight to the information requirements of the pilot-vehicle-display system, and could suggest the need for additional display elements.

For the monitoring task, position and rate information show roughly a balance as to their importance over all configurations. Only V_y seems to dominate y for the lateral error indicator. Considering the control task, we see that position information dominates in the flight director signals — as it should. However, rate information V_x, V_y and (to a lesser extent) V_z dominate in the x, z and y position status indicators.† The attitude indicators θ, ϕ and ψ require little f_{c_i} in all cases, with a mix of position and rate importance.

Finally, we note that the ψ flight-director for System F serves no useful purpose. It can be omitted with no change in control/monitoring performance. Partial flight directors have not been studied for System D.

†Thus, we may wish to consider the possibility of separate V_x, V_y and/or V_z indicators in further evaluations.

4.2.5 PERFORMANCE AT OTHER FLIGHT CONDITIONS

The results presented above are for the hover flight condition. To evaluate fully the performance of each candidate system it is necessary to exercise the pilot model at the other five flight conditions. Fortunately, we need consider only those systems that have acceptable performance at hover. These are, in summary:

Longitudinal D with x, θ flight directors
Longitudinal F with no flight director
Longitudinal H with no flight director
Lateral F with ϕ flight director
Lateral D/H with no flight director

Recall that System F1 is the combination of longitudinal F plus lateral D/H.

Figures 23 through 27 show the control performance versus control workload curves for each system over the remaining flight conditions.

- Approach (3°, 9°, 15°)
- Spiral Approach
- Cruise

These figures clearly reveal that all of the candidate systems achieve control performance well below $P_{c,max} = 1$ for any reasonable attention level $f_c > 0.1$. This verifies our hypothesis that the hover flight condition represents the most difficult piloting task.

The results show the relative difficulty (or ease) of the four different approach paths. By considering performance cost at a constant workload level f_c, the following conclusions may be drawn:

- The 3° approach path produces, in relative terms, the most difficult control regulation (i.e., error minimization) task.
- The 9° approach produces an easier task than the 3° approach. Furthermore, except for System F longitudinal, a 15° angle is easier still, although the P_c difference between 9° and 15° is small.

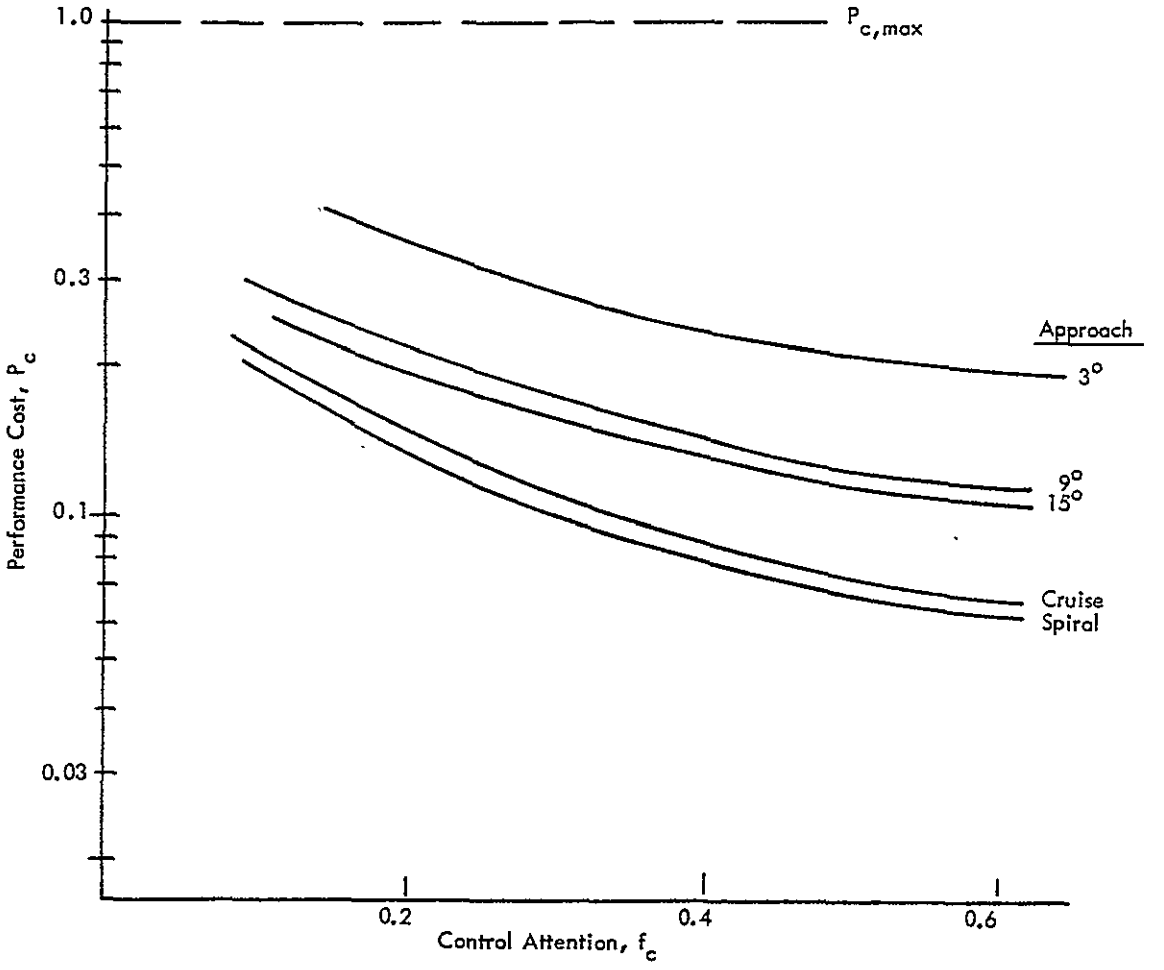

Figure 23. Performance Curves: System D, Longitudinal; With θ, z Flight Directors.

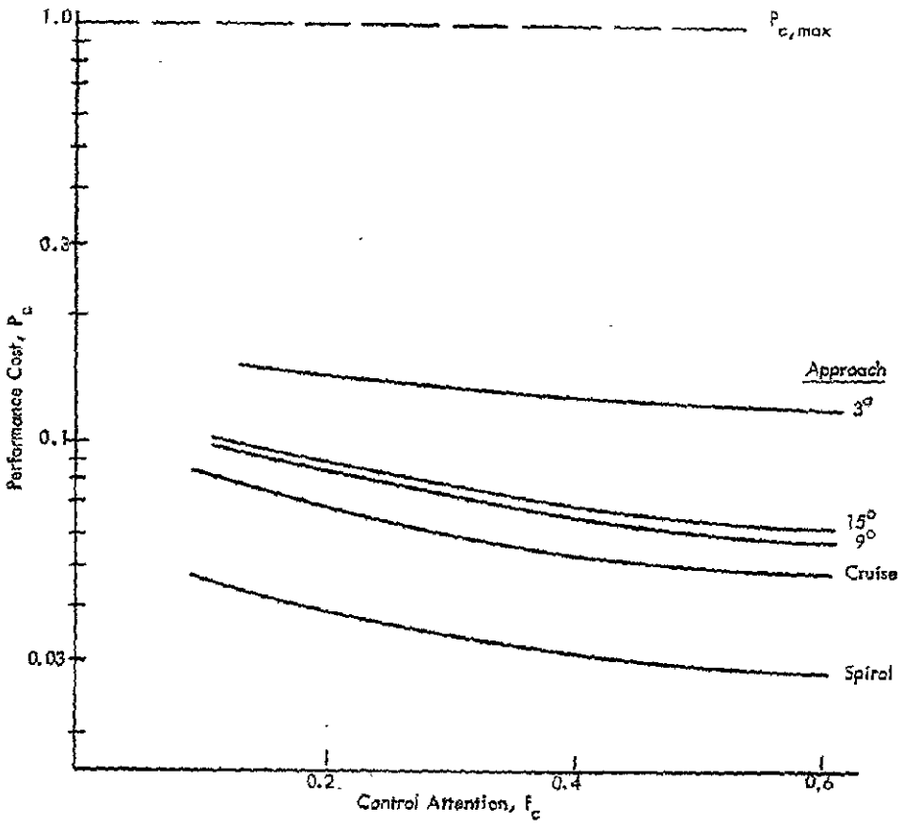

Figure 24. Performance Curves: System F, Longitudinal; No Flight Directors.

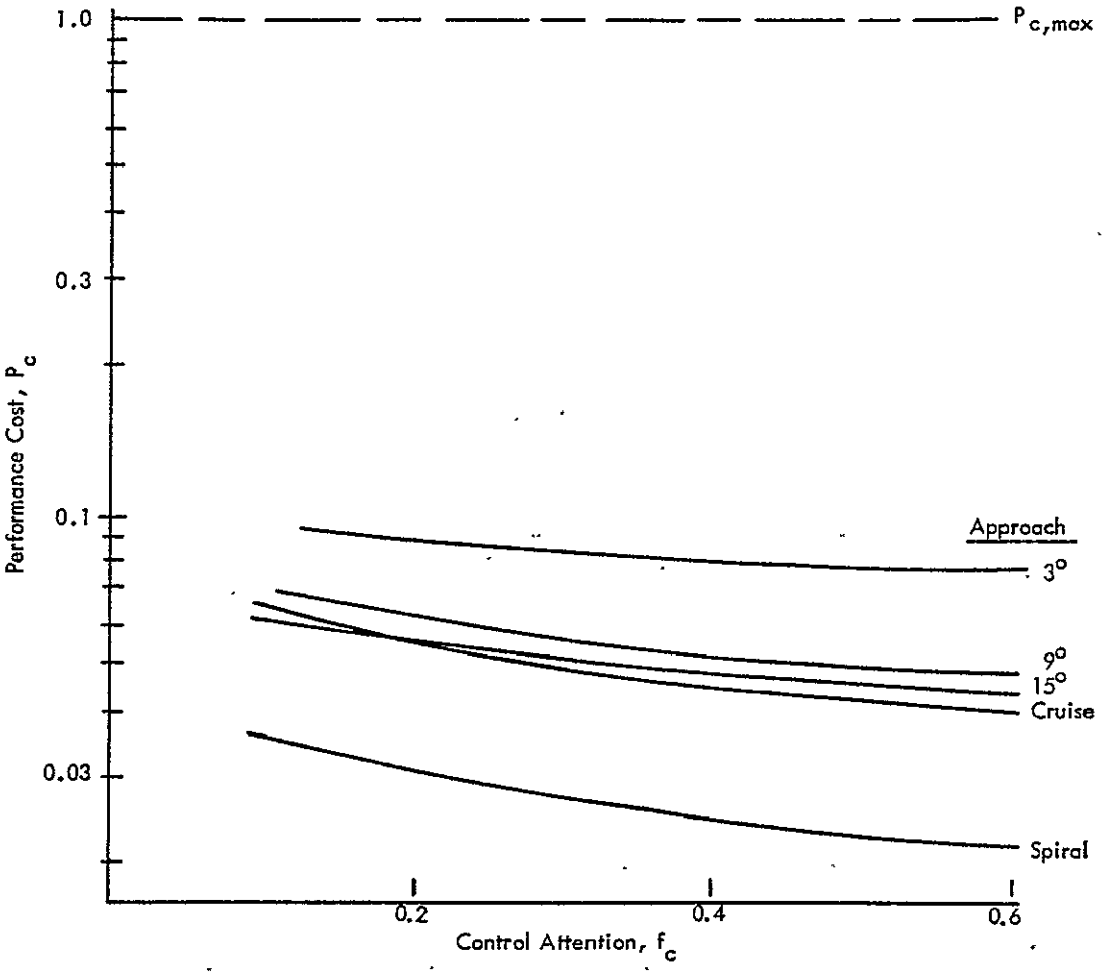

Figure 25. Performance Curves: System H, Longitudinal; No Flight Directors.

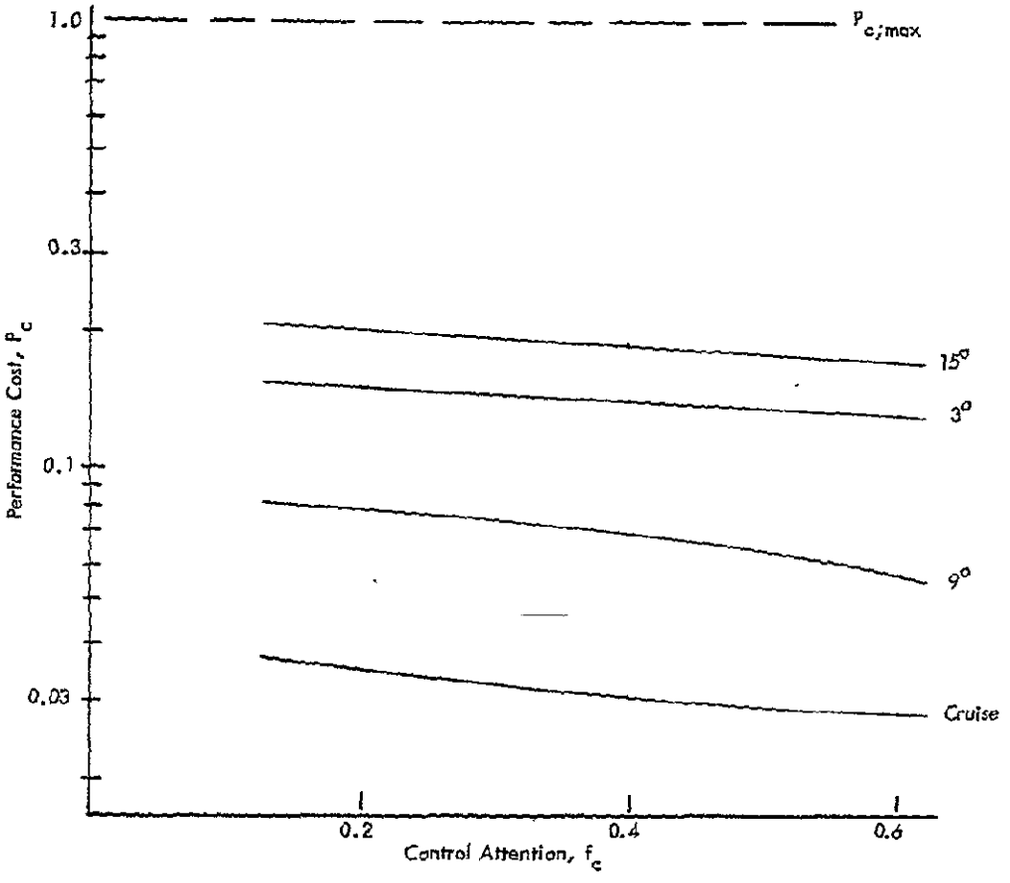

Figure 26. Performance Curves: System F, Lateral; With Flight Directors.

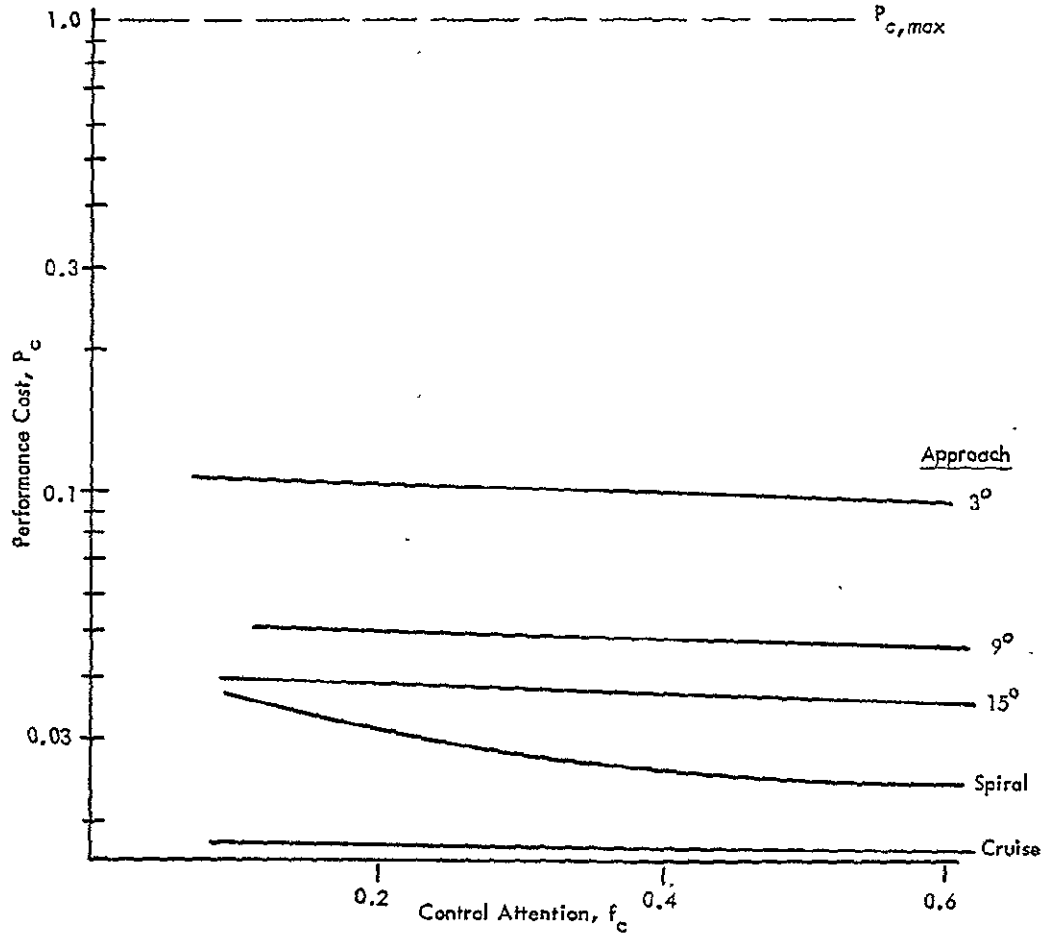

Figure 27. Performance Curves: System D/H Lateral; No Flight Directors.

- A spiral approach path yields better error minimizing performance than do any of the straight-in approach paths.
- Performance during cruise is better than during the straight approaches, but comparisons with spiral approach show no clear trend.

Thus, the model predicts a decreased workload with increasing approach angle, or spiral path. Note, however, that we have not considered the problem of transition from approach path to hover. The results of this (dynamic) control problem may modify the results obtained from our (static) analyses.

Most of the configurations show comparable performance levels for equal workload. An exception is System D, longitudinal, with θ, z flight directors. Compared with System F, performance is only 1/3 as good at the same f_c, i.e., P_c for System D is three times that for System F. Flight director augmentation during approach and cruise is not a necessity. Although not shown herein, the performance P_c versus f_c curves for System D (longitudinal) and System F (lateral) without flight directors are almost identical to the curves of Figure 23 and Figure 26, respectively. Thus, was not the case for hover, where FD information was either necessary or highly desirable for adequate performance.

4.3 CONTROL/DISPLAY SYSTEM SELECTION

The final step of the model-based evaluation process is the recommendation of a control/display system for follow-on simulation tests. This selection is made on the basis of the control and monitoring performance study, in addition to other factors as described in Subsection 2.1.3.

Four potential configurations have been identified in Subsection 4.2.3. Their monitoring performance at hover, and their control performance at other flight conditions have been examined, and discussed. Consolidating these results, we

recommend Configuration IV, i.e., V_x and V_z command system in the longitudinal axis plus y and ψ command in the lateral axis, for experimental use in the CH-47. The reasoning behind this choice is discussed below.

Configuration IV, the hybrid design System F1, does not require flight director automation for adequate control. At hover, the $f_{c,req} = 0.25$, and the control workload is well-balanced between the lateral and longitudinal axes. The monitoring performance (with $f_{m,avail} = 0.55$) meets the specification $P_m \leq 0.4$. The performance results are not highly sensitive to changes in control attention, as the P_c versus f_c tradeoff curves demonstrate. System F1 can still be controlled with an acceptable workload level if the longitudinal automation fails. With successive failures of outermost "loops," System F1 reverts to C/D and/or B which can be controlled to $P_c \approx 1$ using $f_c \leq 0.3$ (see Table 13). The lateral axis is not as robust to outerloop failures (in the roll loop). Figure 20 shows a relatively small performance change in failing from a y-command system to a V_y-command system, but a large performance decrement in a secondary failure to a ϕ-command system.

Overall, the performance attained with Configuration IV is quite comparable to Configuration III, which has a full x-z-y position command system. The equivalence is true across all flight conditions. Thus, System H is not attractive vis-a-vis System F1; the increased automation and complexity yields only small performance improvements.

Configuration II, the full velocity command system, is marginal from a hover performance viewpoint. A lateral flight director (ψ) is needed to meet control specifications. Monitoring performance is relatively poor in the longitudinal axis, and the flight director signal cannot be cross-checked adequately by monitoring the primary status information. The longitudinal "failure" properties of this configuration are the same as

increase in P_c; but a failure in the V_y outer-loop augmentation will pose a serious problem (especially if the flight director is not disengaged!)

The overall performance obtained with Configuration I at hover is similar to that of Configuration IV, as seen in Table 19. Both systems are identical in the lateral axis. In the longitudinal mode, two levels of control automation (one for each channel) have been exchanged for two flight directors (one for each control). This seems to be a "fair" trade, although we tend to prefer control automation. Two flight directors may contribute to display clutter (we have not studied the removal of FD_z). Moreover, the pilot's ability to reconstruct or cross-check the flight director signals through monitoring is poor. The flight directors are not necessary at the other flight conditions. However, the longitudinal performance of System D is considerably worse than System F or F1 in approach mode. On an absolute scale, its performance is still adequate, but this could change if the design parameters $x_{i,max}$ are modified† or if wind turbulence levels are increased.

From the pilot's standpoint, System D is somewhat unusual in terms of the harmony between the longitudinal and lateral axes. Whereas the lateral axis has full position feedback with heading hold, the longitudinal axis provides no automation in the vertical channel and only attitude command in the forward channel. This imbalance in automation level might be difficult for pilots to adjust to, and furthermore, might lead to confusion in the event of an emergency or subsystem failure.

This completes the model-based evaluation procedure. In the next section, the results are assimilated to suggest a potential display format for System F1.

---

†Recall that approach weights $x_{i,max}$ have been set to the more liberal cruise values. Halving $x_{i,max}$ will result in a quadrupling of J_c.

SECTION 5

DISPLAY FORMAT SELECTION

As discussed in Reference 4, there is no unique transformation from analytically determined information requirements to display layout. However, a number of important design principles must be taken into account (Reference 22), particularly when dealing with integrated displays and with the problem of VTOL control. These guidelines, which are outlined below, supplement conventional display criteria relating to instrument design, including location, size, contrast, quantization, and display-control compatibility.

- Operator Centered and Oriented Display - The favored presentation has the aircraft position and orientation fixed in the display, and the other pictorial information (horizon, glide-slope, hover point, velocity impact point, altitude reference, etc.) moving with respect to this reference.

- Geometric Real World Compatibility for Pictorial Displays - Although the integrated display is not in general a contact analog (and typically includes command and/or situation information not present in the VFR view), any pictorial information presented should be compatible with a view of the real world situation. The integrated display is best when the required information can be perceived by the pilot as a single comprehensive picture, rather than as a densely packed code through which he must successively determine the aircraft flight path.

- "Status at a Glance" for Situation Displays - In keeping with geometric real world compatibility, the essential elements of the display must be clearly delineated by size, shape, or color. They should be coordinated with respect to one another so that the status of the aircraft, especially in unusual attitudes, is immediately obvious and does not require element decoding.

- Predictive Capacity - In addition to indicating the current state of the aircraft, the integrated display must show the dynamic situation so that the future state can be really surmised. This kind of information is necessary for lead generation in fast loops (e.g., attitude control) and for planning maneuvers in guidance or collision avoidance. Display quickening, explicit rate symbols, display prediction, and historical trail markers may all be used to this end, and should follow the practice of derivative information "leading" the variable on the display.

- Geometric Sensitivity and Scaling - The symbols and elements in an integrated display must move far enough and fast enough so that the pilot will be able to detect the motion and estimate its magnitude. Maximum range and desired pilot gain in each loop must be considered in scaling the integrated display elements for the various phases of flight.

- Use of Digital Information Where Required - An exception to the pictorial compatible principle is in the display of information which is slowly varying and which must be read accurately over a large range. In this case, the judicious use of some digital presentations on the integrated display is appropriate. Digital information should be minimized, be displayed only when necessary (perhaps on pilot demand), be legible, and contain as few digits as absolutely required.

These design principles were adhered to in the development of Straw-Man display format concepts for the implementation of control/display Configurations IV, III and II, which were analyzed in the previous sections.

The displays for all systems were chosen to meet the assumptions in the analysis regarding state variables observed by the pilot, RMS values, and indifference thresholds. In addition, the displays are designed to be compatible with the underlying linearity assumption of the analysis, wherein the pilot is observing and controlling only small deviations from nominal conditions. This implies, for example, that the pilot controls only deviations of velocity from a nominal provided either by an external guidance loop or by his own trim input. In hover, of course, with the nominal velocity and position command all zero, there is no difference between the incremental control task and the control of total velocity or position. A simple diagram illustrating this display concept is shown in Figure 28. The command to be followed is either generated by a separate guidance function or is entered by the pilot through his trim control. This command value serves as one input to this automatic control system and is displayed to the pilot as a digital signal. If no other pilot control is exerted, the automatic system will follow the command, driving the tracking error to zero. In the case of velocity control, for example, the pilot, or guidance system, could enter a nominal or command approach

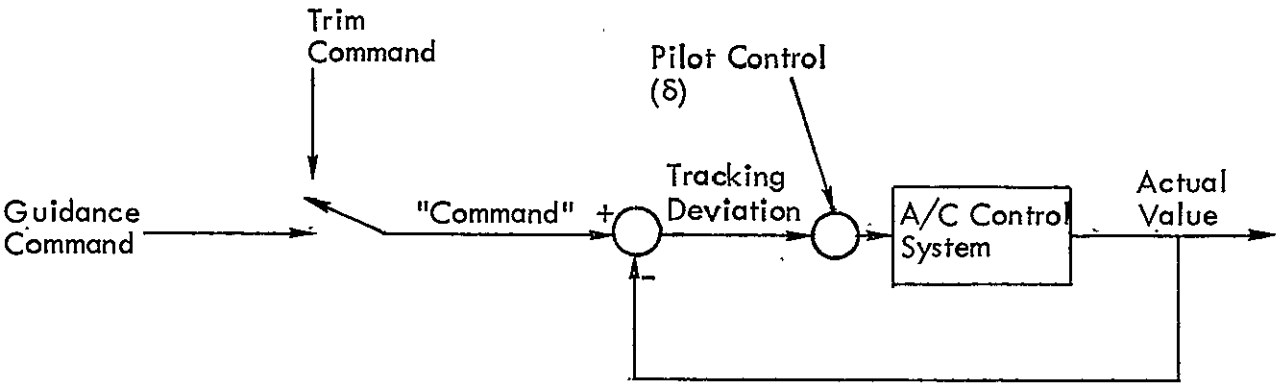

Figure 28. The Display Concept.

velocity, which would be displayed digitally, and would be followed, except for some tracking transients by the automatic system in the absence of any pilot control inputs. The tracking deviations from the nominal are displayed to the pilot in analog form, and are directly under his control through stick, collective or rudder. These control loops, wherein the pilot observes and controls tracking deviations from the nominal, correspond to the tasks considered in the linear analysis. For velocity control, to continue the example, the stick deflection would increase or decrease speed relative to the nominal or commanded speed, and the deviation from nominal would be displayed in analog format. There are many reasons for pilot intervention on the level of controlling deviations from nominal, including the requirements of 4-D navigation, traffic, noise, or corrections based on direct visual observation.

In all cases of these display concepts it is assumed that the conventional aircraft instruments are available to provide the pilot with basic vehicle status information (θ, ϕ, airspeed, etc.).

5.1 DISPLAY CONCEPT — CONFIGURATION IV

As discussed in the previous section, System F1 in Configuration IV is not one of the original control systems developed in Section 3, but was created during the

analysis to improve the lateral performance of System F. In the longitudinal axes, System F1 is a velocity-command system (V_x and V_z), the same as System F. However, in the lateral axes, it is the same as the most automated system, System H, and accepts lateral position (y) and heading (ψ) commands from the pilot (or the guidance system). The primary analytical parameters used in the display format design for System F1 are summarized in Table 20. These were based on the most critical flight condition — hover.

Two choices must be made in the display concept for this system. The first is a choice between

- a longitudinal-lateral display split (with $V_x - V_z$ data on a side-looking display or a vertical integrated display, and $y-\psi$ information on another display)
- a design based on an altitude (h, V_z) - horizontal situation (y, V_x, ψ) display.

Table 20. Analytical Parameters for Configuration IV Display Format (Hover).

Display Element	Units	RMS Hover Value	Design Maximum (1σ Range)	Indifference Threshold	Control Attention (f_{c_i})
x	ft	6.15	5.0	1.25	0.053
V_x	ft/sec	1.11	1.0	0.63	
y	ft	5.12	5.0	1.25	0.125
V_y	ft/sec	1.03	1.0	0.63	
z	ft	3.39	5.0	1.25	0.030
V_z	ft/sec	0.92	1.0	0.63	
θ	deg	0.80	1.0	0.25	0.017
$\dot{\theta}$	deg/sec	0.56	0.5	0.13	
ψ	deg	0.09	1.0	0.25	0.010
$\dot{\psi}$	deg/sec	0.05	0.5	0.13	
ϕ	deg	1.56	1.0	0.25	0.015
$\dot{\phi}$	deg/sec	0.58	0.5	0.13	

Although the latter necessitates an awkward display-control relationship (velocity control in x and position in y), it was selected to avoid the geometric incompatibility of a side-looking or perspective longitudinal display. The choice of a moving map or PPI horizontal display as the major position instrument is in accord with the experimental findings discussed in Reference 23, wherein horizontal situation display formats yielded more accurate piloting than vertical situation displays. Care should be taken in direct use of those results since they were for control systems with minimal augmentation, relying instead upon display quickening for stability.

The second choice was between a heading-oriented moving map horizontal situation indicator (HSI) and a track-oriented display. The former was chosen, because, at least in hover, it provides direct control-display compatibility between stick position and display for V_x and y. When the x-axis is defined as the aircraft longitudinal axis, it provides compatibility with an "out the window" view which is of considerable importance (References 22 and 24).

The suggested HSI and altitude displays for System F1 are shown in Figure 29. The HSI is a "heading-up" moving map display, in which the actual aircraft heading (ψ), defining the x-axis, is at the top of the display. The commanded heading appears as a triangular "bug" at the appropriate place on the compass card. In the absence of any pilot rudder input, the aircraft would turn until that heading were adopted, and the bug appeared at the top of the display. A steady rudder pedal deflection is required to maintain a steady offset between command ψ and actual ψ. The commanded velocity along the aircraft longitudinal (x) axis is shown as a 3-digit display to the right of the A/C symbol, in the center of the HSI. When this nominal velocity is entered by the pilot using the V_x trim button, a small indicator light below the digital meter is illuminated, as a reminder that the value was not a ground command. Pilot x deflection of the control stick thereafter controls V_x, the deviation of the actual x velocity from the

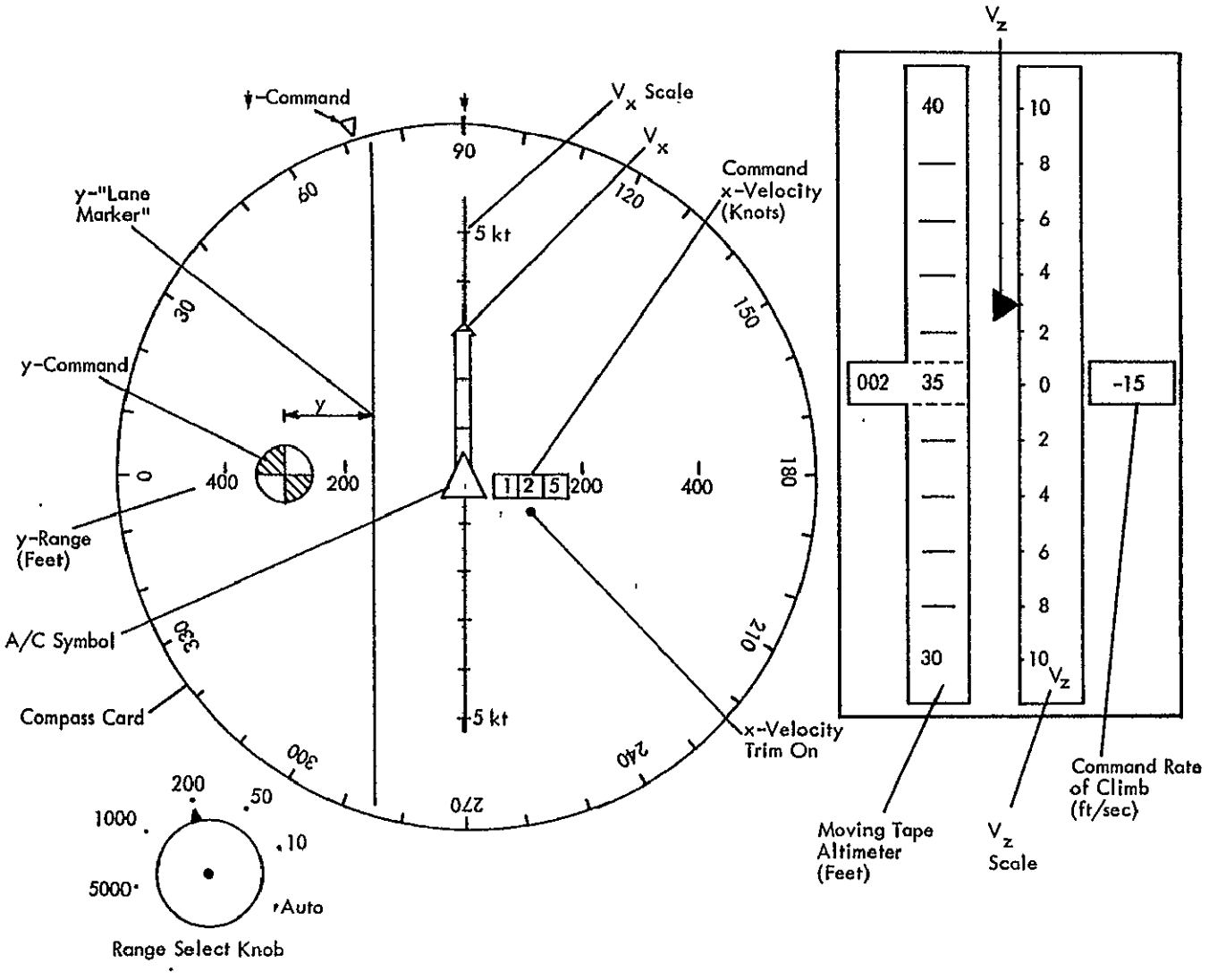

Figure 29. Display Format for Configuration IV.

command, displayed as the length and direction of a continuously variable arrow pointing up or down. Upward displacement indicates that the actual aircraft velocity is greater than the command. The pilot pushes forward on the control stick to increase inertial velocity above the command or trim nominal, and pulls back to slow down. In the hover situation, of course, with command x-velocity equal to zero, the arrow indicates actual total velocity in the x-direction, positive upwards.

Lateral displacement, y, is similarly displayed and controlled as deviations from a nominal. For the cruise condition the nominal or command value of y is normally zero, and the purpose of the y control is to permit the pilot to shift his cruise lane laterally, parallel to his current heading, by any desired amount. The y position of the quartered circle (which represents the landing pad in hover or approach) indicates the nominal or commanded y relative to the current aircraft inertial position. System F1 normally operates through y position feedback to keep the symbol on the center line of the display. The pilot can command short-term lateral deviations (y) without change of heading by lateral control deflection of the stick, which, in turn moves his vertical line "lane marker" laterally. In time, this constant deflection causes the aircraft y-position to change, bringing the line back over the center symbol in the moving map display. If it were desired to now maintain that y-position without continued y stick deflection, the pilot could enter a y-trim command which would bring the quartered circle back to the center and establish the current y as a reference. Thus, the pilot can temporarily "change lanes" with a stick deflection, or cause a semipermanent lane change through his trim. The y "lane marker" rides through the center of the y-command quartered circle in the absence of any lateral deflection, and both are in the center of the display when the automatic system drives y to its commanded value. The variable y used in the analysis is the distance from the center of the quartered circle to the lane marker.

The range on the moving map display, which only affects y for the F1 System, is variable and controlled by the range select knob. In "auto" the lowest range which will keep the y-command or landing pad symbol in view is automatically selected. The pad symbol is a circle when in range, but appears as a semicircle when out of range, placed in the direction of the y-command or of the landing pad to indicate the course to take toward the pad or other navigational point.

The case illustrated in Figure 29 for the HSI on System F1 is an unrealistic one, chosen only to demonstrate the display features. Although the commanded heading is 073°, the pilot is heading 090°, which would require a constant rudder deflection. The aircraft has commanded groundspeed of 125 knots in the direction of current heading, as set in by the pilot (x-velocity trim indicator on). To increase speed, the pilot has pushed forward on the control stick, adding an additional 3 knots (V_x). The aircraft is currently 250 feet to the right of the commanded y position. The pilot has pushed his control stick to the right to drive the aircraft to a steady flying "lane" (y) which is 140 feet to the right of the guidance or trim command (110 feet to the left of current position). The y position feedback loop will, with constant inputs, move the aircraft laterally 110 feet to the left, leaving the lane marker in the center and the y-command symbol 140 feet to the left. When pressure is removed from the stick the lane marker will revert to a position over the y-command symbol, and both will be driven to the center.

Altitude is controlled by setting in a commanded rate of climb on the digital indicator either manually or from guidance. Deviations (V_z) from this command rate are then controlled by the collective pitch control. The actual altitude is shown to the left of V_z on a combined digital and moving tape display, in which the first three numerals give altitude in hundreds of feet and the moving tape shows altitude to the nearest foot (available from radar in the hover case). The portion of the tape centered within the viewing window is the actual altitude. The moving tape has a ten foot

visible range, and is filtered at a corner frequency of about 1 Hz to reduce the difficulty of reading. In the case illustrated, the current altitude is 235 feet and the guidance system calls for a 15 ft/sec sink rate. The pilot has put in a positive V_z control, however, resulting in a 3 ft/sec deviation, or an actual sink rate of only 12 ft/sec.

This display concept permits the pilot to exercise the level of control accuracy and display indifference thresholds indicated in the analysis even under cruise conditions, when the command values are large. In accomplishing this goal, by display and control of deviations from the nominal, it loses the benefit of "status at a glance" for the total aircraft state.

5.2 DISPLAY CONCEPT — CONFIGURATION II

Configuration II differs from IV only in the lateral axes where the pilot has direct control over V_y, rather than y, and he is presented with a flight director signal for V_y. Table 21 summarizes the analytical design parameters for the Configuration II display format. The HSI map display still maintains the heading up orientation, and merely displays V_y commands as a rotation of the velocity vector away from the center-line. Thus, through control stick forward and side displacements the pilot controls the aircraft horizontal ground velocity vector deviations from the nominal or trim velocities. To represent the flight director function a "directed velocity" vector is also displayed. The pilot should attempt to match his $V_x - V_y$ vector with the "directed velocity" in the usual "fly-to" manner. Although only a V_y flight director signal was assumed in the analysis of Configuration II, human factors considerations dictate a $V_x - V_y$ director. By maintaining a heading display orientation, the important control-display directional compatibility is maintained. Figure 30 shows the display for Configuration II, with the landing pad symbol appearing to the left and a commanded deviation of the velocity vector in that direction, over and above the nominal 15-knot command. Note that for Configuration II, lateral as well as fore-aft stick motion controls velocity, which make the use of a single vector appropriate, as well as the use of range rings.

Table 21. Analytical Parameters for Configuration II Display Format (Hover).

Display Element	Units	RMS Hover Value	Design Maximum (1σ Range)	Indifference Threshold	Control Attention (f_{c_i})
x V_x	ft ft/sec	6.15 1.11	5.0 1.0	1.25 0.63	0.053
y V_y	ft ft/sec	5.26 1.01	5.0 1.0	1.25 0.63	0.060
z V_z	ft ft/sec	3.39 0.92	5.0 1.0	1.25 0.63	0.030
θ $\dot{\theta}$	deg deg/sec	0.80 0.56	1.0 0.5	0.25 0.13	0.017
ψ $\dot{\psi}$	deg deg/sec	0.06 0.05	1.0 0.5	0.25 0.13	0.010
ϕ $\dot{\phi}$	deg deg/sec	1.54 0.67	1.0 0.5	0.25 0.13	0.010
FD_ψ $\dot{FD}_\psi$	in in/sec	0.01 0.19	0.1	0.02 0.01	0.020
FD_ϕ $\dot{FD}_\phi$	in in/sec	0.20 1.62	0.3	0.09 0.04	0.350

5.3 DISPLAY CONCEPT — CONFIGURATION III

For Configuration III (Table 22), the full inertial position command system, the attractiveness of a track-oriented display is diminished. However, it is still important to maintain geometric control-display compatibility between control stick direction and display motion, independent of heading. Once again a moving map, heading-up HSI display is used as shown in Figure 31. The HSI display is used to place the line intersection representing pilot stick input over the desired position on the moving map, allowing the position feedback system to bring the aircraft to that spot. In the absence of any control stick input the aircraft is directed to the command position, indicated by

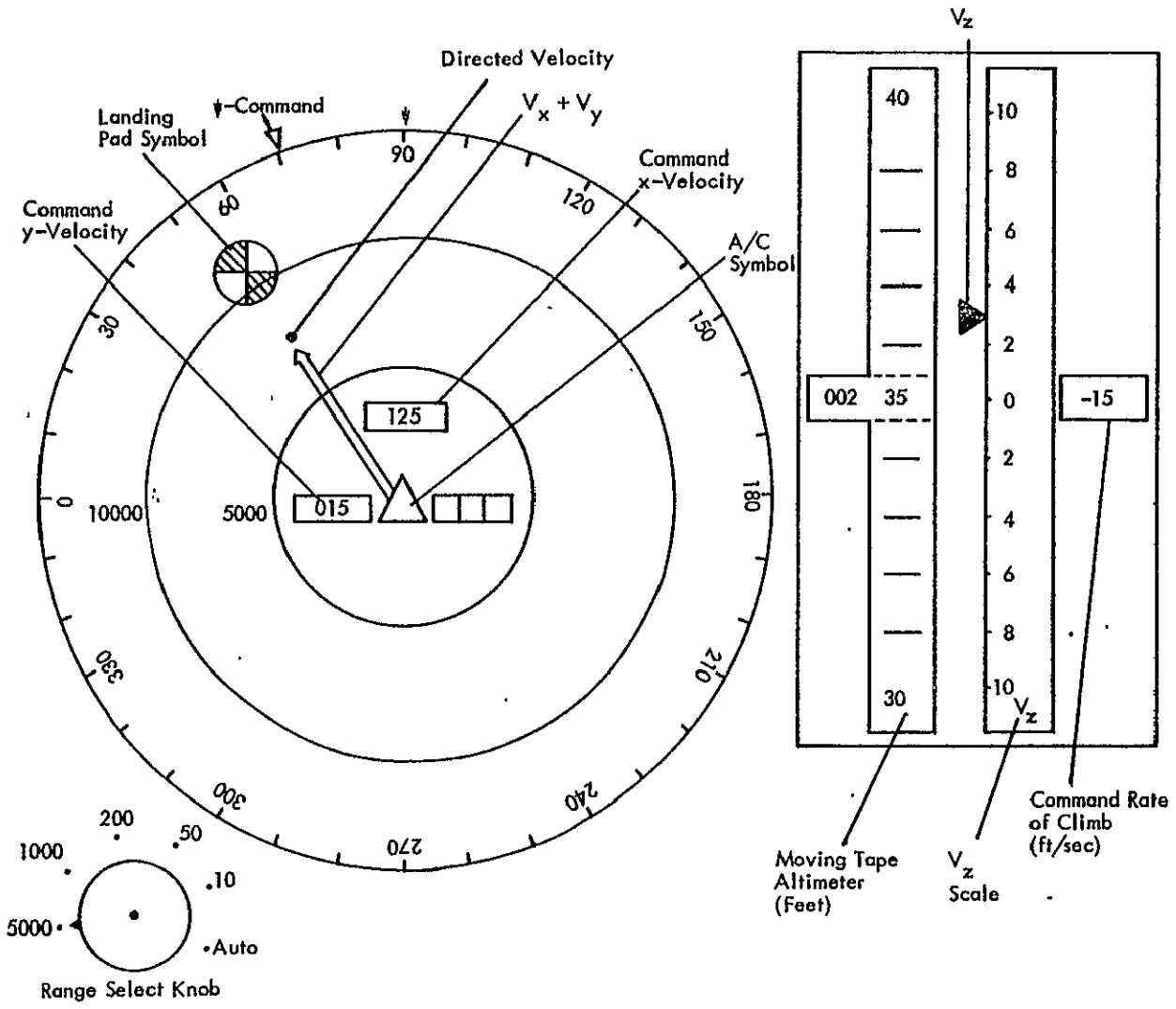

Figure 30. Display Format for Configuration II.

Table 22. Analytical Parameters for Configuration III Display Format (Hover).

Display Element	Units	RMS Hover Value	Design Maximum (1σ Range)	Indifference Threshold	Control Attention (f_{c_i})
x	ft	4.81	5.0	1.25	0.010
V_x	ft/sec	0.76	1.0	0.63	
y	ft	5.12	5.0	1.25	0.125
V_y	ft/sec	1.03	1.0	0.63	
z	ft	3.28	5.0	1.25	0.010
V_z	ft/sec	0.80	1.0	0.63	
θ	deg	0.56	1.0	0.25	0.010
$\dot{\theta}$	deg/sec	0.37	0.5	0.13	
ψ	deg	0.09	1.0	0.25	0.010
$\dot{\psi}$	deg/sec	0.05	0.5	0.13	
ϕ	deg	1.55	1.0	0.25	0.015
$\dot{\phi}$	deg/sec	0.58	0.5	0.13	

the center of the sectored circle, or landing pad symbol. Pilot control for changes from the lateral command are depicted by the lateral displacement of a vertical line from the sectored circle, and controlled by lateral stick deflection as in Configuration IV. X-input is similarly depicted by a horizontal line whose height is controlled by fore-aft stick position. The intersection of these lines is the desired vehicle position over the ground, reflecting both the guidance command and the pilot stick control of deviation. As heading is independently controlled, the orientation of the x and y axes (and their respective controls) remains fixed in aircraft axes to avoid control-display orientation changes. In the example, the pilot is calling for a position ahead and to the right of the commanded position.

Altitude commands are given both by an indicator opposite the moving tape altimeter for fine control within a 15-foot range, and by a digital display which shows the command altitude, as shown in Figure 31. In this example, the guidance system or pilot trim called for a command altitude of 225 feet, to which the pilot added an incremental stick deflection corresponding to 10 feet. The actual altitude is between these two, 230 feet, and would increase to 235 feet.

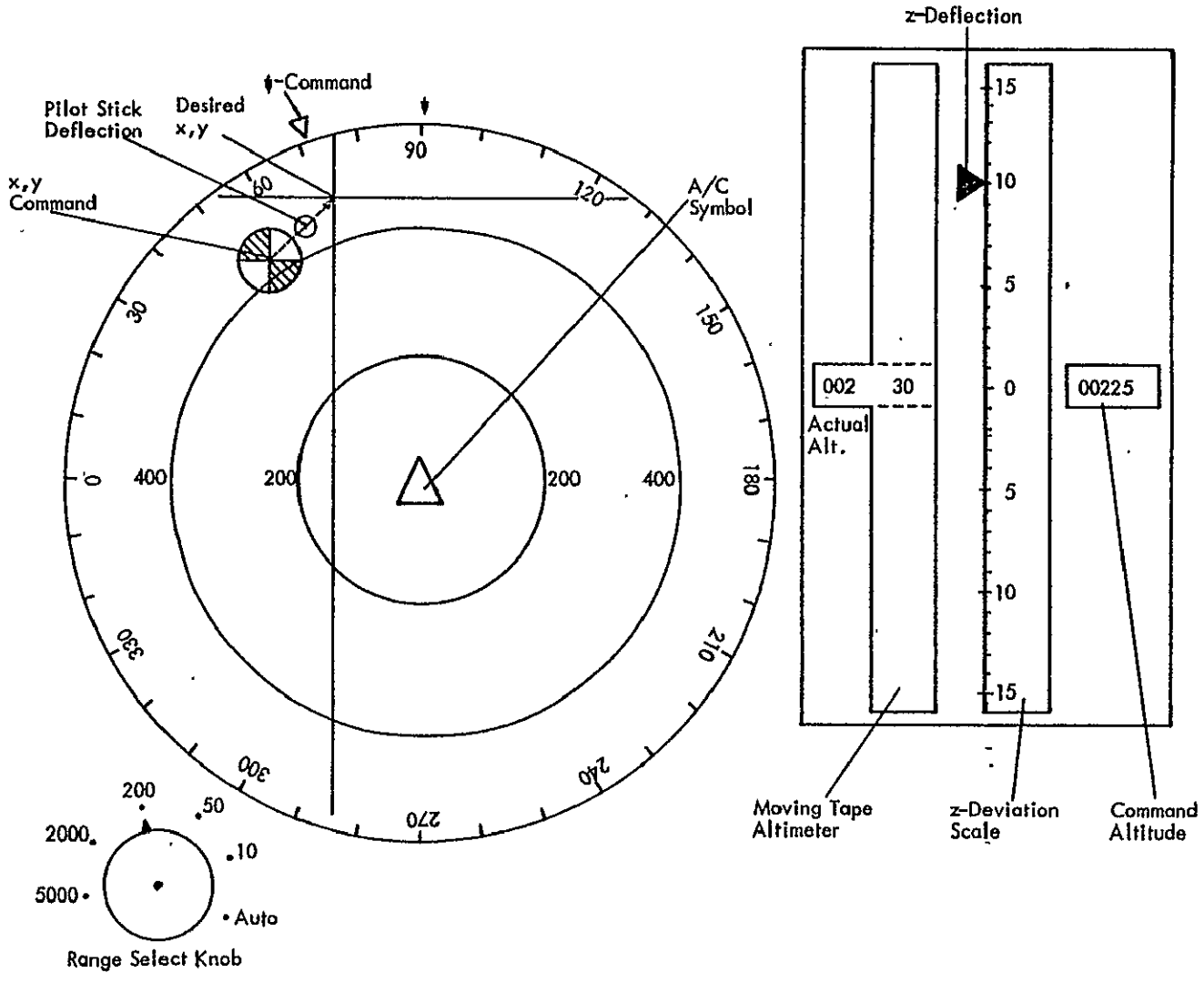

Figure 31. Display Format for Configuration III.

SECTION 6

CONCLUSIONS AND RECOMMENDATIONS

This section presents a summary of the primary accomplishments and significant findings which resulted from the research effort. It also describes briefly several suggestions for additional analysis or experimental investigations based on the results of this study.

6.1 SUMMARY AND CONCLUSIONS

A systematic design methodology for pilot displays in advanced commercial VTOL aircraft has been developed and refined. This methodology provides the analyst with a step-by-step procedure to conduct conceptual display/control configuration evaluations for simultaneous monitoring and control pilot tasks. The approach consists of three phases:

- Formulation of information requirements
- Configuration evaluation
- System selection

Both the monitoring and control performance models are based upon the optimal control model (OCM) of the human operator. The conventional OCM required extensions for its use in the display design methodology:

- Explicit optimization of control/monitoring attention
- Simultaneous monitoring and control performance predictions
- Indifference threshold effects

The monitoring model developed in Reference 4 was reevaluated in depth, but was not substantially changed. The basic concept is that the pilot first allocates whatever attention is necessary to control the aircraft to a desired performance level; then any remaining capacity is used to monitor the situation.

The selection of candidate display/control configurations during the first phase of the analysis is an important step, and one which obviously affects the remainder of the process. These configurations can be either prespecified independent of the main design process, or developed specifically for that effort. For completeness, two corollary design techniques were presented: one provides a systematic means of developing a series of control automation levels based upon simple closed-loop response models; the other is an iterative technique for generating flight director signals which allow the pilot to respond approximately as a pure gain. The result of these ancillary design methodologies is a matrix of vehicle-controller-display system configurations having various levels of control automation on one hand and display sophistication on the other.

The design methodology was applied to NASA's experimental CH-47 helicopter in support of the VALT research program. The objective was to identify one or more control/display configurations which could be evaluated during the flight test phase of the VALT program. The CH-47 application examined the system performance at six flight conditions:

- Cruise
- Straight Approach (3°, 6°, 9°)
- Spiral Approach
- Hover

The longitudinal and lateral axes were decoupled and analyzed separately. The control design technique mentioned above was used to develop a series of eight automation levels for the CH-47, ranging from a completely manual system to a full position feedback system. The flight director design approach was also used to generate flight director signals for each of the four control input channels at each level of automation and for all flight conditions. Four levels of display sophistication were considered:

- Status information only
- Status information and longitudinal flight directors
- Status information and lateral flight directors
- Status information and full flight directors

Thus, a total of 4 x 8 = 32 different control/display configurations was investigated at each of the six flight conditions.

In order to reduce somewhat the computational burden, the performance of all 32 configurations was investigated at the hover flight condition, which poses the most difficult pilot control task. As a result many of the original 32 configurations were eliminated from further consideration, and three configurations were identified as primary candidates. A fourth candidate was also synthesized from the hover analysis results. This was made possible by the decoupling of the longitudinal and lateral axes. The four candidates are summarized below:

- Configuration I: Pitch attitude command
  Collective command
  Lateral position command
  Heading hold
  Longitudinal flight directors
- Configuration II: Three-axis velocity command
  Heading hold
  Lateral flight directors
- Configuration III: Three axis position command
  Heading hold
  No flight directors
- Configuration IV: Forward and vertical velocity command
  Lateral position command
  Heading hold
  No flight directors

The control and monitoring performance of these configurations was carefully analyzed for all six flight conditions. The results verified that hover is the most difficult flight condition for the pilot to control, while cruise is the easiest. The control workload during the approach conditions decreases slightly with increasing approach angle

and for the spiral descent. As expected, the control performance improves with increased control and/or display automation at a fixed workload. The lateral response of the CH-47 is more difficult to control than the longitudinal. Some automation, either control or display, is required at hover to maintain acceptable control performance. The flight directors are the most beneficial to the least automated systems. Of the six flight conditions investigated, a flight director is only essential for hover, but it would undoubtedly be useful for nonsteady conditions such as the transition to hover or a missed approach.

The evaluation of the four candidate configurations led to the selection of Configuration IV as the most favorable, with III and II being the alternate choices. Configuration IV does not require a flight director, and has a reasonable workload that is balanced between the longitudinal and lateral axes. The monitoring performance is acceptable, and the control performance is comparable to the fully automatic system (Configuration III). The control performance is also insensitive to workload variations.

Based upon the analytical results, display formats were developed for Configurations IV, III and II. Accepted display design guidelines were followed in formulating unconventional formats for each configuration which satisfy or exceed the specifications used in the analysis. These candidate formats can be evaluated via pilot-in-the-loop simulations with the NASA Terminal Area Display Research Facility, and eventually flight-tested in the CH-47 research helicopter.

6.2 RECOMMENDATIONS FOR ADDITIONAL RESEARCH

During the course of this study several topics have been identified which warrant additional research or which should be the subject of ground and/or flight experiments. Several of these suggested research efforts are outlined below.

6.2.1 TIME-VARYING ANALYSIS

The present investigation has been restricted to steady-state flight conditions. A time-varying analysis should analyze the performance of candidate control/display configurations along the entire mission profile: takeoff, climbout, cruise, approach, transition to hover, hover, and missed approach. This investigation could be conducted as a Monte Carlo analysis, which would permit the inclusion of nonlinear effects, or it could be carried out as a linear analysis by propagating the error covariance matrix. Besides predicting the full mission performance, this study could examine the transient effects of subsystem failures and the performance of adaptive control and/or flight director algorithms.

6.2.2 EFFECTS OF SYSTEM FAILURES

The effects of system failures on the piloting task should be investigated. Representative failure modes should be defined (i.e., actuator failure, sensor failure, etc.) consistent with the generic augmentation systems. The optimal control model should then be utilized to examine the pilot control workload and performance under the assumed failure mode conditions. For example, results could be obtained that indicate whether a flight director designed for a velocity command system can be used when that augmentation system fails. Consideration should be given to investigation of transient conditions to determine the time required by the pilot to recover from different assumed failures.

The investigation could also examine the failure detection process under various situations. One promising approach would extend the present OCM to provide for a different model in the pilots' estimator than is used to represent the vehicle/display/control system response. A failure would be reflected as a change in the latter model.

6.2.3 GUIDANCE AND NAVIGATION ERRORS

In the present analysis the only errors in the pilot's observations arise from observation noise and from indifference thresholds; that is, the display instruments are being driven with perfect data. In reality, the information which the instruments present is derived from imperfect measurements. Sometimes, these measurement errors may greatly surpass the errors considered in the present study. They generally depend upon the type of navigation and guidance equipment being used, and moreover may be nonlinear or vary with time or position. A complete analysis should evaluate the entire system's performance including the navigation and guidance errors in addition to the "flight technical error" predicted by the present model. Such an investigation would use performance estimates of the navigation/guidance systems anticipated to be operational for VTOL aircraft in the next two decades (Reference 1). This study might also consider the effects of visual "out-the-window" observations and vehicle motion cues as well (e.g., References 25 and 26).

6.2.4 ADAPTIVE CONTROL

The feedback control laws and flight director algorithms developed in the current study change with flight conditions to compensate for the helicopter's response variations. Reference 4 found that a fixed gain flight director would not be satisfactory, while Reference 27 has investigated the design of digital-adaptive controllers for the VALT Research Aircraft. The feedback control laws and the flight director algorithms for a specified control/display configuration should be developed for an adaptive system. Since these adaptive versions would most likely differ from those obtained in the stationary analysis, they should be reevaluated for selected flight conditions. A time-varying analysis should be conducted to verify the adaptive system's continuous performance through the flight profile.

6.2.5 FLIGHT DIRECTOR DESIGN

The systematic flight director design technique developed in this investigation is based on the accepted premise that the pilot normally prefers to participate in the control loop as a pure gain. The composite dynamics results presented in Section 3 verified this assumption for many cases, but in other situations the assumption seems to be extremely inaccurate. A detailed reexamination of the flight director design technique as well as previous research on closed-loop pilot control behavior would be useful to understand the design requirements for VTOL flight directors. This investigation should also examine the effects of control automation level on the flight director characteristics and composite system dynamics.

6.2.6 PILOT INTERACTION WITH AUTOMATIC SYSTEMS

The pilot's interaction with an automatic system has been only briefly addressed by control theory models. Studies of this interaction should be conducted to examine factors such as the pilot's acceptance of the automatic system; the "harmony" of the system (i.e., whether the automatic system responds the way the pilot thinks he would); whether the pilot's interaction with the system is by monitoring a closed-loop system or by controlling the open-loop system. Actuator movement information can be presented to the pilot by dedicated displays, or by control stick motion. In one case only visual information is presented (actuator monitoring is done through the visual channel); and in the other case the monitoring is done through the kinesthetic channel (thus allowing more time to visually monitor other displays). The model should be examined to see whether differences in failure detection times using these two methods can be accurately represented by the model.

6.2.7 FIXED-BASE SIMULATION EXPERIMENTS

A series of fixed-base pilot-in-the-loop simulation experiments should be planned and conducted to (1) validate the extensions in the pilot model accomplished during the initial phase of the study and (2) evaluate and verify the display/control system concept for the CH-47. The experiments should be conducted on the NASA VALT fixed-base display research facility with a good cross section of subject pilots. Consideration should be given to experiments for measuring the performance differences and subjective differences between integrated displays and separate displays. Based on the results of the experiments, methods for representing appropriate changes in the analytical model should be made. Experiments to measure monitoring strategies in the simulation should be included to determine whether the pilot actually uses a normative strategy (i.e., how he should do it) as represented in the present model. Occulometer-scanning tests should be carried out and the results compared with the attention allocation predictions of the analytical model. Experimental control performance versus attention curves could be generated for selected control/display configurations by varying the subjects' total control attention through the use of side tasks. These results would be compared to the OCM predictions, and would also show the performance sensitivity to control attention. The straw-man display formats presented in Section 5 represent only one of an unlimited number of possible designs to satisfy the OCM specifications. Other formats could be developed which provide the same analytical performance predictions; these should then be evaluated in the fixed-base simulator to establish their experimental performance differences and the pilots' subjective ratings of each.

6.2.8 FLIGHT EVALUATION

Ultimately, the candidate display/control configurations should be experimentally evaluated under actual flight conditions in the CH-47 VALT Research Aircraft.

Detailed experiments should be developed using the results of the present study and subsequent analytical and ground-based experimental investigations. The experimental design would include such elements as: scenarios and flight profiles, vehicle control automation levels, instrument and display formats, navigational accuracy, instrumentation and recording requirements (accuracy, data rate, quantization, capacity, etc.) for measuring all performance variables, pilot rating questionnaires. Once the experiments have been designed, the flight research phase must be carefully monitored and supported throughout to ensure that they are conducted effectively, with a minimum need for dedicated flight time, and that all pertinent data is completely documented. Finally, the results of the flight test must be carefully analyzed, both on an absolute basis and in comparison to the previous analytical predictions and simulation studies.

REFERENCES

1. Hoffman, W. C.; Hollister, W. M.; and Howell, J. D.: Navigation and Guidance Requirements for Commercial VTOL Operations. Aerospace Systems, Inc., ASI-TR-74-17, NASA CR 132423, January 1974.

2. Hoffman, W. C.; and Hollister, W. M.: Navigation and Guidance Requirements for Commercial VTOL Operations - Navigation System Sensitivity Analysis. Aerospace Systems, Inc., ASI-TR-75-25, May 1975.

3. Hoffman, W. C.; and Hollister, W. M.: A Spiral Guidance Approach Concept for Commercial VTOL Operations. Aerospace Systems, Inc. Technical Report. ASI-TR-75-21, NASA CR 132651, March 1975.

4. Hoffman, W. C.; et al: Display/Control Requirements for VTOL Aircraft. Interim Technical Report. Aerospace Systems, Inc., ASI-TR-75-26, NASA CR 145028, August 1975.

5. Kleinman, D. L.: Solving the Optimal Attention Allocation Problem in Manual Control. IEEE Trans. Autom, Control, Vol. AC-21, No. 6, December 1976.

6. Kleinman, D. L.; and Curry, R. E.: Some New Control Theoretic Models for Human Operator Display Monitoring. 1976 IEEE Decision and Control Conference, November 1976.

7. Kleinman, D. L.; and Baron, S.: Manned Vehicle Systems Analysis by Means of Modern Control Theory. NASA CR 1753, June 1971.

8. Kleinman, D. L.; Baron, S.; and Levison, W. H.: A Control Theoretic Approach to Manned Vehicle Systems Analysis. IEEE Trans. Autom. Control, Vol. AC-16, No. 6, December 1971.

9. Kleinman, D. L.; and Baron, S.: Analytic Evaluation of Display Requirements for Approach to Landing. NASA CR 1952, November 1971.

10. Kleinman, D. L.; and Killingsworth: A Predictive Model for STOL Aircraft Landing. NASA CR 2374,

11. Levison, W. H.; Baron, S.; and Kleinman, D. L.: A Model for Human Operator Remnant. IEEE Trans. Man-Machine Systems.

12. Levison, W. H.; Elkind, J. I.; and Ward, J. L.: Studies of Multivariable Manual Control Systems: A Model for Task Interference. NASA CR-169, July 1970.

13. Kleinman, D. L.; and Curry, R. E.: An Equivalence Between Two Representations for Human Attention Sharing. IEEE Trans. SMC, Vol. SMC-6, No. 9, September 1976.

14. Kelley, J. R.; Niessen, F. R.; and Sommer, R. W.: Evaluation of a VTOL Flight Director Concept During Constant-Speed Instrument Approaches. NASA TN D 5860, June 1970.

15. Garren, J. R., et al: Flight Investigation of VTOL Control and Display Concept for Performing Decelerating Approaches to an Instrument Hover. NASA TN D-6108, February 1971.

16. Gai, E. G.; and Curry, R. E.: A Model of the Human Observer in Failure Detection Tasks. IEEE Trans. Syst. Man. Cybernetics, Vol. SMC-6, No. 2, February 1976.

17. Gai, E. G.; and Curry, R. E.: Failure Detection by Pilots During Automatic Landing: Models and Experiments. AIAA Journal of Aircraft, 1976.

18. Senders, J. W.: The Human Observer as a Monitor and Controller of Multi-Degree of Freedom Systems. IEEE Trans. on HFE, Vol. HFE-5, No. 1, September 1964.

19. Hoffman, W. C.; and Hollister, W. M.: Simplified Aircraft Control System Design Using Optimal Control Techniques. Paper No. FA 3-1, 1976, IEEE Conference on Decision and Control, Clearwater, Florida, December 1-3, 1976.

20. Ostroff, A. J.; Downing, D. R.; and Rood, W. J.: A Technique Using a Nonlinear Helicopter Model for Determining Trims and Derivatives. NASA TN D-8159, May 1976.

21. Trueblood, R. B.; Bryant, W. B.; and Cattel, J. J.: Advanced Flight Control System Concepts for VTOL Aircraft. USAAML Technical Report 69-95, July 1970.

22. Young, L. R.: Integrated Display Principles and Some Applications to V/STOL Aircraft. AGARD Conference Proceedings No. 96 on Guidance and Control Displays, October 1971.

23. Wolf, J. D.; and Hoppe, R. B.: Aircraft Displays for Steep-Angle Approaches. JANAIR Report 681215, July 1970.

24. Wooding, H. C., Jr.; Simpson, J. A.; Harper, H.; and Sweetnam, R.: Integrated Vertical Display Research. JANAIR Report 680611, July 1970.

25. Curry, R. E.; Hoffman, W. C.; and Young, L. R.: Pilot Modeling for Manned Simulation. USAF AFFDL-TR-76-29. Aerospace Systems, Inc., March 1976.

26. Levison, W. H.; Baron, S.; and Junkers, A. M.: Modeling the Effects of Environmental Factors on Human Control and Information Processing. USAF AMRL-TR-76-74, Bolt Beranek and Newman, August 1976.

27. Stengel, R. F.; Broussard, J. R.; and Berry, P. W.: The Design of Digital-Adaptive Controllers for VTOL Aircraft. NASA CR-144912, The Analytic Sciences Corporation, March 1976.

Appendix A

EXAMPLE RESULTS FOR CH-47 AT HOVER

This appendix contains detailed numerical results to illustrate the design procedures as applied to the CH-47 helicopter. Since it would be impractical to present the numerical results for all flight conditions and all system configurations, we have selected the most difficult flight condition (hover) and the three-axis velocity command system (System F) for these example results.

A.1 LONGITUDINAL AXES

The longitudinal axes state, control and disturbance vectors were defined in Equation (119), repeated below for convenience.

$$x = [u_g, w_g, \dot{w}_{g1}, q_g, x, V_x, z; V_z, \theta, \dot{\theta}]'$$

$$u = [\delta_e, \delta_c]'$$

$$w = [\eta_u, \eta_w]'$$

The open-loop dynamics at hover are given in Figure A-1. Application of the control design technique discussed in Subsections 3.1 and 3.3 yielded the automatic system feedback gains L_{cs} and closed-loop system matrix A_0 shown in Figure A-2. The state and control weightings used to obtain these results were derived from Tables 8 and 9:

$$Q_x = \text{Diag } [0, 0, 0, 0, 0, 0.0013, 0, 0.0178, 5.285, 5.285]$$

$$Q_u = \text{Diag } [0.143, 7.226]$$

Next, the flight director design process was applied as described in Subsections 3.2 and 3.3. The resulting status and flight director observations and corresponding indifference thresholds are given in Figure A-3. The observation vector for these is

$$A_{0L} = \begin{bmatrix} -0.0474 & 0 & 0 & 0 & 0 & 0 & 0 & 0 & 0 & 0 \\ 0 & -0.5060 & 0.2530 & 0 & 0 & 0 & 0 & 0 & 0 & 0 \\ 0 & -0.2530 & 0 & 0 & 0 & 0 & 0 & 0 & 0 & 0 \\ 0 & -0.0040 & 0.0020 & -0.2010 & 0 & 0 & 0 & 0 & 0 & 0 \\ 0 & 0 & 0 & 0 & 0 & 1.0 & 0 & 0 & 0 & 0 \\ 0.0182 & -0.0004 & 0 & -2.620 & 0 & -0.0182 & 0 & 0.0004 & -32.20 & 2.620 \\ 0 & 0 & 0 & 0 & 0 & 0 & 0 & 1.0 & 0 & 0 \\ 0.0073 & 0.2990 & 0 & -0.1350 & 0 & -0.0073 & 0 & -0.2990 & 0 & 0.1350 \\ 0 & 0 & 0 & 0 & 0 & 0 & 0 & 0 & 0 & 1.0 \\ -0.0095 & -0.0013 & 0 & 1.230 & 0 & 0.0095 & 0 & 0.0013 & 0 & -1.230 \end{bmatrix}$$

$$B_0 = \begin{bmatrix} 0 & 0 \\ 0 & 0 \\ 0 & 0 \\ 0 & 0 \\ 0 & 0 \\ 0.1170 & 0.0044 \\ 0 & 0 \\ 0.0170 & -8.120 \\ 0 & 0 \\ 0.3290 & 0.0191 \end{bmatrix} \qquad E_0 = \begin{bmatrix} 1.926 & 0 \\ 0 & 2.358 \\ 0 & 1.362 \\ 0 & 0.0187 \\ 0 & 0 \\ 0 & 0 \\ 0 & 0 \\ 0 & 0 \\ 0 & 0 \\ 0 & 0 \end{bmatrix}$$

Figure A-1. Open-Loop CH-47 Longitudinal Hover Dynamics.

$$A_0 = \begin{bmatrix}
-0.474 & 0 & 0 & 0 & 0 & 0 & 0 & 0 & 0 & 0 \\
0 & -0.5060 & 0.2530 & 0 & 0 & 0 & 0 & 0 & 0 & 0 \\
0 & -0.2530 & 0 & 0 & 0 & 0 & 0 & 0 & 0 & 0 \\
0 & -0.0040 & 0.0020 & -0.2010 & 0 & 0 & 0 & 0 & 0 & 0 \\
0 & 0 & 0 & 0 & 0 & 1.0 & 0 & 0 & 0 & 0 \\
0.0182 & -0.0004 & 0 & -2.620 & 8.9E-6 & -0.0107 & -1.2E-6 & -0.0004 & -33.37 & 1.825 \\
0 & 0 & 0 & 0 & 0 & 0 & 0 & 1.0 & 0 & 0 \\
0.0073 & 0.2990 & 0 & -0.1350 & -3.7E-6 & -0.0049 & -0.0005 & -0.5030 & -0.1211 & 0.0597 \\
0 & 0 & 0 & 0 & 0 & 0 & 0 & 0 & 0 & 1.0 \\
-0.0095 & -0.0013 & 0 & 1.230 & 2.5E-5 & 0.0307 & -2.8E-6 & -0.0010 & -3.278 & -3.464
\end{bmatrix}$$

$$L_{cs} = \begin{bmatrix} 0 & 0 & 0 & 0 \\ 0 & 0 & 0 & 0 \end{bmatrix}$$

Figure A-2. Closed-Loop CH-47 Longitudinal Hover Dynamics - System F.

$$C_0 = \left[\begin{array}{cccccccccc}
0 & 0 & 0 & 0 & 1 & 0 & 0 & 0 & 0 & 0 \\
0 & 0 & 0 & 0 & 0 & 1 & 0 & 0 & 0 & 0 \\
0 & 0 & 0 & 0 & 0 & 0 & 1 & 0 & 0 & 0 \\
0 & 0 & 0 & 0 & 0 & 0 & 0 & 1 & 0 & 0 \\
0 & 0 & 0 & 0 & 0 & 0 & 0 & 0 & 57.3 & 0 \\
0 & 0 & 0 & 0 & 0 & 0 & 0 & 0 & 0 & 57.3 \\
\hline
0 & 0 & 0 & 0 & -0.0418 & -0.2213 & 0.0050 & 0.0183 & 16.46 & 15.71 \\
-0.1525 & -0.0142 & 0 & 19.90 & 0.0004 & 0.4425 & -5.4E-5 & -0.0199 & -44.11 & -38.35 \\
0 & 0 & 0 & 0 & -0.0006 & -0.0049 & -0.0891 & -0.3850 & 0.5336 & 0.4770 \\
-0.0074 & -0.1157 & 0 & 0.6517 & -1.3E-5 & 0.0160 & 0.0002 & 0.1041 & -1.352 & -1.151
\end{array}\right]$$

$$D_0 = 0$$

$$a = \left[\begin{array}{cccccc|cccc} 1.250 & 0.2500 & 1.250 & 0.2500 & 0.2500 & 0.1250 & 0.1301 & 0.0651 & 0.1144 & 0.0572 \end{array}\right]$$

Figure A-3. CH-47 Longitudinal Hover Observations and Thresholds - System F.

$$y = [x,\ V_x,\ z,\ V_z,\ \theta,\ \dot{\theta},\ FD_\theta,\ \dot{FD}_\theta,\ FD_z,\ \dot{FD}_z]'$$

$$= C_0 x + D_0 u$$

The results of the control and flight director design processes were then used in Program PIREP to evaluate the control performance as a function of pilot workload. The following additional input data were required:

- Pilot time delay: $\tau = 0.2$ sec
- Motor noise: $V_{u_i} = -25$ dB
- Observation Noise: $\rho_i^o = -20$ dB

The results for three levels of control attention f_{c_T} are presented in Tables A-1 and A-2, respectively with and without the flight directors. The "Total Cost" shown in the tables is the control cost J_c defined by Equation (28), while the "Performance Cost" is control performance metric P_c given by Equation (5). The "Cost Gradient" is the gradient $g_f = \partial J_c / \partial f_c$ as in Equation (38).

A.2 LATERAL AXES

The lateral axes state, control and disturbance vectors were defined in Equation (120), repeated below:

$$x = [v_g,\ v_{gI},\ p_g,\ r_g,\ y,\ V_y,\ \phi,\ \dot{\phi},\ \psi,\ \dot{\psi}]'$$

$$u = [\delta_a,\ \delta_r]'$$

$$w = [\eta_v,\ \eta_p]'$$

The open-loop dynamics at hover are given in Figure A-4. The control design process produced the closed-loop system matrix and feedback gains shown in Figure A-5. The weighting matrices used to obtain these were also derived from Tables 8 and 9:

Table A-1. Longitudinal Performance Summary — System F With Flight Directors.

Total Control Attention	$f_c = 0.2$		$f_c = 0.4$			$f_c = 0.6$		
Display Variable (y_i)	RMS Value	Control Attention (f_{c_i})	RMS Value	Control Attention (f_{c_i})	Cost Gradient ($-g_{f_i}$)	RMS Value	Control Attention (f_{c_i})	Cost Gradient ($-g_{f_i}$)
x (ft)	3.66	0.016	2.83	0.019	0.09	2.51	0.019	0.07
V_x (ft/sec)	0.75	0.016	0.60	0.019	1.09	0.53	0.019	0.68
z (ft)	1.60	0.016	1.07	0.017	0.04	0.92	0.016	0.01
V_z (ft/sec)	0.58	0.016	0.44	0.017	1.28	0.39	0.016	0.67
θ (deg)	0.61	0.019	0.53	0.036	1.03	0.49	0.105	0.51
q (deg/sec)	0.49	0.019	0.45	0.036	1.40	0.42	0.105	0.86
FD_θ (in)	0.19	0.095	0.16	0.204	2.66	0.15	0.283	1.34
$\dot{FD}_\theta$ (in/sec)	1.22	0.095	1.21	0.204	0.26	1.20	0.283	0.19
FD_z (in)	0.26	0.054	0.19	0.124	1.39	0.17	0.176	0.70
$\dot{FD}_z$ (in/sec)	0.29	0.054	0.30	0.124	1.35	0.30	0.176	0.77
Control Variable (u_i)	RMS Value		RMS Value			RMS Value		
δ_e (in)	0.25		0.25			0.25		
δ_c (in)	0.13		0.13			0.13		
Total Cost (J_c)	3.52		2.49			2.09		
Performance Cost (P_c)	0.47		0.34			0.28		

Table A-2. Longitudinal Performance Summary — System F Without Flight Directors.

Total Control Attention	$f_c = 0.2$			$f_c = 0.4$			$f_c = 0.6$		
Display Variable (y_i)	RMS Value	Control Attention (f_{c_i})	Cost Gradient ($-g_{f_i}$)	RMS Value	Control Attention (f_{c_i})	Cost Gradient ($-g_{f_i}$)	RMS Value	Control Attention (f_{c_i})	Cost Gradient ($-g_{f_i}$)
x (ft)	4.74	0.083	1.34	3.50	0.120	0.46	2.94	0.154	0.23
V_x (ft/sec)	0.90	0.083	10.56	0.68	0.120	3.52	0.58	0.154	1.73
z (ft)	2.32	0.058	1.36	1.77	0.098	0.33	1.47	0.142	0.13
V_z (ft/sec)	0.74	0.058	9.40	0.63	0.098	3.52	0.56	0.142	1.75
θ (deg)	0.69	0.058	7.09	0.57	0.182	2.04	0.51	0.301	0.89
q (deg/sec)	0.53	0.058	4.52	0.47	0.182	2.04	0.44	0.301	1.14
FD_θ (in)	0.24	0.0		0.19	0.0		0.17	0.0	
$\dot{FD}_\theta$ (in/sec)	1.23	0.0		1.21	0.0		1.20	0.0	
FD_z (in)	0.35	0.0		0.29	0.0		0.25	0.0	
$\dot{FD}_z$ (in/sec)	0.28	0.0		0.29	0.0		0.29	0.0	
Control Variable (u_i)	RMS Value			RMS Value			RMS Value		
δ_e (in)	0.25						0.25		
δ_c (in)	0.14			0.13			0.13		
Total Cost (J_c)	4.25			2.85			2.28		
Performance Cost (P_c)	0.68			0.44			0.35		

$$A_{0L} = \begin{bmatrix} -0.0948 & 0.0474 & 0 & 0 & 0 & 0 & 0 & 0 & 0 & 0 \\ -0.0474 & 0 & 0 & 0 & 0 & 0 & 0 & 0 & 0 & 0 \\ 0 & 0 & -0.2000 & 0 & 0 & 0 & 0 & 0 & 0 & 0 \\ 0.0010 & -0.0005 & 0 & -0.2680 & 0 & 0 & 0 & 0 & 0 & 0 \\ 0 & 0 & 0 & 0 & 0 & 1.0 & 0 & 0 & 0 & 0 \\ 0.1370 & 0 & 1.490 & -0.0086 & 0 & -0.1370 & 32.00 & -1.490 & 0 & 0.0086 \\ 0 & 0 & 0 & 0 & 0 & 0 & 0 & 1.0 & 0 & 0 \\ 0.0067 & 0 & 0.7230 & -0.0075 & 0 & -0.0067 & 0 & -0.7230 & 0 & 0.0075 \\ 0 & 0 & 0 & 0 & 0 & 0 & 0 & 0 & 0 & 1.0 \\ 0.0011 & 0 & 0.0547 & 0.0409 & 0 & -0.0011 & 0 & -0.0547 & 0 & -0.0409 \end{bmatrix}$$

$$B_0 = \begin{bmatrix} 0 & 0 \\ 0 & 0 \\ 0 & 0 \\ 0 & 0 \\ 0 & 0 \\ 1.160 & -0.0504 \\ 0 & 0 \\ 0.4370 & -0.0375 \\ 0 & 0 \\ 0.0427 & 0.2000 \end{bmatrix} \qquad E_0 = \begin{bmatrix} 2.360 & 0 \\ 1.360 & 0 \\ 0 & 0.0165 \\ -0.0248 & 0 \\ 0 & 0 \\ 0 & 0 \\ 0 & 0 \\ 0 & 0 \\ 0 & 0 \\ 0 & 0 \end{bmatrix}$$

Figure A-4. Open-Loop CH-47 Lateral Hover Dynamics.

$$A_0 = \begin{bmatrix}
-0.0948 & 0.0474 & 0 & 0 & 0 & 0 & 0 & 0 & 0 & 0 \\
-0.0474 & 0 & 0 & 0 & 0 & 0 & 0 & 0 & 0 & 0 \\
0 & 0 & -0.2000 & 0 & 0 & 0 & 0 & 0 & 0 & 0 \\
0.0010 & -0.0005 & 0 & -0.2680 & 0 & 0 & 0 & 0 & 0 & 0 \\
0 & 0 & 0 & 0 & 0 & 1.0 & 0 & 0 & 0 & 0 \\
0.1370 & 0 & 1.490 & -0.0086 & -0.0001 & -0.1819 & 24.01 & -8.206 & -0.2170 & -0.3487 \\
0 & 0 & 0 & 0 & 0 & 0 & 0 & 1.0 & 0 & 0 \\
0.0067 & 0 & 0.7230 & -0.0075 & -5.0E-5 & -0.0239 & -3.042 & -3.283 & 0.0985 & 0.1246 \\
0 & 0 & 0 & 0 & 0 & 0 & 0 & 0 & 0 & 0 \\
0.0011 & 0 & 0.0547 & 0.0409 & 9.6E-7 & 0.0005 & 0.0612 & 0.0278 & -1.972 & -2.799
\end{bmatrix}$$

$$L_{cs} = \begin{bmatrix} 0 & 0 & 0 & 0 \\ 0 & 0 & 0 & 0 \end{bmatrix}$$

Figure A-5. Closed-Loop CH-47 Lateral Hover Dynamics - System F.

$$Q_x = \text{Diag}\,[0,\ 0,\ 0,\ 0,\ 0.0013,\ 5.285,\ 5.285,\ 5.285,\ 5.285]'$$

$$Q_u = \text{Diag}\,[0.2281,\ 0.0549]'$$

The flight director design process for lateral System F yielded the observation matrices and indifference thresholds shown in Figure A-6. The lateral system observation vector is

$$y = [y,\ V_y,\ \phi,\ \dot{\phi},\ \psi,\ \dot{\psi},\ FD_\phi,\ \dot{FD}_\phi,\ FD_\psi,\ \dot{FD}_\psi]'$$

Program PIREP was used to evaluate the lateral system performance in the same manner as described for the longitudinal axes. The results for three levels of lateral control attention, with and without the flight directors, are presented in Tables A-3 and A-4.

$$C_0 = \left[\begin{array}{cccccccccc}
0 & 0 & 0 & 0 & 1 & 0 & 0 & 0 & 0 & 0 \\
0 & 0 & 0 & 0 & 0 & 1 & 0 & 0 & 0 & 0 \\
0 & 0 & 0 & 0 & 0 & 0 & 57.3 & 0 & 0 & 0 \\
0 & 0 & 0 & 0 & 0 & 0 & 0 & 57.3 & 0 & 0 \\
0 & 0 & 0 & 0 & 0 & 0 & 0 & 0 & 57.3 & 0 \\
0 & 0 & 0 & 0 & 0 & 0 & 0 & 0 & 0 & 57.3 \\
\hline
0 & 0 & 0 & 0 & 0.0351 & 0.1519 & 12.16 & 13.45 & 0.8177 & 2.176 \\
0.1127 & 0 & 10.07 & -0.0137 & -0.0006 & -0.3126 & -37.14 & -33.19 & -2.998 & -3.649 \\
0 & 0 & 0 & 0 & -0.0084 & -0.0260 & -1.699 & -2.380 & 4.625 & 23.07 \\
0.0067 & 0 & -0.4970 & 0.0962 & 0.0001 & 0.0649 & 8.028 & 6.968 & -45.72 & -60.24
\end{array}\right]$$

$$D_0 = 0$$

$$a = [\ 1.250 \quad 0.2500 \quad 0.2500 \quad 0.1250 \quad 0.2500 \quad 0.1250 \quad 0.0859 \quad 0.0430 \quad 0.0240 \quad 0.0120\ ]$$

Figure A-6. CH-47 Lateral Hover Observations and Thresholds - System F.

Table A-3. Lateral Performance Summary — System F With Flight Directors.

Total Control Attention	$f_c = 0.2$			$f_c = 0.4$			$f_c = 0.6$		
Display Variable (y_i)	RMS Value	Control Attention (f_{c_i})	Cost Gradient ($-g_{f_i}$)	RMS Value	Control Attention (f_{c_i})	Cost Gradient ($-g_{f_i}$)	RMS Value	Control Attention (f_{c_i})	Cost Gradient ($-g_{f_i}$)
y (ft)	6.19	0.020	0.21	5.27	0.054	0.04	4.90	0.089	0.02
V_y (ft/sec)	1.18	0.020	9.25	1.00	0.054	2.80	0.93	0.089	1.51
ϕ (deg)	1.59	0.010	0.07	1.54	0.010	0.03	1.52	0.010	0.02
$\dot{\phi}$ (deg/sec)	0.70	0.010	0.51	0.67	0.010	0.41	0.65	0.010	0.31
ψ (deg)	0.07	0.010	0.00	0.06	0.010	0.00	0.05	0.010	0.00
$\dot{\psi}$ (deg/sec)	0.05	0.010	0.01	0.05	0.010	0.00	0.05	0.010	0.00
FD_ϕ (in)	0.20	0.140	10.70	0.19	0.310	2.99	0.19	0.473	1.53
$\dot{FD}_\phi$ (in/sec)	1.64	0.140	0.53	1.63	0.310	0.33	1.62	0.473	0.26
FD_ψ (in)	0.02	0.020	0.48	0.02	0.016	0.03	0.01	0.017	0.01
$\dot{FD}_\psi$ (in/sec)	0.18	0.020	0.43	0.16	0.016	0.32	0.16	0.017	0.26
Control Variable (u_i)	RMS Value			RMS Value			RMS Value		
δ_a (in)	0.28			0.28			0.28		
δ_r (in)	0.03			0.03			0.03		
Total Cost (J_c)	8.16			6.93			6.45		
Performance Cost (P_c)	1.24			1.05			0.88		

Table A-4. Lateral Performance Summary — System F Without Flight Directors.

Total Control Attention	$f_c = 0.2$			$f_c = 0.4$			$f_c = 0.6$		
Display Variable (y_i)	RMS Value	Control Attention (f_{c_i})	Cost Gradient ($-g_{f_i}$)	RMS Value	Control Attention (f_{c_i})	Cost Gradient ($-g_{f_i}$)	RMS Value	Control Attention (f_{c_i})	Cost Gradient ($-g_{f_i}$)
y (ft)	6.53	0.162	0.42	5.50	0.322	0.08	5.04	0.443	0.03
V_y (ft/sec)	1.30	0.162	11.27	1.12	0.322	3.92	1.04	0.443	2.35
ϕ (deg)	1.67	0.020	0.91	1.62	0.059	0.41	1.59	0.137	0.21
$\dot{\phi}$ (deg/sec)	0.76	0.020	3.20	0.73	0.059	2.76	0.71	0.137	1.93
ψ (deg)	0.08	0.018	0.0	0.07	0.019	0.00	0.06	0.019	0.0
$\dot{\psi}$ (deg/sec)	0.06	0.018	0.04	0.05	0.019	0.01	0.05	0.019	0.0
FD_ϕ (in)	0.23	0.0		0.22	0.0		0.22	0.0	
$\dot{FD}_\phi$ (in/sec)	1.67	0.0		1.65	0.0		1.64	0.0	
FD_ψ (in)	0.03	0.0		0.02	0.0		0.02	0.0	
$\dot{FD}_\psi$ (in/sec)	0.20	0.0		0.19	0.0		0.19	0.0	
Control Variable (u_i)	RMS Value			RMS Value			RMS Value		
δ_a (in)	0.28			0.28			0.28		
δ_r (in)	0.04			0.04			0.04		
Total Cost (J_c)	8.77			7.53			6.93		
Performance Cost (P_c)	1.42			1.21			1.11		